Calcium Influx, Diffusion and Extrusion in Fly Photoreceptor Cells

School of Behavorial and
Cognitive Neurosciences

RIJKSUNIVERSITEIT GRONINGEN

Calcium Influx, Diffusion and Extrusion in Fly Photoreceptor Cells

Proefschrift

ter verkrijging van het doctoraat in de
Wiskunde en Natuurwetenschappen
aan de Rijksuniversiteit Groningen
op gezag van de
Rector Magnificus, dr. D.F.J. Bosscher,
in het openbaar te verdedigen op
vrijdag 31 maart 2000
om 16.00 uur

door

Johannes Christoph Oberwinkler

geboren op 16 juni 1969
te Merida/Venezuela

Promotor:	prof.dr. D.G. Stavenga
Beoordelingscommissie:	prof.dr. D. Hoekstra
	prof.dr. W.H. Moolenaar
	prof.dr. W.J. Wadman

ISBN 90-367-1218-1

Meine Musca domestica

Hoch soll sie leben!
Auch tief darf sie leben!
Meine Stubenfliege in der Winterzeit.
Alle Sauberkeit
Darf sie schwarz verkleben.

Was mag sie denken?
Was mag sie lenken,
Wenn sie scheinbar sinnlos auf dem Frühstückstisch
Zwischen Braten, Käse, Milch und Fisch
Immer unbehelligt flugwirr flieht,
Aber plötzlich einen Tischtuchfleck beehrt,
Wo kein Mensch etwas Besonderes sieht?

Ist ein Krümelchen wohl eines Totschlags wert!?

Mag sie meinetwegen
Ihre Eier legen
Wann, wohin und wieviel ihr beliebt!

Immer noch studiere
Ich am kleinsten Tiere:
Welche himmelhohen Rätsel es gibt.

Joachim Ringelnatz

To Sandrine

Contents

1 General introduction

Calcium signals are arguably the most ubiquitous among all intracellular signals and are employed by almost all cell types, from unicellular organisms to highly specialized cells in our own body. Calcium signals are often vital for the proper functioning of the cells and hence for the survival of the whole organism. Well-documented examples where calcium plays a crucial role are the triggering of neurotransmitter release at all chemical synapses in the brain and the calcium wave that runs on the surface of egg cells just after it has been fertilized. Despite, or perhaps because of this widespread occurrence, calcium signals occur in amazingly many different forms. Slow changes in the free calcium concentration -typically in the range of several hundreds of nanomoles per liter- can affect all parts of the cytosol uniformly. The other extreme are so-called calcium microdomains that arise on the intracellular mouth of calcium channels within a few microseconds after the channel opened. These microdomains extend only 20 nm and the calcium concentration there reaches several millimoles per liter but only in a tiny volume (Llinás et al., 1995).

It may therefore not be surprising that cells have evolved a great variety of mechanisms in order to achieve, to regulate and to tightly control the size, shape, and time course of the different calcium signals. Amongst them are calcium influx through channels and calcium extrusion due to the action of exchangers and pumps located in the plasma membrane, as well as calcium release from and calcium uptake into intracellular organelles. Very important are also the amount and nature of calcium-binding molecules, often in the form of special calcium-binding proteins. The precise localization of these calcium-handling molecules with respect to the geometry of the cell is crucial in determining the speed and the extent of the resulting calcium signal. This thesis exemplifies this point by describing the rather extreme, and extremely localized, calcium signals in fly photoreceptor cells.

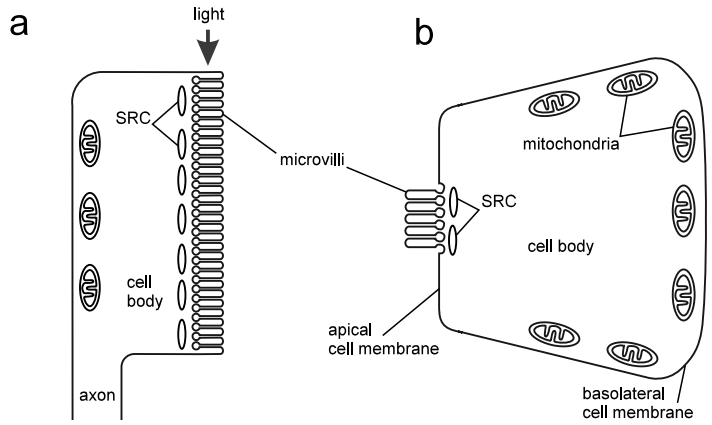

FIGURE 1.1: Schematic drawing of the morphology of fly photoreceptor cells (not to scale). a) longitudinal cross-section. b) transverse cross-section. Photoreceptor cells are highly polarized. Close to the basolateral side, the mitochondria are located. The apical membrane is folded into many small microvilli. All microvilli together are called the rhabdomere. Very close to the mouth of the microvilli the subrhabdomeric cisternae (SRC) are located that are part of the endoplasmic reticulum.

The morphology of fly photoreceptor cells

Fly photoreceptor cells are thin, elongated structures surrounded by the plasma membrane that has two highly different sides, i.e. fly photoreceptor cells are polarized (Figure 1.1). On the so-called basolateral side close to the membrane most mitochondria are located (Boschek, 1971). In the basolateral membrane the ATP consuming Na^+/K^+ pumps are placed (Baumann et al., 1994) that are responsible for maintaining a high concentration of potassium and a low concentration of sodium intracellularly. The basolateral membrane also contains the voltage-gated potassium channels (Weckström et al., 1991; Hardie, 1991b). On the opposite, the so-called apical side, the membrane is folded up into the rhabdomere, a densely packed stack of small tube-like protrusions, called the microvilli. A microvillus is about 0.7-1.6 μm long and 60 nm in diameter (rev.: Hardie, 1985). They are connected to the cell body via a still narrower neck that is 35 nm in diameter (Boschek, 1971; Walz, 1982). At the base of the microvilli, in very close distance to the plasmalemmal membranes, intracellular organelles are located (Walz, 1982) that belong to the endoplasmic reticulum (ER). These organelles are

called sub-rhabdomeric cisternae (SRC). Optically, the rhabdomere acts as a waveguide (rev.: van Hateren, 1989). This means that the light that is falling onto the eye and that is focused by the corneal facet lenses is trapped into the rhabdomere and then travels along the rhabdomere down its length. Consequently, the rhabdomere contains the rhodopsin molecules that are, by absorbing the photons, at the beginning of the biochemical cascade that transduces the optical into an electrical signal. Surprisingly, however, the rhabdomeric microvilli also contain many of the molecules that have been implied in either the primary transduction cascade or in the modulation thereof (rev.: Montell, 1999).

Phototransduction

The transduction of an optical into an electrical signal is exquisitely sensitive. Already the successful absorption of a single photon by a rhodopsin molecule triggers a quantum bump, a measurable, short-lived current (e.g. Scholes, 1966; Wu and Pak, 1978) that is due to the opening of channels in the membrane of microvilli. When the photoreceptor cells are stimulated with stronger lights, many quantum bumps add up and produce a larger light response.

Between the absorption of a photon and the opening of membrane channels, a complex and still not fully understood chain of biochemical events underlies the transduction of the signal (Figure 1.2). It is however clear that the rhodopsin molecule that absorbed a photon activates a G-protein, that, in turn, activates a protein called phospholipase C (PLC; rev.: Montell, 1999; Figure 1.2, steps 1 and 2). This protein, when activated, cleaves a specific type of lipid molecule present in the membrane, the so-called phosphatidylinositol-bisphosphate (PIP_2), into two parts. The first part, called inositol-trisphosphate ($InsP_3$), is soluble in the cytosol, while the other part, diacylglycerol (DAG), remains in the membrane of the microvilli. It is still controversially debated how the phototransduction cascade proceeds from these two substances, $InsP_3$ and DAG. One hypothesis (Figure 1.2a; Hardie and Minke, 1993; Cook and Minke, 1999) suggests that $InsP_3$ causes calcium to be released from the SRC; the reduced concentration of calcium in this compartment of the ER is then thought to activate channels in the plasma membrane. This pathway of signal transduction has already been demonstrated in a variety of other cell types (rev.: Berridge, 1995). More recently, Chyb et al. (1999) have demonstrated that poly-unsaturated fatty acids, substances that can be produced by further metabolizing DAG, can

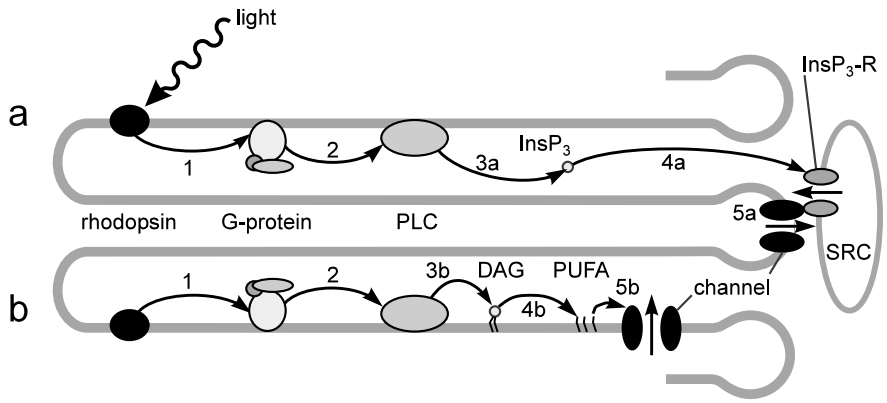

FIGURE 1.2: Two hypotheses of phototransduction. When a rhodopsin molecule is activated due to the absorption of a photon, the G-protein transmits (step 1) the activation to the phospholipase C (PLC) (step 2). The phospholipase C splits a molecule called PIP_2 into $InsP_3$ (step 3a) and DAG (step 3b). The "capacitative calcium entry" hypothesis (a) assumes that $InsP_3$ diffuses to the $InsP_3$-receptor ($InsP_3$-R) that is located in the subrhabdomeric cisternae (SRC; step 4a). The $InsP_3$ in turn opens and lets calcium flow from the SRCs into the cytosol. The reduction of the calcium concentration in the SRCs is thought to constitute the signal for the plasmamembrane channels to open (step 5a). The alternative hypothesis (b) assumes that the other product of the PLC activity, DAG, is metabolized into poly-unsaturated fatty acids (PUFA; step 4a), that are able to directly open the membrane channels (step 5b). The straight arrows indicate the direction of the calcium flux. See text for further explanation.

activate the same channels that are normally activated by light stimuli (Figure 1.2b). Whether this pathway represents the physiological route of activation, however, remains to be demonstrated.

Biophysically, two types of light-activated channels can be distinguished. One type of channel is dependent on the presence of the product of the *trp* gene. This type of channel is highly permeable for calcium ions (Hardie and Minke, 1992; Reuss et al., 1997) and has a small single channel conductance (Reuss et al., 1997). The other type of channels is eliminated when the product of the *trpl* gene is missing. This channel-type is much less specific for calcium ions than the *trp*-dependent channel-type, and its single channel conductance might be as much as 10 times larger (Hardie et al., 1997; Reuss et al., 1997). The product of the *trp* gene is 10 times more abundant in the photoreceptor cells than the product of the *trpl* gene (Xu et al., 1997). This might indicate that the *trp*- and *trpl*-dependent channels

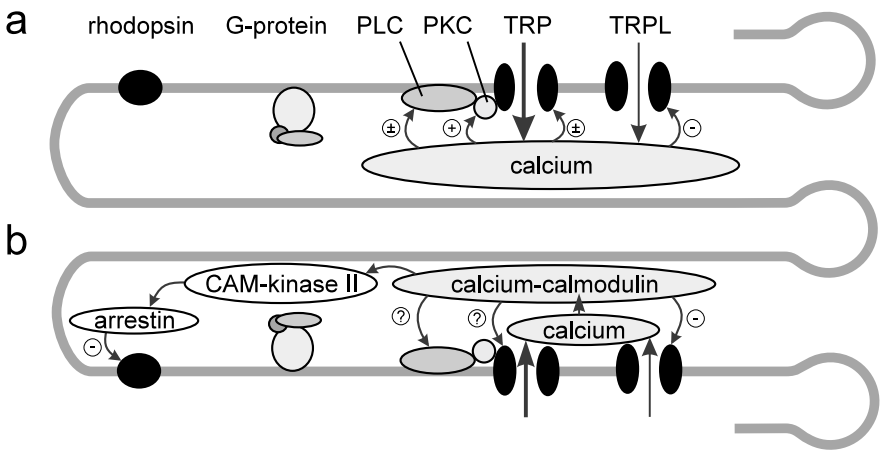

FIGURE 1.3: Diagram of the pathways through wich calcium can modulate the transduction cascade. Calcium flowing through the *trp*- and *trpl*-dependent channels increases the calcium concentration very rapidly in the microvilli (Chapter 3). a) An increased calcium concentration has been shown to directly modulate the *trp*- and *trpl*-dependent channels, but also the phospholipase C (PLC) and the protein kinase C (PKC) that can phosphorylate the *trp*-dependent channels. b) A high concentration of the calcium-binding protein calmodulin is present in the microvilli. In its calcium-bound form, it activates the Cam-kinase II that phosphorylates arrestin. This phosphorylation is necessary for arrestin to turn off activated rhodopsins. Calcium-bound calmodulin furthermore directly inactivates the *trpl*-dependent channels and might also regulate the *trp*-dependent channels and the PLC.

each contribute about 50% of the total light-induced current. However, the contribution of the *trpl*-dependent channels seems to be much less than 50% under physiological recording situations (Niemeyer et al., 1996; Reuss et al., 1997). This apparent contradiction has been resolved by demonstrating that calcium flowing into the microvilli differentially regulates the two types of channels: the activity of the *trp*-dependent channels becomes enhanced by the rising calcium concentration, while the *trpl*-dependent channels are inhibited (Hardie, 1995a; Reuss et al., 1997). This is just one example that illustrates the importance of calcium for the regulation of the light response.

Calcium regulation of phototransduction

A change in the intracellular calcium concentration regulates the sensitivity in almost every sensory cell, e.g., in vertebrate photoreceptor cells, in hair

cells of the inner ear that are used for hearing, and in olfactory neurons that allow us to smell (revs: Torre et al., 1995; Jaramillo, 1995; Menini, 1999). This is also observed in fly photoreceptor cells. When the cells are stimulated with light, their sensitivity for additional light stimulation becomes reduced, i.e. the cells become light adapted. For this light adaptation to take place, the intracellular calcium concentration needs to increase (Muijser, 1979). How calcium brings about light adaptation has recently begun to be unraveled. It has become clear that calcium acts on many different targets (Figure 1.3). Calcium is believed to directly act (Figure 1.3a) on the light-activated channels, because the differential regulation of the two types of light-activated channels described above is observed within at most a few milliseconds of increasing the calcium concentration (Hardie, 1995a). In addition, calcium has been shown to directly affect the activity of the PLC (Running Deer et al., 1995) and a protein termed protein kinase C (PKC), that is also located in the microvilli (Huber et al., 1998). Without this PKC, light adaptation is severely impeded (Hardie et al., 1993). The PLC and PKC are tightly coupled in a complex that is held together by a protein called INAD and that also contains the *trp*-gene product (Huber et al., 1996a).

The calcium-sensing protein calmodulin is present in high concentrations in the rhabdomeric microvilli (Porter et al., 1993). Calmodulin in its active, calcium-bound form is itself an important regulator of phototransduction (Figure 1.3b). It activates a protein named Cam-kinase II that phosphorylates arrestin. Preventing this phosphorylation severely reduces the concentration of arrestin that can bind to activated rhodopsin and terminate its activity (Scott et al., 1997; Alloway and Dolph, 1999). This in turn causes the light response to terminate abnormally slowly (Scott et al., 1997). Calmodulin can also bind to the *trp*- and *trpl*-dependent channels (Phillips et al., 1992; Warr and Kelly, 1996; Scott et al., 1997). It has been shown that this interaction is important to inactivate the *trpl*-dependent channels (Scott et al., 1997). Furthermore, calmodulin might also regulate the PLC (Richard et al., 1997).

While these regulatory actions of calcium all take place in the rhabdomeric microvilli, an increase in the calcium concentration in the cell body also leads to regulatory reactions. It causes small pigment granules to aggregate near the rhabdomere (Kirschfeld and Vogt, 1980) in order to absorb light (Kirschfeld and Franceschini, 1969); this pigment migration has been termed intracellular pupil. Increasing the calcium concentration in the cell body activates the mitochondria (Fein and Tsacopoulos, 1988), presumably to induce the mitochondria to augment the production of ATP. Mitochondria

can also take up calcium (rev.: Bernardi, 1999) and thereby play an important role in the regulation of the calcium concentration in the cell body.

Together, these data show that calcium plays a crucial role in regulating the light response of fly photoreceptor cells. A good understanding of how the light response is regulated, therefore, requires the kinetics and absolute values of the free calcium concentration to be known quantitatively in the different compartments of the photoreceptor cells, especially in the rhabdomere. This thesis is the account of an attempt to provide these data.

Outline of the thesis

Quantitative calcium measurements in fly photoreceptor cells have previously been done only in isolated cells of the fruitfly *Drosophila melanogaster*. Since these cells do not resist to strong, adapting light stimuli when they are isolated, a new preparation was developed. This preparation is introduced in Chapter 2 and the methods employed for measuring calcium quantitatively in the photoreceptor cells in the larger fly *Calliphora vicina* are explained. This method is used to determine how the average intracellular calcium concentration in the photoreceptor cells depends on the stimulating light intensity.

In Chapter 3, this method is refined in order to measure the calcium concentration only in the rhabdomere. It is shown that very high calcium transients, exceeding 200 μM, occur in the rhabdomeres.

In Chapter 4, it is shown, using fast fluorescent imaging, that the calcium concentrations in the rhabdomere and in the cell body are similar in the steady state, after the calcium transients in the rhabdomere have decayed. Using a modeling approach, it is demonstrated that this finding implies that calcium influx and calcium extrusion, which is mediated by Na^+/Ca^{2+} exchangers, must be co-localized.

In Chapter 5, the properties of the calcium-extruding Na^+/Ca^{2+} exchanger in the photoreceptor cells of *Drosophila* are explored by using the patch-clamp technique. The main findings are that the exchanger does not require potassium to function, and that it tightly regulates the activity of calcium-activated potassium channels.

In Chapter 6, finally, the data obtained in the previous Chapters are integrated into a model that allows simulating the ion fluxes in fly photoreceptor cells. The model shows that the quantitative measurements of the calcium concentration in the rhabdomere are consistent with what is known about the geometry and physiology of the photoreceptor cells. Furthermore, it is

shown that experimental data of changes of extracellular ion concentrations match the predictions of this model reasonably well.

2 Light dependence of calcium and membrane potential measured in blowfly photoreceptors in vivo

Abstract

Light adaptation in insect photoreceptors is caused by an increase in the cytosolic Ca^{2+} concentration (Ca_i). To better understand this process, we measured Ca_i in vivo as a function of adapting light intensity in the white-eyed blowfly mutant *chalky*. We developed a technique to measure Ca_i under conditions as natural as possible. The calcium indicator dyes Oregon Green 1, 2 or 5N were iontophoretically injected via an intracellular electrode into a photoreceptor cell in the intact eye; the same electrode was also used to measure the membrane potential. The blue-induced green fluorescence of these dyes could be monitored by making use of the optics of the facet lens and the rhabdomere waveguide. The use of the different Ca^{2+}-sensitive dyes that possess different affinities for Ca^{2+} allowed the quantitative determination of Ca_i in the steady state. Determining Ca_i as a function of the adapting light intensity shows that Ca_i is regulated in a graded fashion over the whole dynamic range where a photoreceptor cell can respond to light. When a photoreceptor is adapted to bright light, Ca_i reaches stable values higher than 10 μM. The data are consistent with the hypothesis that the logarithm of the increase in Ca_i is linear with the logarithm of the light intensity. From the estimated values of Ca_i we derive that the Ca^{2+}-buffering capacity is limited. The percentage of the Ca^{2+} influx that is buffered gradually decreases with increasing Ca_i. At Ca_i levels above 10 μM, buffering becomes minimal.

The research presented in this Chapter has been published as:
Oberwinkler J, Stavenga DG (1998) J Gen Physiol 112:113-124.

Introduction

The cytosolic free concentration of Ca^{2+} ions (Ca_i) is one of the most important regulation factors in biological cells, influencing a great number of cellular processes. This holds particularly for insect photoreceptor cells, where Ca_i has been shown to play a key role in the regulation of the light-sensitivity (Bader et al., 1976; Autrum, 1979; Muijser, 1979; Tsukahara, 1980; Walz, 1992). More specifically, Ca_i has been implicated in the control of numerous cellular processes in fly photoreceptors, e.g., in the modulation of the light-activated ion-channels (Hardie, 1991a, 1995a, b; Hardie and Minke, 1994b), the activation of the Na^+/Ca^{2+} exchanger (Hardie, 1995a, b), the regulation of many enzymes involved in the transduction cascade (revs: Selinger et al., 1993; Minke and Selinger, 1996; Montell, 1999), the activation of mitochondria (Fein and Tsacopoulos, 1988; Mojet et al., 1991), and the migration of pigment granules in the photoreceptor cells (Kirschfeld and Vogt, 1980; Howard, 1984; Hofstee and Stavenga, 1996).

Ca_i has been reported to rise in insect photoreceptors cells during light stimulation (Howard, 1984; Hardie, 1991a, 1996a; Peretz et al., 1994b; Ranganathan et al., 1994; Walz et al., 1994). In fly photoreceptors, the main part of this increase in Ca_i is caused by the influx of extracellular Ca^{2+} through the light-activated channels (Howard, 1984; Hardie, 1991a, 1996a; Hardie and Minke, 1994b; Peretz et al., 1994b; Ranganathan et al., 1994). Therefore, in an intact eye Ca_i will not only depend on processes inside the photoreceptors themselves, but also on the ionic conditions in the extracellular space. With respect to Ca^{2+}, these can vary considerably (Sandler and Kirschfeld, 1988, 1991; Ziegler and Walz, 1989; Rom-Glas et al., 1992; Peretz et al., 1994a).

In the past, Ca_i of insect photoreceptors and its dynamic regulation has been measured either in isolated ommatidia (Peretz et al., 1994b; Ranganathan et al., 1994; Hardie, 1995a, 1996a,b) or in slice preparations of the retina superfused with Ringer solutions (Coles and Orkand, 1985; Hochstrate and Juse, 1991; Walz et al., 1994). Both of these techniques are likely to strongly influence the extracellular ion concentrations and hence to affect Ca_i. In an alternative approach, the light dependence of the Ca^{2+} homeostasis in insect photoreceptors has been studied via measurements of the Ca^{2+} concentration in the extracellular space (Sandler and Kirschfeld, 1988, 1991, 1992; Rom-Glas et al., 1992; Peretz et al., 1994a); however, the possibly strong influence of intracellular Ca^{2+} buffering (Hardie, 1996a) and of

Ca^{2+} release from intracellular stores (Walz et al., 1995; Hardie, 1996b; Cook and Minke, 1999) on Ca_i could not be studied in this way.

To better understand the regulation of Ca_i under natural, physiological conditions, we developed a technique to directly measure Ca_i in the intact eye, by using fluorescent Ca^{2+} indicator dyes with varying affinity for Ca^{2+}. We thus were able to estimate Ca_i as a function of adapting light intensity. We find that bright illumination of fly photoreceptors causes surprisingly high levels of Ca_i, probably even exceeding 10 μM.

Materials and Methods

PREPARATION All experiments were performed on female blowflies (*Calliphora vicina*, white-eyed mutant *chalky*) taken from a laboratory culture. The mutant *chalky* was chosen because screening pigments and a functional pupil mechanism are lacking. The animals were immobilized with wax and a small hole was cut in the cornea that was immediately sealed with silicon grease. A silver wire was placed as reference electrode in the same eye. The intactness of the optics of the eye was checked before and after preparation, by inspecting the deep pseudopupil (Franceschini and Kirschfeld, 1971). The animal was placed in a holder that allowed adjustment of its orientation. The holder with the animal was then positioned on the micromanipulator-controlled stage of a Leitz Orthoplan epi-fluorescence microscope.

ELECTROPHYSIOLOGY Conventional electronic equipment was used to measure the intracellular membrane potential and to pass current through the electrode (Axoclamp 2A, Axon Instr.; operated in bridge mode). The electrodes were pulled on a P-87 (Brown and Flaming, Sutter Instr.) from borosilicate glass (1.5 mm outer diameter, 0.86 mm inner diameter, Clark Instr.), and their tip was filled with a solution containing 5 mM of calcium indicator dye (Oregon Green 1, 2 or 5N, Molecular Probes, in the following abbreviated as OG1, OG2 and OG5N, respectively) in 0.1 M KCl. The shank was then backfilled with 0.1 M KCl solution. The electrodes had a resistance of 150-250 MΩ in the tissue. The procedure of electrical recording was as follows. First, the tip of the electrode was adjusted at the optical axis of the objective, at a level 150 μm below the focal plane. The stage of the microscope with the fly in the holder was then moved under the objective, so that the electrode penetrated the eye through the hole at a level 150 μm below the corneal surface and the fly was advanced so far that a penetrated cell was approximately co-axial with the objective.

DYE FILLING After impalement, the cell was dye-filled by applying pulses of -1.2 to -2.2 nA at 0.5 Hz (50% duty cycle). The process of filling lasted at most 5 min, but was usually complete after 1-2 min. Sometimes no current was necessary, because cells filled simply by diffusion of the dye from the tip of the electrode. The filling of a cell was immediately apparent from the distinct fluorescence emerging from one of the facet lenses. As outlined in the Results, excessive concentrations of the dye induced alterations of the electrical response of the photoreceptor cells. Therefore, as a precaution, the process of dye filling was checked in regular intervals by visually judging the intensity of the fluorescence and filling was stopped when the intensity of the fluorescence reached values sufficient from optical recordings. Recordings of cells that were subsequently found to display alterations in their peak-plateau transitions (indicative of excessive additional Ca^{2+} buffering) were rejected (see Results).

OPTICAL SETUP Two light sources, a 75 W xenon lamp and a 100 W halogen lamp, delivered the test and adapting light beam, respectively. Shutters (Uniblitz, Vincent Associates; rise time < 3 ms) and grey filters controlled the light flux in both light paths independently. A 50% mirror combined the beams, which then passed the microscope's fluorescence cube (Leitz DM 510, i.e. blue excitation causing green emission). A 10x objective (NA 0.25, Spindler and Hoyer) projected the blue illumination onto the fly eye. The green emission was measured by a photomultiplier (R928, Hamamatsu). A small diaphragm (diameter 0.2 mm) in the image plane was adjusted so that only the fluorescence emerging from the brightly shining facet lens was selected. The background due to a distinct autofluorescence of the cornea thus was minimized.

DATA ACQUISITION The signals from the electrode amplifier and the photomultiplier were filtered at 2 kHz (Krohn-Hite, model 3343) and sampled at 5 kHz per channel by a CED 1401 interface (Cambridge Electronic Design). Further processing of the data was performed off-line.

PHOTOGRAPHY After filling a cell with OG1 the fly was placed in a fluorescence microscope (Nikon Diaphot) equipped with a Nikon F-601M camera containing a black and white film (Ilford SFX; 200 ASA pushed to 800 ASA). The blue (477 nm) induced green ($>$510 nm) fluorescence was photographed with a dry objective (4x, NA 0.1, Spindler and Hoyer; Figure 2.1) as well

as a water immersion objective (SW25, NA 0.6, Leitz; Figure 2.1c and d). In Figure 2.1a, a halogen light source delivered additional side illumination for recognition of the eye and facet pattern. To identify the stained cell, the eye was first illuminated during 5 s with 380 nm light for creating the highly fluorescent visual pigment state M′ (Stavenga et al., 1984). Then the green (546 nm) induced red emisssion (>580 nm) was photographed (water immersion SW25; Figure 2.1d).

QUANTITATIVE DATA ANALYSIS To estimate Ca_i quantitatively as a function of the adapting light, we first adapted the photoreceptor cells for 5 s to a given light intensity, and then probed the fluorescence with a bright test flash. The fluorescence signal at the beginning of the test flash thus represents the Ca_i signal due to the adapting light. At the end of the test flash the signal is dominated by the Ca^{2+} influx caused by the much brighter test flash. Because we used non ratiometric Ca^{2+} indicators it was necessary to ensure that changes in dye concentration (caused by bleaching or by active transport out of the cell) did not corrupt the measurements. When using the high affinity dyes OG1 or OG2, we therefore took the difference in the fluorescence signal between the beginning and the end of the fluorescence trace for the quantitative analysis. Any change in the magnitude of the fluorescence signal at the end of the test flash, i.e. when the dye is saturated, indicated that the concentration of the dye changed. For the data from OG5N, this procedure was not possible, because due to the low affinity of OG5N for Ca^{2+} the signal does not saturate. We therefore took the difference between the initial fluorescence of the photoreceptor cell adapted to different light intensities and the initial fluorescence signal of the dark adapted photoreceptor cell. This method requires regular checks for changes in the magnitude of the fluorescence signal from the dark adapted photoreceptor. Because the magnitude of the fluorescence signal of our single wavelength dyes depends on the concentration of the dye, we normalized the data in order to be able to compare data from different cells. The quantitative values from a single cell describing the influence of the adapting light were normalized between the value of the lowest adaptation intensity and the value of the highest adaptation intensity, and subsequently plotted as a function of the light intensity. To estimate the dependence of Ca_i on the light intensity, we calculated the expected fluorescence signal as a function of the light intensity with the function $F(Ca_i) = {Ca_i}^h / ({Ca_i}^h + {K_d}^h)$. Since our in vivo method does not allow a direct calibration of the indicators, we used the K_d values published by

Haugland (1996): OG1: $K_d = 0.16$ μM; OG2: $K_d = 0.58$ μM; OG5N: $K_d = 20$ μM. Hill-coefficients were taken equal to 1, except for OG5N, for which repeatedly Hill-coefficients lower than one have been reported (e.g. Ukhanov et al., 1995); we used a value of 0.7, derived from fitting the data published for Calcium Green 5N (Haugland, 1996). Using this function, we calculated the expected fluorescence as a function of the light intensity, for functions of Ca_i depending on the light intensity. The resulting functions of fluorescence depending on the light intensity were normalized (again between the value for the lowest light intensity and the value for the highest light intensity, i.e. between $\log I = -3$ and $\log I = 2$), to allow comparison with the measured data.

Results

A new method to measure cytosolic Ca^{2+} dynamics in photoreceptors of insect compound eyes in vivo

The preferred method for recording the membrane potential of individual insect photoreceptors in intact animals is to insert an electrode through a small hole in the cornea and to subsequently impale a photoreceptor cell. Here we demonstrate that this technique can also be used to inject calcium indicator dyes into a penetrated cell. Figure 2.1a shows an eye of a blowfly where one cell was dye-filled, photographed through a dry objective. One facet lens clearly shines up. Neutralizing the cornea by using a water immersion objective (Kirschfeld and Franceschini, 1969) allows examination of the subcellular distribution of the dye, because it is then possible to focus onto the tips of the rhabdomeres and the cell bodies; Figure 2.1b depicts this optical situation diagramatically (for a detailed account of the anatomy of the fly retina see Hardie, 1985). Figure 2.1c shows the blue-induced green fluorescence of the stained cell. Both the soma and rhabdomere of one of the photoreceptor cells fluoresce, indicating that the dye is distributed throughout that photoreceptor cell and that part of the excited fluorescence is efficiently guided by the rhabdomere. To visualize the localization of the stained cell within the ommatidial lattice of the fly's eye, we exploited the bright red fluorescence of the M′ state of the visual pigments (Stavenga et al., 1984, see Materials and Methods) when illuminated with green light. The green-induced red fluorescence (Figure 2.1d) of the same part of the retina as in Figure 2.1c shows the rhabdomere of the stained cell (arrow), an R5 cell, and the regular pattern of fluorescing rhabdomeres; of course, the green-induced red fluorescence of the dye is much weaker than the blue-induced green fluorescence.

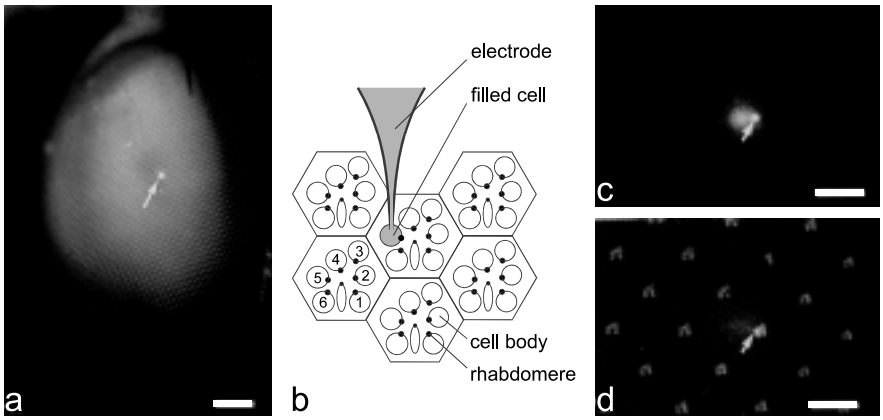

FIGURE 2.1: Photographs of a dye injected photoreceptor cell. a) Left eye of a white-eyed mutant blowfly *Calliphora vicina* photographed with a dry objective. The facet lens overlying the dye-injected cell clearly shines up (scale bar 0.2 mm). b) Diagram of the photoreceptor organization and the recording situation after optically neutralizing the cornea with a water immersion objective (Kirschfeld and Franceschini, 1969). c) Blue-induced green fluorescence photographed through a water-immersion objective, showing that the rhabdomere and the cell body of the stained cell fluoresce. d) Green-induced red fluorescence of the same eye region showing the characteristic pattern of the rhabdomeres; one rhabdomere -belonging to the stained cell- is brighter than the others (arrow), allowing to identify the stained cell as an R5 photoreceptor (scale bar in c) and d) 20 μm).

Under the physiological optical conditions used in the experiments, light emitted from the rhabdomere leaves the eye within an angle of 1-2° (van Hateren, 1984), while the fluorescence coming from the cell body is expected to irradiate from the cornea within an angle of $\sim$11° (assuming a diameter of the cell of $\sim$10 μm and a focal distance of 50 μm of the facet lens). Because the objective aperture is $\sim$14°, the photomultiplier samples a mixture of light emitted by the rhabdomere and the cell body; however, the ratio of the amount of light sampled from the two cellular compartments depends on the precise alignment of the investigated cell's visual axis with the microscope objective. This inevitably varied from one recording to another.

From such a dye-filled cell, we recorded simultaneously the light-induced changes of the membrane potential and the accompanying fluorescence, using the low affinity dye OG5N (Figure 2.2). As in all experiments presented here, the cell was dark adapted for 1 min before and between the recordings. Illumination causes, after a delay of a few ms, a rapid depolarization

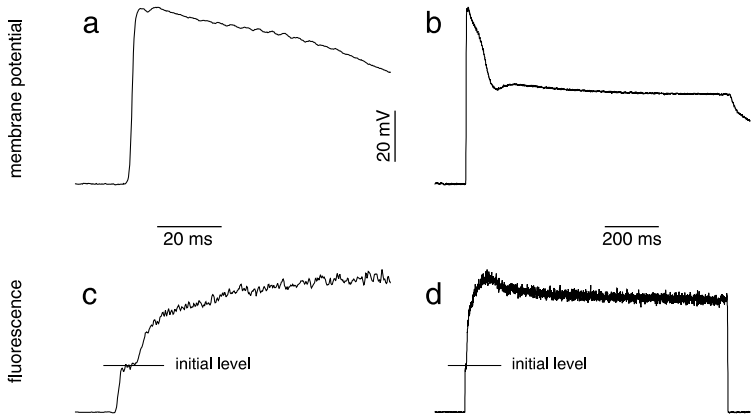

FIGURE 2.2: Simultaneous recording of membrane potential (a, b) and Ca^{2+} induced fluorescence (c, d) from a dark adapted photoreceptor illuminated with saturating light. The same data are shown with high (a, c) and with low temporal resolution (b, d). The cell was injected with the low affinity dye OG5N. The fluorescence signal increases very fast after opening the shutter and peaks after ~100 ms before levelling off towards a plateau. The depolarization of the membrane, however, displays still faster kinetics. All traces are averages of 9 recordings.

of the cell membrane, reaching a peak after ~10 ms (Figure 2.2a); subsequently, the receptor potential levels off to a plateau value (Figure 2.2b). The blue-induced green fluorescence appears to follow a similar, although somewhat slower time course. First, during the opening of the shutter the fluorescence signal rises to an initial plateau (initial level, Figure 2.2c, d). This is the sum of tissue autofluorescence and fluorescence of the dye due to resting Ca_i. Then, after a short delay (~3 ms), the emission very rapidly increases, indicating an abrupt rise in Ca_i (Figure 2.2c). The peak occurs after ~100 ms, and the subsequent decrease to a plateau of the fluorescence distinctly lags that of the receptor potential (Figure 2.2d).

The effect of the Ca^{2+} indicator dyes on the membrane potential

All Ca^{2+} indicator dyes are also Ca^{2+} buffers. Increasing the intracelluar Ca^{2+} buffering capacity by introducing the dyes can considerably alter the dynamics and the regulation of Ca_i (e.g. Neher, 1995). Because fly photoreceptors are thought to react sensitively to changes in the Ca^{2+} homeostasis (Muijser, 1979; Hardie, 1995b) we checked for changes in the waveform of

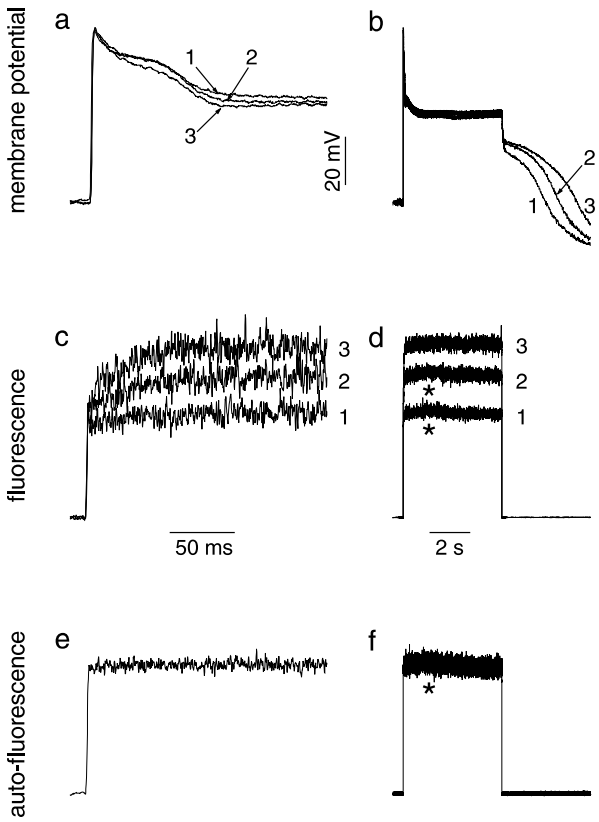

FIGURE 2.3: The effects of dye filling on the membrane potential. The photoreceptor cell was impaled with an electrode containing OG2 and then filled without applying current. Traces 1, 2 and 3 were measured 1 min, 4 min and 6 min after impalement, respectively, by a 1 s stimulus of saturating intensity. While the fluorescence signal (c, d) increases with time of impalement, indicative for an on-going dye-loading, the membrane potential response (a, b) of the cell during the light stimulus is hardly changed. Only after turning the stimulus off, a distinct prolongation of the depolarizing afterpotential can be seen, due to an increase in the concentration of the dye (b). The fluorescence traces in d) are smoothed by adjacent averaging with a window size of 20 sample points (equivalent to 4 ms) and therefore the rising phase that is visible in c) is not discernible in d). The traces in e) and f) were obtained from a different preparation in which no cell had been dye-filled; these traces are averages of 5 recordings. They show that the tissue autofluorescence is essentially constant, except for a small, transient increase in fluorescence signal ($\star$) that can be attributed to a light induced change in redox state of mitochondrial flavoproteins (Stavenga and Tinbergen, 1983).

the membrane potential due to loading with the dyes. The cell of Figure 2.3 spontaneously filled with OG2, i.e. without the need to apply current. The first measurement was taken at ∼1 min after impalement of the cell, the following after 4 and 6 min, respectively. The fluorescence signal (Figure 2.3c, d) increased with time, indicating that the cell progressively took up more of the dye. Following light-off, the time course of the afterdepolarization became prolonged. The afterdepolarization is -at least partially- caused by the Na^+/Ca^{2+} exchanger (Hochstrate, 1991), which in *Calliphora* photoreceptor cells can generate currents stronger than 1 nA (Gerster, 1997). Therefore, the prolongation of the afterpotential indicates that the Na^+/Ca^{2+} exchanger extrudes more Ca^{2+} when the dye concentration increases. This is in line with an increased buffering of Ca^{2+} ions by the dye, which leads to an increase in the total concentration of Ca^{2+} at comparable concentrations of free Ca^{2+}. We consistently found that the dyes prolonged the duration of the afterdepolarization, even at concentrations that were difficult to detect photometrically. However, the waveform of the receptor potential during light-on remained virtually unchanged (Figure 2.3a, b), suggesting that the rising dye concentration did not appreciably affect the phototransduction process.

Generally, the effect of the dye on the membrane potential during the light stimulus was inconspicuous, but peak values sometimes increased by a few mV after filling the cell; in some cases the peak to plateau transition of the membrane potential at the onset of light stimulation was accelerated after dye filling. When cells were filled too much, the typical reduction of the peak-plateau transition, caused by a substantial increase in Ca^{2+} buffering (Bader et al., 1976; Muijser, 1979; Tsukahara, 1980; Walz et al., 1994) could be observed; these cells then were rejected.

In addition to the fluorescence from the dyes, we measured the tissue autofluorescence from an eye of which no cell was injected with a Ca^{2+} indicator. This tissue autofluorescence remained essentially constant upon illumination (Figure 2.3e, f). Nevertheless, occasionally a very slight, transient increase in autofluorescence could be noticed in this background ($\star$ in Figure 2.3f), probably due to the light-induced, transient redox changes of the flavoproteins in the photoreceptor mitochondria (Stavenga and Tinbergen, 1983; Mojet et al., 1991). Sometimes, such a small increase in fluorescence also was observed when measuring from a cell filled with the high affinity dyes, i.e. in Figure 2.3d ($\star$); this small increase might also be attributable to the observed increase of the autofluorescence, that is, to transient changes in the redox state of the flavoproteins. In the processed experiments, this variation

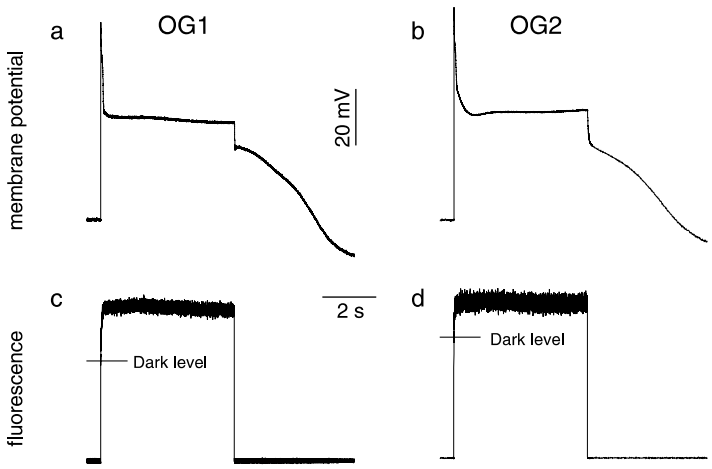

FIGURE 2.4: Membrane potential (a, b) and fluorescence (c, d) signal from two cells injected with the high affinity dyes OG1 (a, c) and OG2 (b, d), respectively. The dark adapted cells were illuminated for 5 s with light of saturating intensity. The fluorescence signal increases monotonically upon stimulation and does not display the peak that can be seen when using the low affinity dye OG5N (Figure 2.2). This indicates that the high affinity dyes OG1 and OG2 are saturated by the levels of Ca_i reached under bright illumination. This implies that in these conditions Ca_i exceeds 10 μM, the concentration where OG2 saturates (Haugland, 1996). Traces in a) and c) are averages of 5 recordings, traces in b) and d) are averages of 7 recordings.

in the background signal was fully negligible compared to the light-induced changes in dye fluorescence.

Bright light causes Ca_i to increase into the high micromolar range

Fluorescence measurements of cells injected with the low affinity dye OG5N ($K_d = 20$ μM; Haugland, 1996) yielded somewhat variable results. The time to peak ranged from 100 ms to almost 1 s; the time required for reaching a stable plateau takes 2-4 s. This variability might be the result of slight differences in the alignment of the investigated cells. Because the Ca^{2+} influx occurs in the rhabdomeres, and the Ca^{2+} ions diffuse from the rhabdomere into the cell body rather slowly (Ranganathan et al., 1994), a variation in the ratio of light sampled from the rhabdomere and from the cell body could cause a variation in the observed time course of the fluorescence signal.

No peak in the fluorescence signal was observed when high affinity dyes (OG1 or OG2; K_d = 0.16 μM and 0.58 μM, respectively; Haugland, 1996) were used (Figure 2.4a, b). The fluorescence signal then increased monotonically towards a stable plateau that was reached after 100-400 ms. These findings are fully consistent with the difference in affinity for Ca^{2+} of the dyes used, suggesting that Ca_i attains values where the high affinity dyes OG1 and OG2 are saturated. Because OG2 saturates at $Ca_i \approx 10$ μM (Haugland, 1996), Ca_i exceeds this range during the peak observed with the low affinity dye OG5N.

Steady state Ca_i after adaptation to different light intensities

To measure the dye fluorescence with an acceptable signal to noise ratio, it is necessary to use very high light intensities. To assess Ca_i at moderate and intermediate intensities, we employed a double pulse paradigm, where an adapting light stimulus was followed by a bright test flash. We adapted the photoreceptors for 5 s at a given intensity, and then probed the fluorescence with a short (0.2-0.5 s) test flash. An adaptation time of 5 s was considered sufficient, because both the stability of the membrane potential and the fluorescence measurements indicated that after 5 s Ca_i reached a stable plateau value and that diffusion of the Ca^{2+} ions had reached an equilibrium. We assume, therefore, that the subcellular distribution of Ca_i in the cytosol is fairly homogeneous after 5 s.

Figure 2.5 shows an example of such an experiment. The high affinity dye OG1 was used. The fluorescence signal at the beginning of the bright test flash increases with increasing adapting light intensity in the low intensity range, but it saturates at high intensities. Again, we confirmed that this is caused by saturation of the dye by using the low affinity dye OG5N. This dye reports an increase in Ca_i, even up to the highest intensities used (see below).

We repeated the experiment of Figure 2.5 with all three dyes (OG1, OG2, OG5N) in nine cells (three for each dye) from six animals. Figure 2.6 summarizes the experiments. In order to correct for the different absolute sensitivities of the different cells, the $V/\log I$ curve of the peak receptor potential of each cell was fitted separately to a logistic function: $V = V_{\max} I^n/(I^n+1)$ (Laughlin, 1981). The light intensity I is taken here relative to the light intensity that causes a half maximal peak depolarization; this intensity was assigned the value $\log I = 0$. Furthermore, the potential values were normalized to the maximal peak depolarization ($V_{\max}$). Figure 2.6a presents the

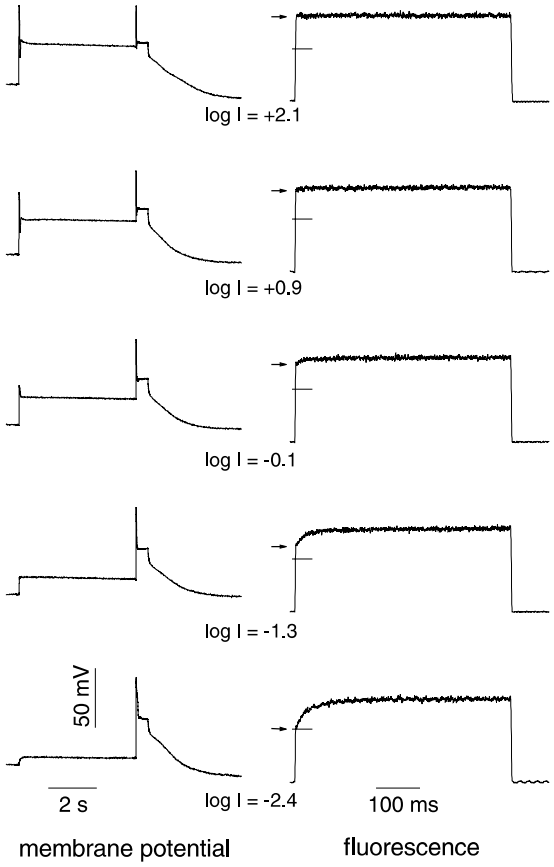

FIGURE 2.5: Example of the double pulse experiments used to determine Ca_i as a function of light intensity. Membrane potential traces are given in the left hand column. The dye-injected (OG1) and dark-adapted cell was stimulated with an adapting light (5 s), the intensity of which is indicated for each experiment. Intensities are expressed relative to the light intensity that caused a half maximal peak depolarization; this intensity was assigned the value $\log I = 0$. After adapting for 5 s, the level of Ca_i was probed with a bright test flash (500 ms). The fluorescence signal measured during this test flash is shown in the right hand column on an expanded time scale. The horizontal line at the beginning of the fluorescence traces indicates the initial fluorescence value when no adapting light was given. With increasing adapting intensity, the initial value of the fluorescence (indicated by arrows) increases. At the highest adapting intensities used, no increase in fluorescence can be observed during the test flash due to saturation of the high affinity dye OG1. All traces shown are averages of 5 recordings.

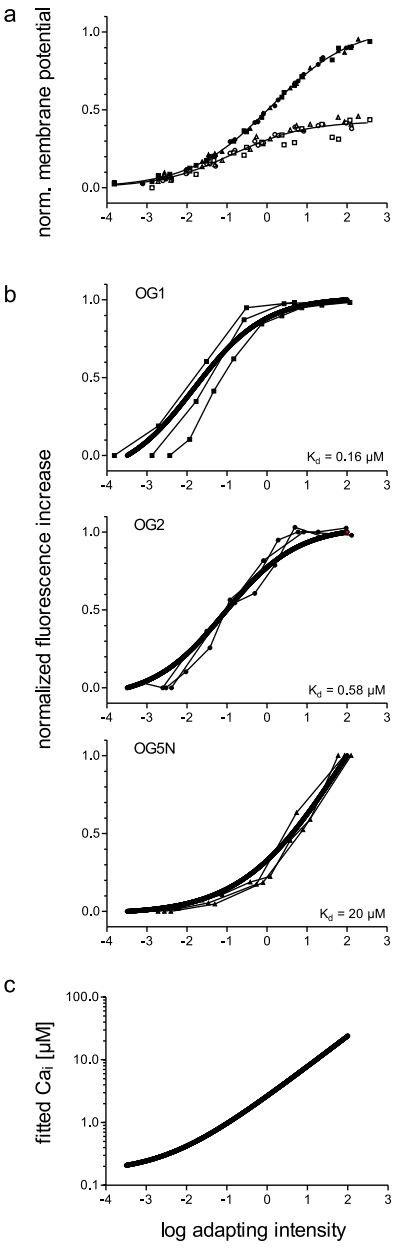

FIGURE 2.6: Summary of the double pulse experiments. a) Normalized depolarization of the peak (filled symbols) and plateau (open symbols) of the membrane potential are given as a function of adapting light intensity. The smooth curves are obtained by fitting the logistic function $V = V_{\max} I^n/(I^n+1)$ to the experimental data (exponent $n = 0.45$ for peak values and 0.47 for plateau values; the normalized $V_{\max}$ for plateau values was fitted to be 0.43). The light intensity I is taken relative to the light intensity that causes a half maximal peak depolarization; this intensity was assigned the value $\log I = 0$. b) Normalized fluorescence increase caused by the adapting light for the three dyes used (symbols connected by thin lines); data from three different cells are shown for each dye. Normalization procedures for all panels are explained in Materials and Methods. The membrane potential and fluorescence data obtained with a specific dye are indicated with the same symbol. The fluorescence increase reported by OG1 and OG2 rises with increasing adapting light intensity and saturates at bright light. The signal that was obtained with OG5N continues to increase up to the highest intensities. This shows that Ca_i is regulated in a graded fashion over the whole intensity range and that Ca_i levels exceed 10 μM at high light intensities. The bold lines are fits to the experimental data obtained by calculating the fluorescence (F) as a function of Ca_i according to $F(Ca_i) = {Ca_i}^h / \left({Ca_i}^h + {K_d}^h\right)$ and normalizing, as detailed in the Materials and Methods section. Ca_i was assumed to increase with a simple power function of adaptation light intensity yielding the curve shown in c) (see Results).

resulting peak and plateau values as a function of relative light intensity. The $V_{\max}$ values ranged for the peak from 60 to 82 mV (average 72 $\pm$ 6 mV SD) and for the plateau from 19 to 40 mV (average 30 $\pm$ 6 mV SD); the exponent n for the peak values ranged from 0.40 to 0.47 (average 0.44 $\pm$ 0.02 SD) and for the plateau values from 0.42 to 0.58 (average 0.50 $\pm$ 0.05 SD). The $V/\log I$ curves appeared to be homogeneous and are fully consistent with similar measurements reported in the literature (Laughlin and Hardie, 1978; Matić and Laughlin, 1981; Sandler and Kirschfeld, 1988; Roebroek and Stavenga, 1990); this suggests again that the dyes did not seriously affect the membrane potential. The fluorescence signals measured during the test flashes were evaluated quantitatively as described in Materials and Methods. Figure 2.6b shows the resulting dependency of the fluorescence signal on the adapting light intensity for the three different dyes.

Obviously, the results for the high affinity dyes OG1 and OG2 are quite different from those for OG5N (Figure 2.6b). While the signals obtained with OG1 or OG2 both show saturation, the signal obtained with OG5N increases with light intensity even up to the highest intensities used. In addition, while the signals of OG1 and OG2 already show a pronounced increase at the lowest intensities, with OG5N this occurs only at $\log I \geq 0$. The differences between OG1 and OG2 are rather inconspicuous. Mainly, OG1 seems to become activated in average at intensities half a log-unit lower than OG2, as can be seen from the leftward shift in the activation curves of OG1 with respect to the curve of OG2. Taken together, the important findings of these experiments are (1), that Ca_i is regulated over the whole intensity range where the photoreceptor can respond to light, and (2), that OG1 and OG2 are saturated at intensities about one log-unit above the intensity for half-maximal activation of the peak membrane potential. This demonstrates that at bright adaptation intensities, the plateau values of Ca_i exceed 10 μM, the saturation value of OG2 (Haugland, 1996).

The slope of the fluorescence vs $\log I$ plots is almost linear in the low intensity region for OG1, in the region between $\log I = -2$ to $\log I = 0.5$ for OG2 and in the high intensity region for OG5N. This seems to imply that log Ca_i rises linearly with $\log I$. To get a more quantitative picture of the changes of Ca_i caused by light adaptation, we have therefore tried to describe the dependency of Ca_i on the light intensity with a simple power function: $Ca_i(I) = Ca_{i,da} + aI^b$; $Ca_{i,da}$ denotes here Ca_i in the dark-adapted state, assumed to be 0.16 μM, the value found for *Drosophila* (Hardie, 1996a). The experimental data were then fitted by taking $a = 2.5$ μM and $b = 0.5$, resulting in the curve shown in Figure 2.6c; the bold lines in Figure 2.6b represent

the simulated fluorescence values, calculated as described in the Materials and Methods section. The similarity between measured and simulated data suggests that the function chosen for describing Ca_i is appropriate. As shown in Figure 2.6c, at $\log I = 2$, Ca_i equals 25 μM. We are well aware that the accuracy of this approach is limited. With slight variations of the parameters a and b, reasonable good fits can still be obtained, whilst yielding considerably different values for Ca_i, especially for high light intensities. It was no longer possible to obtain a good fit between the simulated fluorescence functions and our data, when the parameter a was chosen smaller than 2 or the parameter b smaller than 0.5. Yet even with this combination of parameters, Ca_i at $\log I = 2$ is still estimated reach 20 mM. Therefore, the values of Figure 2.6c can be considered to be a conservative estimate. The value for $Ca_{i,da}$, the dark adapted Ca_i, influences the simulated fluorescence curves neglibly, and it was thus not possible to estimate it with our data. We therefore used 0.16 μM, the value measured in *Drosophila* (Hardie, 1996a) throughout the simulations.

Discussion

Measuring calcium in insect photoreceptors

We demonstrate in this Chapter that it is possible to measure the light-induced changes of Ca_i in photoreceptor cells in the intact eye of flies by using fluorescent Ca^{2+} indicators. The fluorescence signal can be measured simultaneously with the light-induced receptor potential. Dye filling causes alterations of the membrane potential (Figure 2.3a, b) that appear to be consistent and at least qualitatively explainable with the buffer action of the dyes. An increase in buffer capacity leads to an increased amount of Ca^{2+} ions to enter the cell before a given concentration is reached. This in turn causes the Na^+/Ca^{2+} exchanger to be activated for a longer period to extrude the extra load of Ca^{2+}; the afterdepolarization is therefore prolonged.

Increasing the intracellular buffer capacity by introducing Ca^{2+} buffers normally induces pronounced changes in the light response. The peak to plateau transition is diminished and the response kinetics are slowed down (Bader et al., 1976; Muijser, 1979; Tsukahara, 1980; Walz et al., 1994; Hardie, 1995b). We also observed these effects at high dye loads. However, usually this could be avoided and we carefully checked for these alterations of the waveform. Since the membrane potential is a sensitive measure of photoreceptor function, we conclude that our manipulations have not, or at most weakly, influenced the Ca^{2+} homeostasis during the light response.

Changes in Ca_i induced by light stimulation

Bright light stimulation of insect photoreceptors in isolated ommatidia (Peretz et al., 1994b; Ranganathan et al., 1994; Hardie, 1996a) or perfused eye slices (Walz et al., 1994) rapidly increases Ca_i to high concentrations. In *Drosophila* (Hardie, 1996a) and the drone (Walz et al., 1994), the increase in Ca_i is fast and consistently saturates high affinity dyes after ∼200 ms. Using Mag-Indo-1, Hardie (1996a) estimated that Ca_i reaches values up to 50 μM in isolated *Drosophila* photoreceptor cells. Here we show that Ca_i reaches similar values in photoreceptor cells of *Calliphora* in vivo (Figures 2.2, 2.4). The saturation of OG2 upon bright illumination indicates that in *Calliphora* Ca_i reaches values exceeding 10 μM.

The adaptation experiments (Figures 2.5, 2.6) allow to estimate how Ca_i depends on the light intensity (Figure 2.6c). Quantitative measurements of Ca_i with fluorescent indicators are often complicated by the fact that the indicators have different properties in the cytoplasm of cells than in solutions. However, since the K_d-values of the indicators only have been reported to increase when the indicator is brought into the cytosol (e.g. Hardie, 1996a), it is unlikely that we overestimated Ca_i. We conclude that Ca_i reaches values at least up to 20 μM when illuminated with the brightest intensity used in this study. Surprisingly, these high values are not only reached during short and local Ca^{2+} peaks, but are maintained after several seconds of light adaptation, implying that these high concentrations are sustained during prolonged periods. The fluorescence signal at high light intensities reaches a stable level after at most 2-4 s (Figures 2.4-2.6), showing that the distribution of Ca^{2+} ions then is in a steady state. In *Limulus*, only the R-lobe shows a dramatic increase in Ca_i; this increase is spread over a distance of at least 20 μm (Ukhanov and Payne, 1995). Therefore it seems likely that high values of Ca_i are also reached in the cell bodies of *Calliphora* photoreceptor cells that have a diameter of ∼10 μm.

Buffering of the Ca^{2+} influx

The finding that Ca_i reaches very high values is supported by measurements of changes of the extracellular calcium concentration with Ca^{2+}-selective electrodes (Sandler and Kirschfeld, 1988). In the drone, the glia cells do not take up Ca^{2+} (Coles and Orkand, 1985) and volume changes in the retina are small (Orkand et al., 1984; Ziegler and Walz, 1989). Assuming that this is also the case in the blowfly, and that there is no substantial Ca^{2+} release from internal stores (Ranganathan et al., 1994; Hardie, 1996a; Cook and Minke,

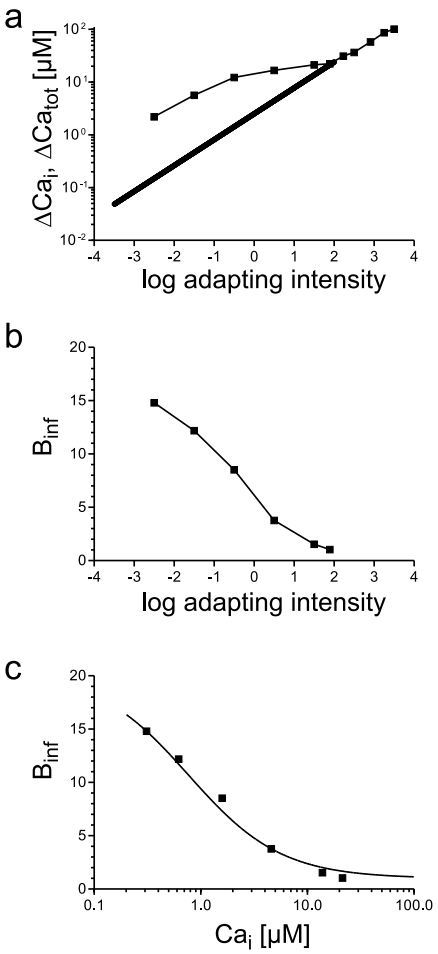

FIGURE 2.7: a) Comparison of changes in Ca_i ($\Delta Ca_i = Ca_i - Ca_{i,da} = aI^b$, continuous bold line, taken from Figure 2.6c) and changes in the total Ca^{2+} concentration (ΔCa_{tot}, ■) measured by Sandler and Kirschfeld (1988, their Figure 1c). The ΔCa_{tot} values were derived using the formula $\Delta Ca_{tot} = \Delta Ca_o/R$. The ratio R between the volume of the photoreceptors and the extracellular space was assumed to be 6.3 (Sandler and Kirschfeld, 1991), and the change in extracellular Ca^{2+} concentration (ΔCa_o) was calculated assuming that in the dark adapted state the extracellular Ca^{2+} concentration amounts to 1.4 mM (Sandler and Kirschfeld, 1991). At $\log I = 2$ the two curves approximate each other. At lower intensities, however, ΔCa_{tot} values are larger than the values obtained with the dyes. This indicates that the influx of Ca^{2+} is buffered. b) Buffering coefficient of the Ca^{2+} influx ($B_{inf} = \Delta Ca_{tot}/\Delta Ca_i$) shown as a function of adapting light intensity. c) Same data plotted as a function of Ca_i. The continuous line was obtained by fitting a simple buffer model (see Discussion). The buffering of the Ca^{2+} influx reduces with increasing Ca_i, and at Ca_i levels above 10 μM buffering becomes minimal.

1999) we can calculate from the decrease in extracellular calcium measured by Sandler and Kirschfeld (1988, their Figure 2.1c) the amount of Ca^{2+} entering the photoreceptors (ΔCa_{tot}; symbols in Figure 2.7a) and compare the resulting values with our estimates of the increase in Ca_i (ΔCa_i; bold line in Figure 2.7a). The calculated values appear to be in good agreement with the values of the light induced Ca_i increase at $\log I \geq 2$. Both curves have a similar slope at these high intensities.

However, at light intensities below $\log I = 2$, $\Delta Ca_{tot} > \Delta Ca_i$, or, the amount of Ca^{2+} entering the photoreceptor cells from the extracellular space is larger than the increase of Ca_i (Figure 2.7a). This difference can be explained by assuming that the Ca^{2+} influx is buffered, e.g. by uptake in organelles or binding to proteins. The buffering coefficient $B_{inf} = \Delta Ca_{tot}/\Delta Ca_i$ is presented in Figure 2.7b as a function of light intensity, and in Figure 2.7c as a function of Ca_i. Clearly, the buffering capacity is limited, and at $Ca_i \geq 10$ μM (corresponding to $\log I = 1.5$) buffering becomes minor. The values of 10-20 obtained for the buffering coefficient at $Ca_i \leq 1$ μM are more than an order of magnitude lower than the estimates for photoreceptors of *Drosophila* (Hardie, 1996a) or *Limulus* (O'Day and Gray-Keller, 1989). We note that the obtained buffering values are subject to a number of uncertainties. Firstly, mismatching the stimulation intensities of Sandler and Kirschfeld's (1988) measurements with respect to our experiments might have affected the estimation of the values for B_{inf}. In addition, our calculations assume that there is no extracellular Ca^{2+} buffering; the buffering coefficients for the Ca^{2+} influx would be underestimated by the factor of extracellular Ca^{2+} buffering, if this assumption does not hold. Also, if the assumptions of a constant extracellular volume and the non-involvement of the glial cells in the Ca^{2+} homeostasis do not hold, this will obviously modify the quantitative values of B_{inf}. However, if Ca^{2+} buffering is assumed to be constant at a high buffering coefficient B_{inf} throughout the light intensity range studied, there would not be enough extracellular Ca^{2+} to sustain a Ca^{2+} influx that causes Ca_i to rise to 20 μM. We calculate a maximal value for B_{inf} of 11 under those conditions, by dividing the extracellular Ca^{2+} concentration (1.4 mM; Sandler and Kirschfeld, 1991) with the product of the maximal value of Ca_i (20 μM) and the ratio of intracellular to extracellular volume (6.3; Sandler and Kirschfeld, 1991). Hereby we assume again that the following conditions hold: (1) there is no extracellular Ca^{2+} buffering; (2) the glial cells do not participate in the Ca^{2+} homeostasis; (3) there is no substantial Ca^{2+} release from internal stores. Therefore, the important point that we wish to emphasize here is that the ratio of buffered to free calcium very likely is not constant and this limitation of the buffering capacity results in high Ca_i values in bright light. This conclusion is not affected by the uncertainties in calculated values for B_{inf}.

Another possible reason for the high discrepancy between the values for B_{inf} derived here and those reported by Hardie (1996a) is the different method. The estimate of Hardie (1996a) is based on the ratio of influx (measured by integrating the current) to free Ca_i measured with optical methods.

Any Ca^{2+} extruded in the period of integrating the current (possibly by the Na^+/Ca^{2+} exchanger) contributes to the buffering, while in our approach, this Ca^{2+} reappears in the extracellular space, and thus does not contribute to the buffering. Therefore our values are necessarily lower than the estimate made by Hardie (1996a).

Probably, there are many different buffer mechanisms with different affinities and capacities. However, it is possible to calculate the parameters of a single, equivalent buffer from the values of Figure 2.7c. We have fitted the data points of Figure 2.7c to a simple buffer model, taking

$$\frac{\mathrm{Ca_{tot}}}{\mathrm{Ca_i}} = 1 + \frac{B}{K_d + \mathrm{Ca_i}}$$

where $\mathrm{Ca_{tot}}$ is the total Ca^{2+} concentration and B the total concentration of a buffer with dissociation constant K_d. The buffering coefficient of the Ca^{2+} influx (B_{inf}) was calculated by

$$B_{\mathrm{inf}}(I) = \frac{\mathrm{Ca_{tot}}(I) - \mathrm{Ca_{tot,da}}}{\mathrm{Ca_i}(I) - \mathrm{Ca_{i,da}}}$$

where $\mathrm{Ca_{tot,da}}$ is the total Ca^{2+} concentration in the dark. The smooth line in Figure 2.7c was obtained by taking $B = 18$ μM and $K_d = 0.77$ μM.

Comparison with other cellular processes dependent on calcium

Illumination of invertebrate photoreceptors with bright light induces a rapid activation of mitochondrial respiration, presumably due to a rise in $\mathrm{Ca_i}$ (Fein and Tsacopoulos, 1988). In the white-eyed blowfly mutant *chalky*, illumination causes a rapid change in the redox state of mitochondrial flavoproteins (Stavenga and Tinbergen, 1983). A comparison of the intensity dependence of this process (Mojet et al., 1991) with the present calcium measurements yields that the transient shift in the redox state of flavoproteins occurs when $\mathrm{Ca_i}$ levels rise above $\sim$1 μM. At these concentrations, the mitochondria are indeed likely to take up considerable amounts of Ca^{2+} (e.g. Miyata et al., 1991; Babcock et al., 1997).

The pupil mechanism of wild type fly photoreceptors, existing of pigment granules migrating inside the cell soma, has also a distinct dependence on Ca^{2+} influx (Kirschfeld and Vogt, 1980; Howard, 1984; Hofstee and Stavenga, 1996). The measurements of the intensity dependence of this system, together with that of the receptor potential (Roebroek and Stavenga, 1990),

also show that the pupil gets activated at Ca_i levels ≥ 1 μM. In addition to increasing the signal to noise ratio of the receptor potential at high light intensities (Howard et al., 1987), the function of the pupil in wild type photoreceptors may therefore be to avoid very high Ca_i levels.

A change in both the membrane potential and Ca_i is caused by the same underlying event, i.e. a change in the permeability of the light activated channels. Curiously, whereas the plateau membrane potential saturates at $\log I \approx$ 1-2, Ca_i shows a continous rise with intensity (Figure 2.6). Apparently, the light-dependent permeability increases with illumination intensity even at the brightest light intensities. Because buffering becomes minimal with large calcium loads, i.e. $Ca_i > 10$ μM (Figure 2.7), the rise in light-dependent permeability translates superlinearly into a rise in Ca_i. In addition, high Ca_i possibly activates a K^+ conductance (Weckström, 1989) resulting in a reduced rise in membrane potential.

3 Calcium transients in the rhabdomeres of dark- and light-adapted fly photoreceptor cells

Abstract

The light response of fly photoreceptor cells is modulated by changes in free Ca^{2+} concentration. Fly phototransduction and most processes regulating it take place in or very close to the rhabdomere. We therefore measured the kinetics and the absolute values of the free Ca^{2+} concentration in the rhabdomere of fly photoreceptor cells in vivo by making use of the natural optics of the fly's eye. We show that Ca^{2+} flowing into the rhabdomere upon light stimulation of dark-adapted cells causes fast Ca^{2+} transients that reach peak values higher than 200 μM in less than 20 ms. About 500 ms later, the free Ca^{2+} concentration has declined again to $\sim$20 μM. The duration of the Ca^{2+} transients becomes still shorter, and their size reduced, when the photoreceptor cell is light-adapted. This reduction in duration and size of the Ca^{2+} transients is graded with the intensity of the adapting light. The kinetics and absolute values of the free calcium concentration found to occur in the rhabdomere are suitable to mediate the fast feedback signals known to act on the fly phototransduction cascade.

The research presented in this Chapter has been published as:
Oberwinkler J, Stavenga DG (2000) J Neurosci 20:1701-1709.

Introduction

Fly photoreceptor cells are the prototypical model system for the PLC mediated activation of ion-channels encoded by members of the *trp* gene family (rev.: Hardie and Minke, 1995). In fly photoreceptors, these channels are highly permeable for Ca^{2+} (Hardie and Minke, 1992; Reuss et al., 1997) and exclusively found in the rhabdomeres (Ranganathan et al., 1994; Huber et al., 1996a; Niemeyer et al., 1996). The rhabdomere consists of microvilli, tube-like protrusions of the plasma membrane (rev.: Hardie, 1985), which contain most known molecules of the transduction cascade as well as many molecules involved in the regulatory control of the cascade (rev.: Montell, 1998).

Invertebrate photoreceptor cells can adjust their sensitivity to the average light level they encounter, i.e. they show pronounced light adaptation (rev.: Laughlin, 1989). Light adaptation comprises many different processes and crucially depends on an increase of intracellular Ca^{2+} concentration (Lisman and Brown, 1975; Bader et al., 1976; Muijser, 1979). Recent studies have started to unravel the mechanisms by which Ca^{2+} exerts its regulatory action. Ca^{2+} has been proposed to act directly on the light-activated channels (Hardie and Minke, 1994b; Hardie, 1995a; Obukhov et al., 1998), or via binding to calmodulin that interacts with the light-activated channels (Phillips et al., 1992: Warr and Kelly, 1996; Scott et al., 1997). Additionally, a Ca^{2+}-regulated PKC (Huber et al., 1998) is crucial for Ca^{2+}-dependent deactivation of the light response (Ranganathan et al., 1991) and light adaptation (Hardie et al., 1993). Other important molecules in the phototransduction cascade that have been suggested to be modulated by Ca^{2+} or by Ca^{2+}/calmodulin include NINAC (Porter et al, 1993), INAD (Chevesich et al., 1997) and PLC (Running Deer et al., 1994). Together these findings suggest that Ca^{2+} plays a central role in the regulation of the light response. However, it is poorly understood how the different Ca^{2+}-dependent processes interact. A key element missing for a more rigorous understanding of Ca^{2+}-mediated regulation of phototransduction is the knowledge of the magnitude and the time course of the free Ca^{2+} concentration in the rhabdomere (Ca_{rh}).

Previous studies have shown that light stimulation causes a rapid rise in free Ca^{2+} concentration throughout the photoreceptor cell that can exceed 10 μM (Hardie, 1996a; Chapter 2). The anatomy of the rhabdomere, however, suggests that the kinetics and absolute values of Ca_{rh} might be considerably different from those encountered in the cell body. Indeed, Postma et al. (1999) have found in a modeling study that the free Ca^{2+} concentra-

tion might rise to millimolar values in the microvilli after the absorption of a single photon. In this study we describe a method to quantitatively measure Ca_{rh} in vivo. We show that illumination of dark-adapted photoreceptor cells increases Ca_{rh} to values possibly as high as 600 μM, while light adaptation reduces the peak amplitude of the Ca^{2+} signal.

Material and Methods

All experiments were performed on female blowflies (*Calliphora vicina*). These large flies allow long lasting and stable intracellular recordings of photoreceptor cells with intracellular electrodes that are blunt enough for iontophoretic injection of fluorescent Ca^{2+} indicators (see below), which might be difficult in *Drosophila*. Many genes of molecules involved in the phototransduction or in its regulation have been cloned in *Calliphora* and found to be about 80% homologous to corresponding genes of *Drosophila* (e.g. Huber et al., 1996a, b, 1998). This indicates that the results obtained in *Calliphora* will be of direct relevance to the interpretation of data from *Drosophila*. Either wild-type or white-eyed mutant *chalky* flies were used. The *chalky* flies were obtained from a laboratory culture, while the wild-type flies were from F1 generations raised from animals caught in Groningen (The Netherlands).

Preparation and electrophysiological methods were as described in Chapter 2. Briefly, the animal was immobilized and placed on the stage of a Leitz Orthoplan epi-fluorescence microscope (Leitz, Wetzlar, Germany). The photoreceptor cells were impaled with borosilicate glass electrodes (1.0 mm o.d., 0.58 mm i.d.; Clark Electromedical Instruments, Reading, UK) pulled on a P-97 electrode puller (Brown and Flaming, Sutter Instr. Co., Novato, CA). Electrodes were filled with a 0.1 M KCl solution containing 5 mM of the Ca^{2+} indicator dyes Oregon Green 1 (OG1), Oregon Green 5N (OG5N) or Fluo5N (Molecular Probes, Eugene, OR), yielding resistances between 150 and 250 MΩ in the tissue. The Ca^{2+} indicator dyes were injected into the cell by applying 0.5-1 nA negative current pulses of 1 s duration in a 0.5 Hz duty cycle for $\sim$1 min. An Axoclamp 2A amplifier (Axon Instruments, Foster City, CA) was used for all electrophysiological experiments. After capacity compensation, the electrodes could be used in the switched current-clamp mode (DCC mode) with switching frequencies typically exceeding 3 kHz, indicating that the time constant of the electrode did not limit the frequency range of the membrane potential measurements. All measurements of the membrane potential presented, however, have been done in the non-switching "bridge" mode.

In experiments where we aimed to simultaneously record the fluorescence and the membrane potential of the photoreceptor cell, it was essential to record from a photoreceptor cell that had its direction of view very well aligned (within 2°) with the optical axis of the microscope. We therefore took care to place the animal on the microscope stage in such a way as to insure that the electrode would follow a path crossing the region of the deep pseudopupil (Franceschini and Kirschfeld, 1971). The electrode was subsequently advanced into the region of the deep pseudopupil, and a photoreceptor cell was impaled there. When we only wanted to record the fluorescence from the Ca^{2+} indicator dye, the electrode was withdrawn after dye-filling the cell. The animal was then aligned under visual control to yield the maximum fluorescence from the dye-filled cell.

The blue-induced green fluorescence of the Ca^{2+} indicator dye was measured with a photomultiplier (R928, Hamamatsu Corp., Bridgewater, NJ) that was shielded with a pinhole of 0.2 mm diameter to reduce background from the autofluorescence of the eyes. Light from a 75 W Xenon arc lamp was focused through a fast shutter (L2, Uniblitz, Vincent Associates, Rochester, NY), then passed through a 510 nm fluorescence cube and was subsequently focused with an objective onto the specimen. Either a 10× (NA 0.25; Spindler and Hoyer, Göttingen, Germany) or a Luminar objective (f = 25 mm; Zeiss, Oberkochen, Germany) with a variable numerical aperture (NA 0.031-0.15) were used.

The signals from the photomultiplier and the electrode amplifier were low-pass filtered at 2 or 4 kHz before being sampled at 5 or 10 kHz, respectively. Data analysis was performed off-line; all recordings shown represent averages of the same experiment repeated 6 to 40 times. We always checked that the waveform of the recorded traces did not considerably change during the experiment. Usually however, the fluorescence signal decreased throughout the experiment; whether this represents bleaching or removal of the dye from the cytosol is not known. In some cases, the fluorescence traces and calculated free Ca^{2+} concentrations have been smoothed by averaging 10 consecutive values (always representing 1 ms). To calculate the free Ca^{2+} concentration from the fluorescence traces the minimum and maximum fluorescence levels were determined as outlined in the Results, and the free Ca^{2+} concentration was calculated as: $Ca_{rh} = K_d(F - F_{min})/(F_{max} - F)$ (Grynkiewicz et al., 1985). The K_d value for OG5N was assumed to be 20 μM (Haugland, 1996). In all calculations we hence assume that the characteristic curve of Ca^{2+} binding to the indicator has a Hill-coefficient of 1. Importantly, the direct measurement of F_{max} and F_{min}, as outlined in the text, both include

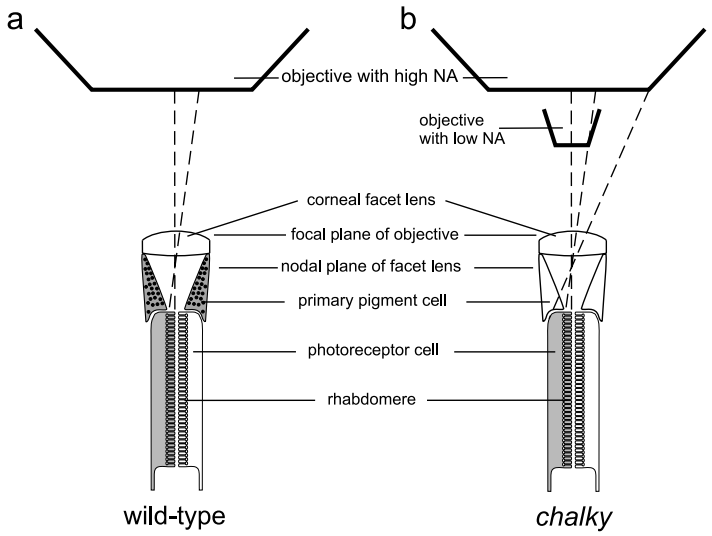

FIGURE 3.1: Method for recording Ca^{2+} induced fluorescence only from the rhabdomere of fly photoreceptor cells. Light leaving the rhabdomere is focused by the corneal facet lens to form a beam that diverges by 1-2° (van Hateren, 1984), while the light originating from the other parts of the photoreceptor cell leaves the eye under a wider angle ($\sim$10°, Chapter 2). In wild-type flies, the screening pigments in the primary pigment cells (indicated by the dark dots and the shading in the primary pigment cells) absorb the light coming from parts of the cell other than the rhabdomere. Therefore, only light originating from the rhabdomeres can leave the eye through its natural optics (a). When using *chalky* flies the same optical principle can be exploited. Because the primary pigment cells no longer contain pigment granules (indicated by the empty primary pigment cells), it is necessary to reduce the NA of the objective to preferentially sample the light coming from the rhabdomere and to reject the light coming from other parts of the cell (b).

the background fluorescence, which was found to be constant over the time scale of our experiments, as much as the signal F. Additional background subtraction is therefore not necessary.

Results

Recording Ca^{2+} induced fluorescence from the rhabdomere of fly photoreceptor cells

We have recently demonstrated that the free Ca^{2+} concentration can be measured by recording the fluorescence emitted from Ca^{2+} indicator dyes in

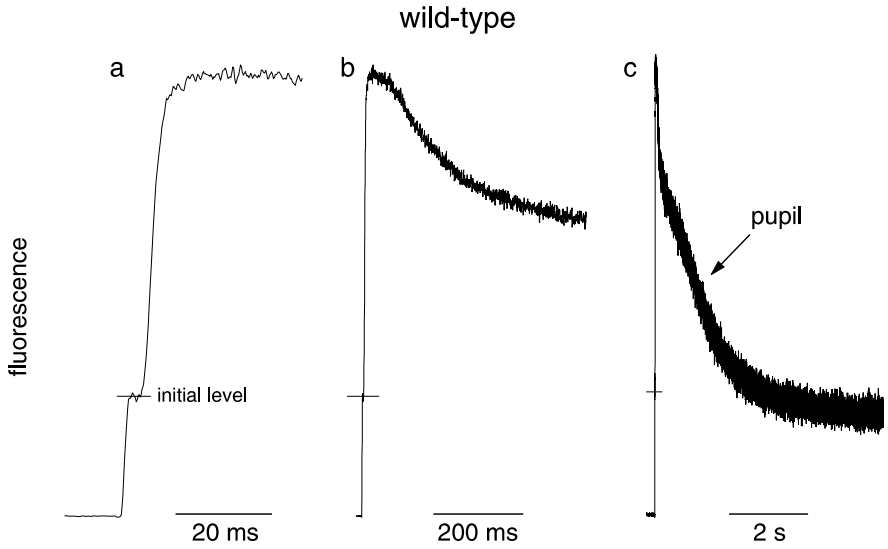

FIGURE 3.2: Fluorescence signal recorded from a photoreceptor cell of a wild-type fly with the Ca^{2+} indicator dye OG5N on three different time scales. When the light is turned on, the fluorescence signal stays at the initial level (indicated by the small horizontal lines) for about 5-6 ms, before a measurable increase in the free Ca^{2+} concentration is observed (a). The initial level of fluorescence is caused by the autofluorescence of the tissue and the fluorescence of the Ca^{2+} indicator dye at low Ca^{2+} concentrations. The fluorescence signal shows an initial plateau at its maximum value (a, b), from which it decreases to about 50% (calculated between the initial level and the peak) during the first 500 ms of light stimulation (b). Wild-type flies possess a powerful pupil mechanism (Kirschfeld and Franceschini, 1969) that efficiently reduces the fluorescence from the rhabdomere (Stavenga, 1983). This pupil mechanism cuts in after about 500 ms (c, arrow).

single photoreceptor cells of blowflies in vivo (Chapter 2). In these earlier measurements, the fluorescent signal was sampled from the entire cell. Since Ca^{2+} influx in fly photoreceptor cells is a highly localized process, only occurring in the rhabdomere (Ranganathan et al., 1994; Huber et al., 1996a; Niemeyer et al., 1996), averaging the Ca^{2+} induced fluorescence across the entire cell might have obscured important kinetic details. We reasoned that it should be possible to record exclusively the fluorescence emanating from the rhabdomere by making use of the natural optics of the fly's eye, because the rhabdomere samples light only from a narrow angle of view which in blowflies amounts to 1-2° (van Hateren, 1984). In fact, in wild-type flies, light that

hits a facet lens under an angle exceeding 1-2° is absorbed by the dense pigmentation in the primary pigment cells. Light emitted from fluorophores in the rhabdomeres follows the reverse path and is consequently focused by the ommatidial lenses to form a beam with 1-2° divergence. Light originating from other parts of the cell would pass through the facet lenses forming a much wider beam of about 10° (Chapter 2). This light, however, is to a very large extent absorbed by the pigment granules in the primary pigment cells (Figure 3.1a), allowing only the light emanating from the rhabdomere to leave the eye.

In Figure 3.2 the fluorescence signal from the Ca^{2+} indicator dye OG5N ionotophoretically injected in a photoreceptor cell of a wild-type fly is shown on three different time scales. The recordings show that, when the bright light is turned on, the fluorescence stays at a low initial level for about 5-6 ms before a pronounced increase is observed (Figure 3.2a). This initial level of fluorescence is due to the autofluorescence of the retina and the fluorescence of the OG5N indicator dye at the low Ca^{2+} levels found in resting photoreceptor cells (0.16 μM; Hardie, 1996a). From this initial level the fluorescence increases rapidly to reach its maximum $\sim$20 ms after the beginning of the light stimulation. The fluorescence stays for a short period at this maximum level before it decreases to reach a level of about 50% 500 ms after the peak (Figure 3.2b). For still longer periods of illumination the fluorescence decreases strongly to values below the initial level (Figure 3.2c, arrow). This decrease is due to the pupil mechanism (Kirschfeld and Franceschini, 1969) present in wild-type flies that is known to drastically reduce the fluorescence emanating from the rhabdomere (Stavenga, 1983).

The pupil mechanism, albeit serving an important function for the fly's vision (Howard et al., 1987), makes it impossible to quantitatively analyze the fluorescence signals of dark-adapted photoreceptors stimulated for longer than 500 ms; the same problem occurs when light-adapted photoreceptors are to be studied (see below). To avoid the problems arising from the pupil mechanism we devised a way to record the fluorescence from the rhabdomeres of white-eyed *chalky* flies that lack the pupil mechanism. However, in these mutants also the pigment granules in the primary pigment cells are missing, allowing the fluorescence from the cell soma to leave the eye. We therefore narrowed the NA of the objective and thereby the angle of the measured light beam. According to the optical situation outlined above, this isolates the signal from the rhabdomere and rejects light coming from other parts of the cell (Figure 3.1b).

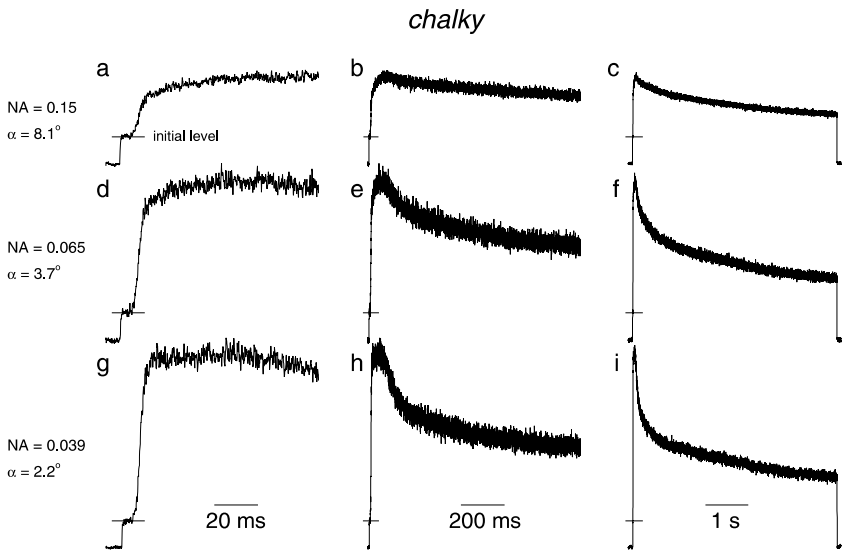

FIGURE 3.3: Effect of the NA of the objective on the fluorescence signal recorded from a *chalky* fly. The fluorescence signals from the Ca^{2+} indicator dye OG5N recorded with three different NAs (values as indicated in the figure) are shown; the data are shown on three different time scales. The traces shown for the 3 different NA have been normalized to the initial level of fluorescence (indicated by the small horizontal lines) to facilitate comparison between recordings. Reducing the NA of the objective increases the size and the speed of the initial transient. This shows that the kinetics and the concentrations of the free Ca^{2+} concentration inside the rhabdomere are different from that of the free Ca^{2+} concentration in the cell body. When using small NAs (g-i), the recordings shown are very similar in the first 500 ms to those obtained with wild-type flies (Figure 3.2). In particular, the fast rise $\sim$5 ms after the onset of light stimulation, the plateau at the highest fluorescence values and the decrease to about 50% fluorescence level (between the initial level and the peak) are highly similar to recordings from wild-type flies. This indicates that the isolation of the fluorescence from the rhabdomere in *chalky* flies is as good as in wild-type flies. The important advantage of using *chalky* flies is the absence of a pupil effect (i).

In Figure 3.3 the results of an experiment with the Ca^{2+} indicator dye OG5N injected in a *chalky* photoreceptor cell are shown. In the upper panels (Figure 3.3a-c) the fluorescence is recorded with a NA of 0.15, i.e. an acceptance angle $\alpha = 8.1°$; in the other panels the NA was reduced to 0.065 ($\alpha = 3.7°$; Figure 3.3d-f), and to 0.039 ($\alpha = 2.2°$; Figure 3.3g-i). All traces are normalized to the initial level to facilitate comparison of the size of the

signal. The striking difference between the different recording situations is the increased size of the initial transient when the NA is reduced. Additionally, the rising and falling flanks of the initial fluorescence transient are steeper in recordings with reduced NA (Figure 3.3a vs Figure 3.3g for the rising flank; Figure 3.3b vs Figure 3.3h for the falling flank). This indicates that the Ca^{2+} increase in the rhabdomere is faster and reaches much higher concentrations than the Ca^{2+} increase in the rest of the cell. Importantly, recordings from dark-adapted *chalky* flies made with low NAs (Figure 3.3g-i) are essentially identical to the recordings from wild-type flies for the first 500 ms (Figure 3.2a, b), showing that the rhabdomeral fluorescence signal in *chalky* mutants can be isolated with comparable quality as in wild-type flies. Photoreceptor cells of *chalky* mutants, however, need to be very well aligned to match the reduced NA of the objective; imperfect alignment results in reduced signal amplitudes and increased noisiness compared to recordings from wild-type flies.

These experiments clearly demonstrate that it is possible to measure the fluorescence from the rhabdomeres in vivo in both wild-type flies and *chalky* mutants. They show the distinct size and kinetics of the free Ca^{2+} concentration in the rhabdomere as compared to the rest of the cell body. Recordings with larger NAs in *chalky* therefore integrate over different compartments of the photoreceptor cells with largely different Ca^{2+} kinetics.

The size of the initial Ca^{2+} transient in the rhabdomere exceeds 200 μM

The Ca^{2+} induced fluorescence measured with OG5N rises very fast to a plateau that is maintained for approximately 30-50 ms before the fluorescence declines again (Figures 3.2a, b and 3.3g, h). This plateau might be caused by either the Ca^{2+} concentration being constant during this phase or by saturation of the indicator dye. To decide between these possibilities, we used the Ca^{2+} indicator Fluo5N that has a higher K_d (90 μM) than OG5N (20 μM). The recordings with Fluo5N (Figure 3.4a, b) clearly do not show a plateau. Furthermore, the fluorescence has declined after 500 ms illumination to 10-20% of the peak value (relative to the initial level; Figure 3.4b, c), being a much lower level than in the recordings with OG5N, where the fluorescence level after 500 ms illumination still is 40-60% of the peak value (Figure 3.4e, f). These observations are consistent with the lower Ca^{2+} affinity of Fluo5N with respect to OG5N and show that OG5N saturates during the initial peak.

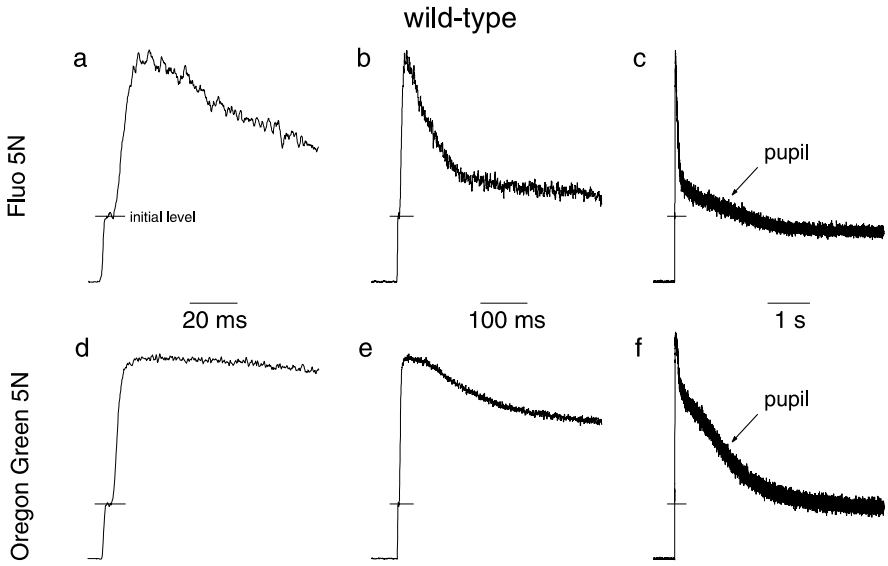

FIGURE 3.4: Comparison of fluorescence obtained with Fluo5N (a-c) and OG5N (d-f; traces are identical to Figure 3.2 and are reproduced for better comparison). The two recordings are each shown on three different time scales. While the recordings with OG5N show a flat plateau at their maximum value (d, e), the recordings with Fluo5N show a sharp peak (a, b). Furthermore, in the Fluo5N recordings, the fluorescence levels off to only about 10% of the dynamic range, but the OG5N traces maintain a level of about 50% (after 500 ms). Both these observations are consistent with the lower affinity of Fluo5N with respect to OG5N. Accordingly, the flat peak seen in the traces obtained with OG5N and not with Fluo5N should be interpreted as due to saturation of the OG5N dye. Consequently, the free Ca^{2+} concentration in the rhabdomere rises to levels between 200 and 1000 μM during this plateau phase. Since these recordings were performed with wild-type flies, the pupil effect is visible at times longer than 0.5 s (c, f). The initial level of fluorescence is indicated by the small horizontal lines.

From its K_d value of 20 μM OG5N is expected to saturate at Ca^{2+} concentrations above 200 μM, while, given its K_d of 90 μM, Fluo5N should saturate at Ca^{2+} concentrations higher than 1 mM. We therefore estimate that the Ca^{2+} concentration reached in the rhabdomeres of dark-adapted fly photoreceptor cells during the initial peak shortly after light onset is in the range between 0.2 and 1 mM.

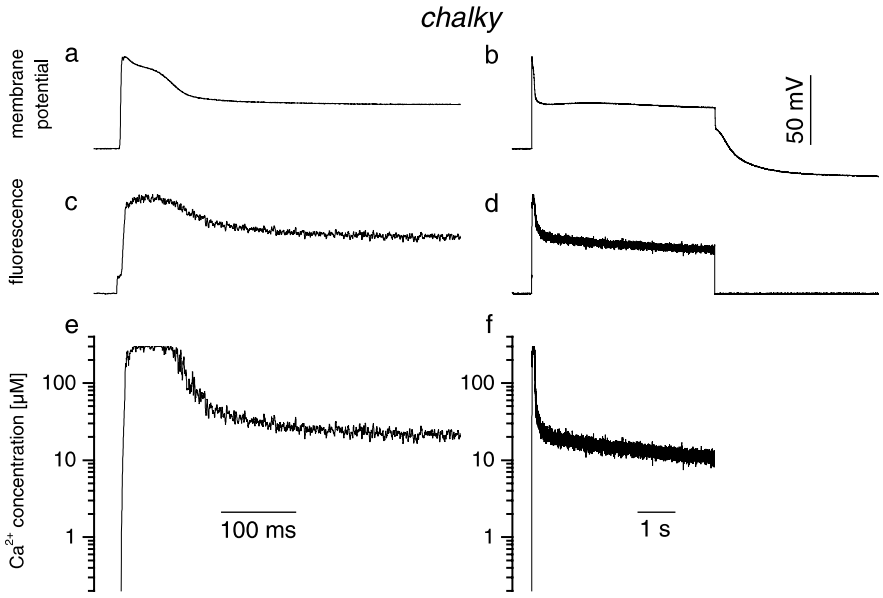

FIGURE 3.5: Membrane potential (a, b), concomitantly measured OG5N fluorescence (c, d) and calculated free Ca^{2+} concentrations in the rhabdomere (e, f) during illumination of a dark-adapted photoreceptor cell. The data are displayed twice, at high temporal resolution (a, c, e) and at lower temporal resolution (b, d, f). The method used for calculating the free Ca^{2+} concentration from the fluorescence signal is explained in the Results; note that only fluorescence values in the dynamic range of the Ca^{2+} indicator OG5N (representing free Ca^{2+} concentrations between 2 and 200 μM) can be converted into free Ca^{2+} concentrations. During the peak of the membrane potential, the free Ca^{2+} concentration in the rhabdomere exceeds this range; the free Ca^{2+} concentration in the rhabdomere during this short period can therefore not be determined, but must exceed 200 μM. From its peak, the free Ca^{2+} concentration in the rhabdomere reduces quickly to 20 μM in 500 ms (e). At longer illumination times, the free Ca^{2+} concentration slowly reduces further, in this cell to 11 μM after 5 s (f).

Quantification of the free Ca^{2+} concentration in the rhabdomere

We can convert the fluorescence traces obtained with OG5N into Ca^{2+} concentrations for fluorescence values that are not close to saturation at either end of the dynamic range of the indicator dye OG5N. The saturation of OG5N at the onset of the light stimulus can be used to obtain the maximum fluorescence signal ($F_{\max}$). Because the resting free Ca^{2+} concentration in the photoreceptor cells is lower than 1 μM (Hardie, 1996a; Chapter 2), we

can take the initial level of fluorescence (before the light-induced fluorescence increase, Figures 3.2-3.4) as the minimum fluorescence, $F_{\min}$. Using $F_{\max}$, $F_{\min}$ and the published K_d values of 20 μM for OG5N (Haugland, 1996), we obtain the free Ca^{2+} concentration as described in Materials and Methods (Figure 3.5e, f). It shows an enormous peak exceeding 200 μM soon after the beginning of the light stimulation that rapidly levels off to values between 10 and 30 μM that are reached already 500 ms after light onset (Figure 3.5e). For longer illumination times, the free Ca^{2+} concentration continues to decay with a slow time constant (Figure 3.5f).

Figure 3.6 shows the average of the free Ca^{2+} concentrations found after 500 ms and 5 s of illumination for several experiments similar to the one shown in Figure 3.5. After 500 ms, both in wild-type flies and in *chalky* mutants the free Ca^{2+} concentration in the rhabdomere is 20 μM ($\pm$ 5 μM SD; min: 12 μM; max: 30 μM). These data can be used to further narrow down the estimate for the Ca^{2+} concentration at the peak. We find that the fluorescence level in Fluo5N recordings after 500 ms illumination is 21% ($\pm$ 8% SD; n = 4) of the fluorescence level at the peak. Given a K_d of 90 μM and assuming that -on average- also in the Fluo5N recordings Ca_{rh} after 500 ms illumination is 20 μM, the Ca^{2+} concentration at the peak can be estimated to reach $\sim$600 μM.

Because of the pupil mechanism, the Ca^{2+} concentration after 5 s illumination can only be determined for *chalky* flies. In the mutant flies, Ca_{rh} has declined to 8 μM ($\pm$ 3 μM SD; min: 6 μM; max: 11 μM) after 5 s illumination (Figure 3.6). This shows that modulation of the light response has components that work on the time scale of seconds. Interestingly, the membrane potential changed only moderately (Figure 3.5b), declining from 51% ($\pm$ 3% SD) of its peak value after 500 ms light stimulation to 45% ($\pm$ 4% SD) of the peak value after 5 s light stimulation.

Light adaptation decreases the duration and the size of the Ca^{2+} transient

In Figure 3.7 responses of a cell adapted to three different background intensities are shown, differing from each other by a logarithmic unit; OG5N was used as the fluorescent Ca^{2+} indicator. Light adaptation shortens the duration of the fluorescence transient at the onset of the light stimulus to about 30 ms (Figure 3.7d-f); in dark-adapted cells this transient lasts at least 100 ms (Figures 3.2-3.4). Comparing the different levels of light adaptation shows that the transient phase of both the fluorescence signal and the mem-

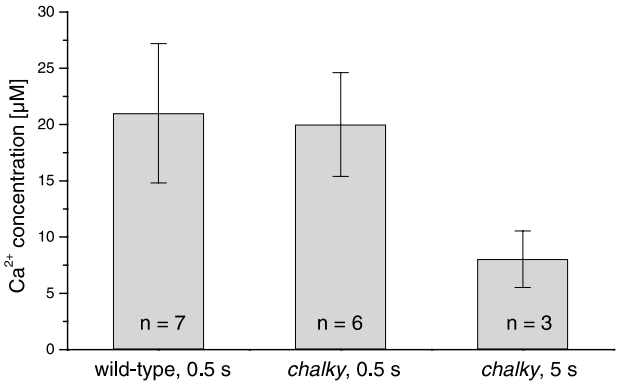

FIGURE 3.6: Summary of several experiments similar to the one shown in Figure 3.5. 0.5 s after the onset of bright illumination the free Ca^{2+} concentration in the rhabdomeres of wild-type and *chalky* flies is on average 20 μM. 5 s after the onset of bright illumination the free Ca^{2+} concentration has declined to 8 μM in *chalky* flies. The pupil mechanism present in wild-type flies makes it impossible to obtain quantitative data for Ca_{rh} later than 0.5 s after the onset of the light stimulus. The error bars indicate the SD.

brane potential are shortened when the background intensity is increased. Additionally, the size of the transient fluorescence peak is reduced when the cell is adapted to stronger background lights (Figure 3.7d vs f). The initial transient of the membrane potential measured simultaneously with the fluorescence also shows a decrease in duration when the background intensity is increased (Figure 3.7a-c). These observations are consistent with the notion that the increase in Ca_{rh} measured with the low affinity indicator OG5N is predominantly caused by Ca^{2+} entering through the light activated channels (Hardie and Minke, 1992; Ranganathan et al., 1994; Peretz et al., 1994b; Huber et al., 1996a; Niemeyer et al., 1996; Reuss et al., 1997).

In addition to its effect on the duration of the transients of membrane potential and fluorescence signal, light adapting a photoreceptor cell increases the free Ca^{2+} concentration throughout the cell (Chapter 2). This can also be seen in Figure 3.7d-f, where the initial level of Ca_{rh} increases with increasing intensity of the adapting background (arrows).

Quantification of the Ca^{2+} signal of light-adapted cells

In order to quantify the free Ca^{2+} concentration in the rhabdomere of light-adapted cells, we have employed a double pulse protocol (Figure 3.8) for

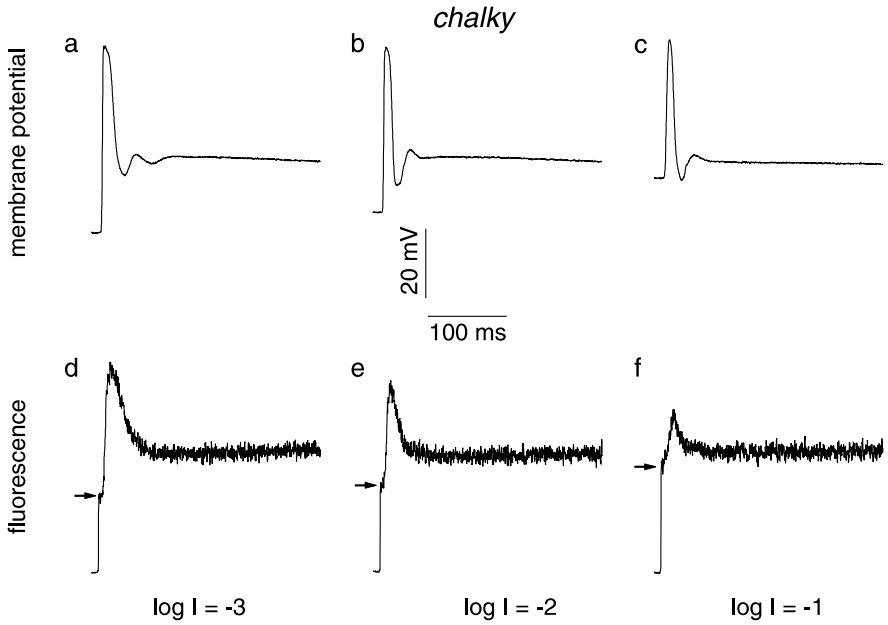

FIGURE 3.7: Increasing the intensity of the adapting light reduces both the duration of the transient of the membrane potential and the duration and the size of the transient of the fluorescence signal at the onset of the light stimulation. The electrical response of a light-adapted *chalky* photoreceptor cell to a test stimulus (a-c) and the accompanying fluorescence signal (d-f) is shown. Three different intensities, each differing by a log-unit, were used as adapting background light. Additional to the effect on the initial transients, increasing the light adaptation also increases the steady state Ca^{2+} concentration (arrows) seen before the test stimulus-induced increase (e.g. Chapter 2). The fluorescence was recorded with an increased NA, equivalent to a visual angle of $\sim 8°$.

recording the responses. The rationale behind this procedure is to record light-adapted response shortly after the dark-adapted response. This reduces errors caused by bleaching or otherwise reduced concentration of the indicator dye as well as errors due to changes in the health of the cell recorded from. In Figure 3.8 we exposed a dark-adapted cell to a 500 ms flash that was followed by a 200 ms period of darkness followed by a second light stimulus.

Figure 3.8a shows that the second light stimulation evoked an electrical response with the reduced duration and size characteristic of light-adapted cells. From the simultaneously recorded fluorescence trace (Figure 3.8b) we

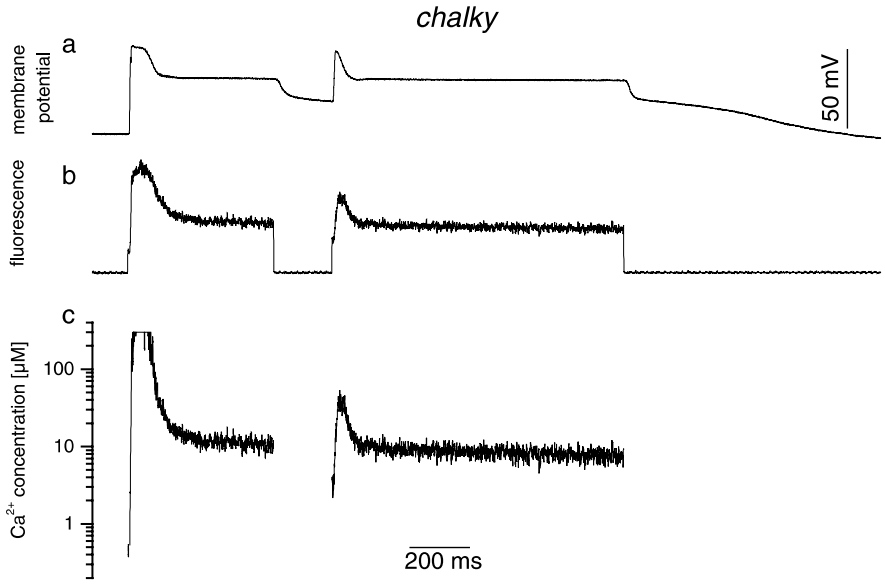

FIGURE 3.8: Quantification of the free Ca^{2+} concentration in the rhabdomere of light-adapted photoreceptor cells. Light adaptation was induced by a 500 ms light stimulus onto a dark-adapted photoreceptor cell. This stimulus was followed by a dark interval lasting 200 ms and a subsequent stimulus to record the light-adapted response. This protocol allows to directly compare the dark- and the light-adapted response and to calculate the free Ca^{2+} concentration in the rhabdomere (c), as shown in Figure 3.5, from the OG5N fluorescence trace (b). To avoid the pupil mechanism a *chalky* fly was used in this experiment. The traces show that the Ca^{2+} concentration reached in the rhabdomere exceeds 200 μM in dark-adapted rhabdomeres, but changes between 3 and 50 μM during the light-adapted response.

hence can calculate Ca_{rh} during the dark-adapted and the light-adapted light response (Figure 3.8c), as outlined above (Figure 3.5). Figure 3.8c shows that Ca_{rh} reaches -as already found in Figure 3.5- values exceeding 200 μM when the cells are dark adapted. During the light-adapted response, however, the Ca^{2+} transient starts from $\sim$3 μM to reach 50 μM before it declines again. Interestingly, physiologically important feedback regulations can be observed in this range of concentrations (Hardie, 1995a).

The membrane potential leads the Ca^{2+} signal in dark- and light-adapted cells.

Invertebrate photoreceptors possess Ca^{2+} stores located in close vicinity to the rhabdomeric membrane, the so-called subrhabdomeric cisternae, that are able to take up Ca^{2+} (Walz, 1982). In *Drosophila*, Ca^{2+} can be released from these stores by treating the cells with thapsigargin or ionomycin (Hardie, 1996b). For *Drosophila*, it is controversially debated if a Ca^{2+} release from stores also occurs as a consequence of light stimulation. Hardie (1996a) found that the free Ca^{2+} concentration in the cytosol increased at most by 20 nM when eliminating Ca^{2+} influx through the light activated channels. Cook and Minke (1999), on the other hand, reported that excitability of the cells correlated with the ability to release Ca^{2+} from the stores and argued that the release might increase the free Ca^{2+} concentration only locally. In *Limulus*, it could be demonstrated that Ca^{2+} is released prior to any electrical signal (Ukhanov and Payne, 1995), while this was found not to be the case in the honey bee drone (Walz et al., 1994) and *Drosophila* (Hardie, 1996a). We reinvestigated this question because in the in vivo preparation it is possible to confine the measurements to the rhabdomeres, where any light-induced Ca^{2+} release should be larger than in other regions. Furthermore, our preparation allows to investigate this question also for light-adapted cells.

We determined the latencies for the membrane potential and the fluorescence trace by calculating the minimal and the maximal values during a 1 ms period starting 1 ms after the fluorescence trace had reached 50% of the initial level, i.e. 1 ms after the shutter was half open. The value obtained by adding twice the difference between the minimal and the maximal value to the maximal value was taken as the threshold. The latencies, defined by the moment when the membrane potential or the fluorescence signal crossed the threshold, are indicated in Figure 3.9 by dotted lines. In Figure 3.9, the leftmost dotted line always indicates the latency of the membrane potential. Therefore, also in *Calliphora*, the electrical signal leads any detectable increase in Ca_{rh} (Figure 3.9). The latencies observed with the high affinity Ca^{2+} indicator OG1 (reported K_d: 0.16 μM, Haugland, 1996; Figure 3.9a, d) and the low affinity Ca^{2+} indicator OG5N (reported K_d: 20 μM, Haugland, 1996; Figure 3.9b, e) show no essential difference. Ca_{rh} at the initial level during the latency period is 0.16 μM (Hardie, 1996a). Using this value we calculate that the criterion for determining the latency for the fluorescence signal in Figure 3.9d corresponds to 0.04 μM. While 0.04 μM is an increase that potentially has physiological functions in many cell types, it corresponds

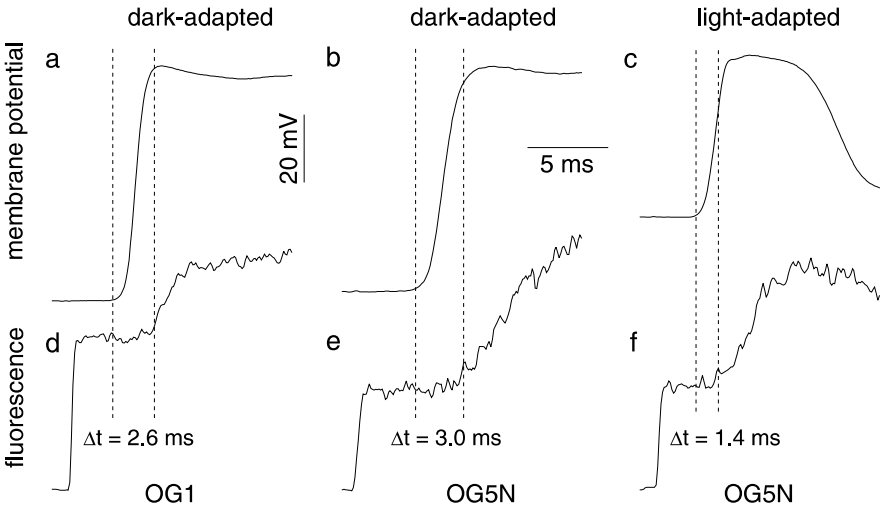

FIGURE 3.9: The first discernible changes of the membrane potential precede the first discernible changes of the fluorescence signal. The first noticeable changes have been determined as outlined in Results and are indicated as dotted lines. The leftmost dotted line in each panel indicates the end of the latency period of the membrane potential. In dark-adapted photoreceptor cells, the delay between the membrane potential and the fluorescence amounts to 2-3 ms, independent of the use of either high affinity (OG1; a, d) or low affinity (OG5N; b, e) Ca^{2+} indicators, confirming earlier results in other insects (Walz et al., 1994; Hardie, 1996a). Wild-type flies were used for the experiments on dark-adapted photoreceptor cells (a, b, d, e). Also in light-adapted cells the membrane potential rises earlier than the fluorescence signal (c, f). This particular recording represents the shortest delay we measured. It was performed in a *chalky* mutant adapted to a steady state background and is identical to the recordings of Figure 3.7b, e.

to only a single additional free Ca^{2+} ion in the volume of 11 microvilli (taking a microvillus to be a cylinder of 1.5 μm length and 0.06 μm diameter). This calculation shows that probably neither an insufficient signal-to-noise ratio nor an insufficient sensitivity of the Ca^{2+} indicator have hindered the detection of an early increase in Ca_{rh}; it might also explain why we did not observe any difference in latency whether using high or low affinity indicators. In light-adapted photoreceptor cells (Figure 3.9c, f), we equally found that the depolarization of the membrane precedes any detectable increase in Ca_{rh}. Figure 3.9f shows the shortest latency observed; typically the delay between the earliest detectable depolarization and the earliest detectable increase in Ca_{rh} was 2-3 ms also in light-adapted cells.

Discussion

In this Chapter we demonstrate the feasibility of measuring -with high temporal resolution- the free Ca^{2+} concentration exclusively from a small cellular compartment of blowfly photoreceptor cells, the rhabdomere. This compartment is of special interest as it contains the phototransduction machinery including the Ca^{2+} permeable *trp*- and *trpl*-dependent channels (Huber et al., 1996a; Niemeyer et al., 1996) that are activated by light stimulation. The Ca^{2+} signals in this compartment are of extraordinary size and speed. We find that the free Ca^{2+} concentrations exceed 200 μM and possibly reach 600 μM within 20 ms after the beginning of light stimulation. These Ca^{2+} concentrations exceed by far the concentrations measured in small compartments of other neurons (e.g. stereocilia of haircells: Lumpkin and Hudspeth, 1998; spines of central neurons: Petrozzino et al., 1995). Even the concentrations measured in the rhabdomeric region of *Limulus* ventral photoreceptor cells, the only other invertebrate species where quantitative data are available, are smaller ($\sim$150 μM; Ukhanov and Payne, 1995). The concentrations we measured in rhabdomeres of fly photoreceptor cells more closely resemble the concentrations measured in microdomains in the immediate vicinity of clusters of Ca^{2+} channels (Llinás et al., 1992).

Precise localization of the fluorescence signal

The rhabdomere optically acts as a waveguide and therefore a part of the light, the so-called boundary wave, is transported outside the rhabdomere. Our measurements hence necessarily include fluorescence that originated outside the rhabdomere, i.e. from dye molecules in the cell soma. Possibly, therefore, the intended spatial localization was compromised. Light at the wavelengths of 470-490 nm, which maximally excites the indicator dyes, is transported predominantly in the first mode and in this mode only a small fraction of the light actually travels outside of the rhabdomere (revs: Snyder, 1979; van Hateren, 1989). Only the intracellular part of the boundary wave will excite indicator dyes, the rest of the boundary wave being at the extracellular side of the rhabdomere. Additionally, fluorescence excited outside the rhabdomere has a reduced probability to be trapped by the rhabdomeric waveguide. We therefore conclude that the contamination of the fluorescence signal measured from wild-type photoreceptor cells with fluorescence from outside the rhabdomere will be minor. In *chalky* photoreceptor cells it is conceivable that a more substantial fraction of the light comes from other parts of the cell than the rhabdomere due to scattering. However, the

close resemblance of the traces obtained from wild-type and from *chalky* flies when using low NAs indicates that also in *chalky* a good isolation of the fluorescence signal from the rhabdomere is possible (Figures 3.2, 3.3).

An independent argument supports the notion that the measured fluorescence signals predominantly stem from inside the rhabdomeric microvilli. The extracellular Ca^{2+} concentration in the fly retina is 1.4 mM (Sandler and Kirschfeld, 1991). Our measurements indicate that Ca_{rh} reaches values as high as 600 μM. The reversal potential for Ca^{2+},

$$E_{rev} = \frac{RT}{zF} \ln\left(\frac{Ca_o}{Ca_i}\right),$$

then works out to be +11 mV, which is very close to the reversal potential of the light-induced current in *Drosophila* (Reuss et al., 1997). It is also close to the peak values we measure for the membrane potential, as in good recordings we measured depolarizations of 70 mV (e.g. Fig 9a), and the resting potential of *Calliphora* photoreceptors is close to −60 mV. During the initial transients elicited by strong illumination of dark-adapted photoreceptor cells the Ca^{2+} gradient therefore is strongly reduced and our estimates for the peak values of Ca_{rh} might approach the maximum value attainable given the strongly depolarized membrane. Therefore, it seems likely that the estimated values for Ca_{rh} reflect the free Ca^{2+} concentration inside the microvilli. These considerations can also explain why the peak values of Ca_{rh} are smaller than the estimates by Postma et al. (1999) who calculated that Ca^{2+} concentration changes in the millimolar range might occur in the rhabdomeric microvilli, when the membrane potential is clamped to −70 mV. Furthermore, the close correspondence of the calculated reversal potential for Ca^{2+} ions and the membrane potential can be taken as an indication that the K_d of our Ca^{2+} indicators was not changed considerably by the intracellular environment. The K_d of Ca^{2+} indicators typically is shifted to larger values when used intracellularly as compared to an aqueous solution (Haugland, 1996; for invertebrate photoreceptors: Ukhanov et al., 1995; Hardie, 1996a). As the estimated values for Ca_{rh} are linearly related with the K_d of the indicator, a three to fivefold increase in K_d (Ukhanov et al., 1995; Hardie, 1996a) would also increase the estimated values Ca_{rh} by the same factor. This, however, would be inconsistent with the measured membrane potentials.

Our results confirm earlier reports on insect photoreceptors (Walz et al., 1994; Hardie, 1996a) that a period of 2-3 ms lies between the first discernible

change of the membrane potential and that of the cytosolic free Ca^{2+} concentration. This seems to be independent of the use of low or high affinity indicators (e.g. Figure 3.9). As more than 50% of the light-induced current is carried by Ca^{2+} ions (Hardie and Minke, 1992; Reuss et al., 1997; Postma et al., 1999), such a delay is counterintuitive because the influx of cations through light-activated channels should cause a simultaneous change in both the electrical signal and Ca_{rh}. By limiting the origin of the fluorescence signal to the rhabdomere, we could provide evidence that our signal-to-noise ratio should be sufficient to detect early rises in Ca_{rh}. To resolve this discrepancy, one might argue that the Ca^{2+} indicators cannot come close to the Ca^{2+} channels. However, Ca^{2+} released from photolabile Ca^{2+} buffers, molecules of sizes similar to the sizes of fluorescent Ca^{2+} indicators, affects the phototransduction within one millisecond (Hardie, 1995a). An alternative, not mutually exclusive, explanation is that endogenous Ca^{2+}-binding proteins are present in the close vicinity of the light-activated channels that instantly bind all of the incoming Ca^{2+} during the first 2 to 3 ms of the light response. Calmodulin might be a good candidate for such a Ca^{2+}-binding protein, as it is present in high concentration in *Drosophila* rhabdomeres (Porter et al., 1993) and binds to several proteins that are thought to participate in a macromolecular assembly containing the light-activated channels (Huber et al., 1996a; Chevesich et al., 1997; rev.: Montell, 1998).

Regulation of the membrane potential by Ca^{2+} in fly photoreceptors

An increase in the Ca^{2+} concentration rapidly inhibits the light response in light-adapted photoreceptors (Hardie, 1995a). Hardie (1995a) also showed that increasing the free Ca^{2+} concentration in the range between 1 and 20 μM strongly inhibits the light response. The observed changes in Ca_{rh} are in this range or exceed it in both light- and dark-adapted cells (Figure 3.8), and are therefore well suited to convey physiologically important feedback signals. In particular, the transients in Ca_{rh} might be important in providing the feedback signal for the fast peak-to-plateau transitions seen in the membrane potential, as those transitions are severely reduced when an increase of the free Ca^{2+} concentration is blocked by loading the cells with Ca^{2+} buffers (Muijser, 1979). Interestingly however, upon light adaptation the size of the Ca^{2+} transients in the rhabdomere is reduced, but the speed of the peak-plateau transition of the membrane potential is increased (Figures 3.7, 3.8). Considering that the Ca^{2+} transients provide the feedback signal for the membrane potential these findings seem paradoxical. A possible explanation

is that photoreceptor cells can react faster or with higher affinity to the feedback signal from the Ca^{2+} transients when they are light adapted. The measurements of Figure 3.7 suggest that the increase in speed of the feedback or in its sensitivity for Ca^{2+} is graded with the intensity of the adapting light. In this scenario -an extension of the findings of Hardie (1995a)- the level of light adaptation defines the way and/or the speed the cells react to an increase in Ca_{rh}.

Additionally to the fast events at the beginning of light stimulation we observed that Ca_{rh} continues to decline in the time range of seconds, at least up to 5 s after the onset of light stimulation (Figures 3.5, 3.6). This was an unexpected finding, as the membrane potential, which is indicative of the Ca^{2+} influx through the light activated channels, seemed to be rather stable during this period. This suggests that additional regulatory mechanisms exist in the photoreceptor cells that work relatively slowly, i.e. in the range of seconds.

4 Calcium imaging demonstrates co-localization of calcium influx and extrusion in fly photoreceptors

Abstract

During illumination, Ca^{2+} enters fly photoreceptor cells through the light-activated channels that are located in the rhabdomere, the compartment specialized for phototransduction. Ca^{2+} then diffuses from the rhabdomere into the cell body. We visualize this process by rapidly imaging the fluorescence in a cross-section of a photoreceptor cell injected with a fluorescent Ca^{2+} indicator in vivo. The free Ca^{2+} concentration in the rhabdomere shows a large transient shortly after light onset. The free Ca^{2+} concentration in the cell body rises slower and displays a much smaller transient. After $\sim$400 ms of light stimulation, the Ca^{2+} concentration in both compartments reaches a steady state, indicating that thereafter an amount Ca^{2+}, equivalent to the of amount Ca^{2+} flowing into the cell, is extruded. Quantitative analysis demonstrates that during the steady state, the free Ca^{2+} concentration in the rhabdomere and throughout the cell body is the same. This shows that Ca^{2+} extrusion takes place very close to the location of Ca^{2+} influx, the rhabdomere, since otherwise gradients in the steady state distribution of Ca^{2+} should be measured. The close co-localization of Ca^{2+} influx and Ca^{2+} extrusion ensures that, after turning off the light stimulus, Ca^{2+} removal from the rhabdomere is faster than from the cell body. This is functionally highly significant because it ensures rapid dark adaptation.

Introduction

Many neurons, including sensory neurons, localize Ca^{2+} influx channels to small, often diffusionally isolated, compartments of the cell body (Koch and Zador, 1993). This localized Ca^{2+} influx into a small volume often results in sizeable, but local changes in free Ca^{2+} concentration (Ca_i; Lenzi and Roberts, 1994; Augustine and Neher, 1992). Photoreceptor cells of flies exemplify this strategy. Upon light stimulation, channels that are highly permeable for Ca^{2+} (Hardie and Minke, 1992; Reuss et al., 1997) and exclusively located in the membranes of the microvilli (Huber et al., 1996a; Niemeyer et al., 1996) are activated. The microvilli, tube-like protrusions of the plasma membrane with exceptionally small dimensions, are regularly packed together to form a dense stack, the rhabdomere (rev.: Hardie, 1985). Ca_i in the rhabdomere rises up to 600 μM when the cells are stimulated with bright light (Chapter 3). Calculations indicate that similar or even higher concentrations also occur in one or a few microvilli already after the absorption of a single photon (Postma et al., 1999). From the rhabdomeric microvilli, Ca^{2+} diffuses into the cell body (Ranganathan et al., 1994), where measured increases in Ca_i are more moderate, but still exceed 10 μM (Hardie, 1996a; Chapter 2). These changes of Ca_i are functionally highly significant as they mediate light adaptation (Lisman and Brown, 1972; Muijser, 1979).

Creating high local Ca_i values by confining the influx to specialized compartments potentially causes the problem that Ca_i in these compartments diminishes only slowly after the stimulus has ceased. This problem can be counteracted by co-localizing proteins that efficiently extrude Ca^{2+}. The implementation of this design principle has been demonstrated e.g. in stereocilia of haircells (Yamoah et al., 1998), in synaptic terminals of rods (Morgans et al., 1998; Krizaj and Copenhagen, 1998) and in presynaptic boutons of hippocampal cells (Reuter and Porzig, 1995). In fly photoreceptor cells, highly active Na^+/Ca^{2+} exchangers extrude Ca^{2+} (Armon and Minke, 1983; Hochstrate, 1991; Hardie, 1995a; Gerster, 1997). Two genes encoding two different types of Na^+/Ca^{2+} exchangers (Ruknudin et al., 1997; Schwarz and Benzer, 1997; Haug-Collet et al., 1999) have been shown to be expressed in the photoreceptor cells of *Drosophila* (Schwarz and Benzer, 1997; Haug-Collet et al., 1999), but the subcellular locations of the proteins are unknown. In squid photoreceptor cells, however, the rhabdomeric membranes show Na^+/Ca^{2+} exchange activity (Bauer et al., 1999). Using a novel approach, we show here that Ca^{2+} extrusion in fly photoreceptors takes place close to the location of Ca^{2+} influx, the rhabdomere, suggesting that the

Na^+/Ca^{2+} exchangers are also located in or close to the rhabdomere. We show that this has profound physiological consequences, as it increases the speed of Ca^{2+} removal in the rhabdomere and avoids large gradients of Ca_i in the cells during continuous stimulation.

Material and Methods

HIGH-SPEED FLUORESCENT IMAGING AND DATA ANALYSIS Single photoreceptor cells of female, white-eyed mutant *chalky* blowflies (*Calliphora vicina*) were impaled with intracellular electrodes and iontophoretically injected with the fluorescent Ca^{2+} indicator dye Oregon Green 5N (OG5N, Molecular Probes, Eugene, OR) as described previously (Chapters 2, 3). The electrode was withdrawn and the fly was placed on a goniometer that served as stage of a standard microscope (Nikon Optiphot-2, Nikon Inc., Melville, NY) connected to a confocal microscope (Odyssey XL, Noran Instr., Middletown, WI), from which the confocal pinhole was removed in order to maximize light intensity. The fly was re-oriented to ensure that the rhabdomere of the dye-filled cell was co-axial with the optical axis of the objective (25× water-immersion, NA: 0.6; SW25, Leitz, Wetzlar, Germany). Light came from the 488 nm line of a krypton-argon laser, and the emitted fluorescence light passed a triple-filter (Noran) or a 510 nm fluorescence cube (Nikon). An LS2 shutter (Uniblitz, Vincent Associates, Rochester, NY) was added in the light path of the confocal microscope before the beam expander to rapidly turn the light on or off. Several sequences of images were recorded at a rate of 480 images/s, and averaged off-line; care was taken to insure that the preparation did not move between the recordings.

MODELING THE STEADY STATE DISTRIBUTION OF Ca^{2+} For the calculations of the steady state distribution of Ca_i we assume that a constant influx of Ca^{2+} (see Results) occurs in the rhabdomere homogeneously along the entire length of a photoreceptor cell (l = 225 μm; Hardie, 1985), reducing diffusion to two dimensions. This assumption seems justified since the light intensities used for measuring the fluorescence are saturating the light response: each microvillus was hit at least once in a few milliseconds. The cross-section through the modeled cell was assumed square with side-lengths of 7.1 μm. The diffusion coefficient for free Ca^{2+} ions (D_{Ca}) was assumed to be 220 $\mu m^2/s$ (Allbritton et al., 1992). The diffusion coefficient of the mobile buffer, whether bound to Ca^{2+} or not, was equally assumed to be D_B = 220 $\mu m^2/s$ (Hall et al., 1997), as it is possible that most of the mobile buffer

stems from the Ca^{2+} indicator. Accordingly, the dissociation constant of the buffer ($K_{d,B}$) was taken to be 20 μM, the value reported for OG5N (Haugland, 1996; Dabdoub and Payne, 1999). As only the steady state distribution of Ca^{2+} was investigated here, fixed (i.e. non-diffusing) Ca^{2+} buffers do not need to be considered (Roberts, 1994). Equally, Ca^{2+} release (Cook and Minke, 1999) from or Ca^{2+} uptake (Walz, 1982) into organelles that might occur in fly photoreceptor cells do not influence the steady state distribution of Ca_i.

The square cross-section was divided by a grid into 40 × 40 compartments of equal size. In the middle of one side a 1.5 μm large region was designated to be the region of Ca^{2+} influx. The concentration of Ca^{2+} ions, either free or bound to a Ca^{2+} buffer, was calculated at the intersections of the grid-lines. The volume that was assigned to each grid-point was 1/1600 of the total cell volume ($v_{\mathrm{tot}} = 11$ pl), but the points lying on one of the cell borders were assigned half that value and the points in the corners a quarter. Diffusion was calculated to occur along the grid-lines. The change of both free and bound calcium at position x and y ($\Delta C_{x,y}$) during a time step ($\Delta t = 28$ μs) caused by diffusion with coefficient D is then given by:

$$\Delta C_{x,y} = \frac{D\Delta t}{\Delta x^2}\left(C_{x-1,y} + C_{x+1,y} + C_{x,y-1} + C_{x,y+1} - 4C_{x,y}\right),$$

for both, x and y, > 1 and < 41. For the border given by $x = 1$ and $1 < y < 41$, ΔC was calculated as:

$$\Delta C_{1,y} = \frac{D\Delta t}{\Delta x^2}\left(2C_{2,y} + C_{1,y-1} + C_{1,y+1} - 4C_{1,y}\right).$$

For the corner given by $x = y = 1$, ΔC is given by:

$$\Delta C_{1,1} = \frac{D\Delta t}{\Delta x^2}\left(2C_{2,1} + 2C_{1,2} - 4C_{1,1}\right).$$

To calculate ΔC for the other borders and corners, the indices were changed appropriately. The distance between two grid points is equal to 1/40 of the side length of the model cell, or, $\Delta x = 177$ nm. After calculating ΔC for every grid-point, the new total Ca^{2+} concentration was obtained. From the total Ca^{2+} concentration, the concentrations of free and bound Ca^{2+} were determined with the assumption that the buffer reactions are in equilibrium. The calculations continued until a stable distribution of Ca_i was reached, i.e. until the amount of Ca^{2+} extruded differed less than 0.1% from the amount of Ca^{2+} flowing in.

The activity of Na^+/Ca^{2+} exchangers, the proteins that extrude Ca^{2+} from fly photoreceptor cells (Armon and Minke, 1983; Hochstrate, 1991; Hardie, 1995a, b; Gerster, 1997) depends on many parameters, including the membrane potential, the intra- and extracellular Na^+ and Ca^{2+} concentrations (rev.: Blaustein and Lederer, 1999). As we are only interested in the steady state distribution of Ca_i, all these parameters can be assumed constant, with the possible exception of Ca_i. Ca^{2+} binding to the transport site of the exchanger proteins is typically described with a Hill-function (Hill-coefficient $h = 1$), for which two parameters, the dissociation constant $K_{d,X}$ and the maximal current $I_{X,\max}$ need to be determined (Blaustein and Lederer, 1999). A rough estimate of the $K_{d,X}$ value for the Ca^{2+} extrusion can be inferred from data by Hardie (1995a), who showed that the Na^+/Ca^{2+} exchanger is 10 times more active when $Ca_i = 20$ μM than when $Ca_i = 1$ μM. This yields 18 μM for $K_{d,X}$, which, however, is rather high compared to the values reported for other preparations (Blaustein and Lederer, 1999). The maximum calcium current transported by the Ca^{2+} extrusion process was set to $I_{X,\max} = 1.3$ nA, a value that insures that the calculated Ca_i values at the location of extrusion lie between 12 and 40 μM, as found experimentally for Ca_i in strongly light-stimulated cells (Chapter 2). The choice of the parameters for the Ca^{2+} extrusion, however, is rather uncritical for the conclusions drawn in the Results, because changing $K_{d,X}$ or $I_{X,\max}$ strongly affects the average Ca^{2+} concentration, but only very weakly the calculated gradients.

Results

Imaging the Ca^{2+} induced change in fluorescence in a cross-section of a photoreceptor cell

The kinetics and the absolute values of Ca_i can be measured in vivo in the photoreceptor cells of blowflies, both in the whole cell (Chapter 2) or only in the rhabdomere (Chapter 3), by making use of the natural optics of the fly's eye. The optics can also be functionally eliminated in this preparation by using a water-immersion objective and placing a drop of water between the objective and the cornea of the eye (Kirschfeld and Franceschini, 1969). It is then possible to image the distal cross-section of a photoreceptor cell (Figure 4.1) that has been iontophoretically injected with the fluorescent Ca^{2+} indicator OG5N. Taking images in rapid succession allows visualization of the changes in Ca^{2+}-induced fluorescence that occur during light stimulation of the photoreceptor cells.

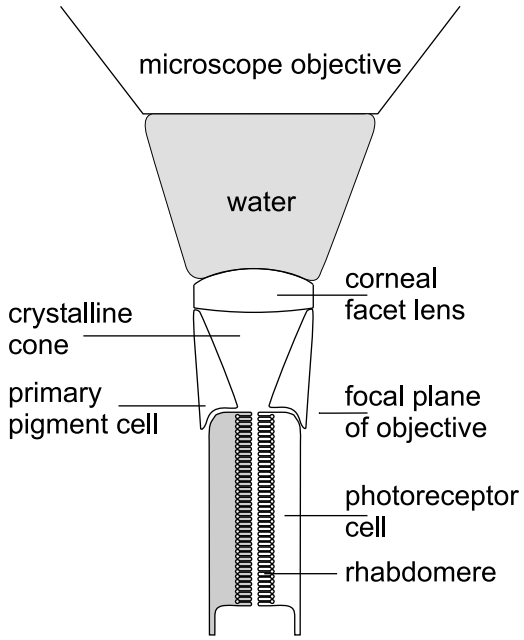

FIGURE 4.1: Optical situation for imaging the distal cross-section of a photoreceptor cell in vivo. The optical function of the corneal facet lens is eliminated by using a water-immersion objective and placing a drop of water between the cornea and the objective (Kirschfeld and Franceschini, 1969). This allows focusing through the cornea and the crystalline cone onto the distal part of the photoreceptor cells, one of which has been filled with a fluorescent Ca^{2+} indicator (indicated by the gray shading).

Figure 4.2a shows grayscale images representing raw intensity values taken from a time series recorded with high temporal resolution (480 images/s). The image at 0 ms is the first image recorded after the light was turned on. Because the photoreceptor cells have a latency period of approximately 4-6 ms before an increase in Ca_i can be detected (Chapter 3; Hardie, 1996a), this first image represents the autofluorescence of the tissue together with the fluorescence of the Ca^{2+} indicator at low values of Ca_i. The intense light used for measuring the fluorescence strongly activates the phototransduction cascade, resulting in opening channels that are permeable for Ca^{2+} (Hardie and Minke, 1992; Reuss et al., 1997). This leads to a substantial inflow of Ca^{2+}, visible in the image taken 10 ms after light onset. The fluorescence intensity in the area that corresponds to the rhabdomere has increased, but not in the rest of the cell. This observation confirms that the Ca^{2+} influx through the light-activated channels is localized exclusively to the rhabdomere (Ranganathan et al., 1994; Huber et al., 1996a; Niemeyer et al., 1996). The subsequent images show that the Ca^{2+} increase spreads into the cell body and concomitantly reduces in the rhabdomere. The im-

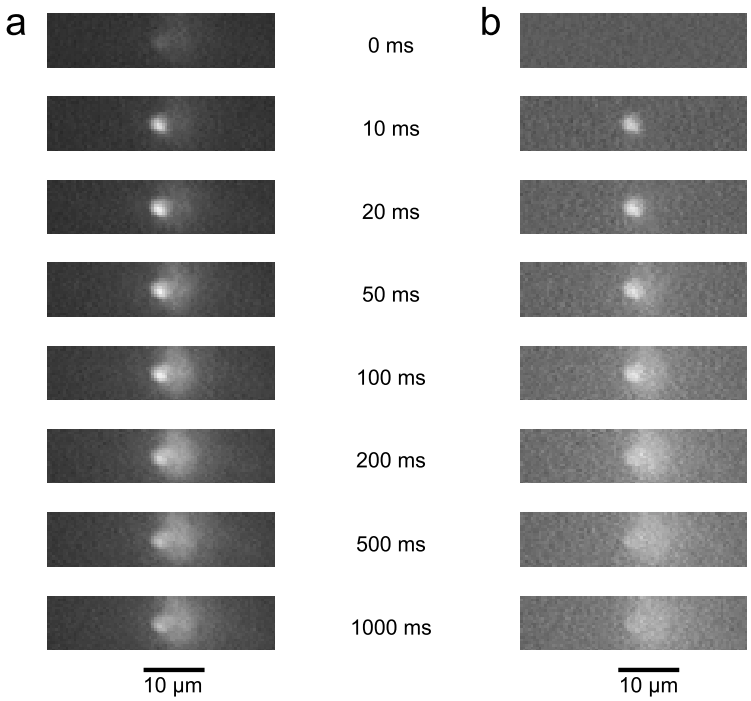

FIGURE 4.2: A time series of images showing the change of the Ca^{2+}-induced fluorescence of the low-affinity dye OG5N during light stimulation. a) Raw intensity values plotted as grayscale images. At 0 ms, the first image was recorded, immediately after the light has been turned on. It represents the initial level of fluorescence during the latency period of the cell, due to autofluorescence of the tissue and the residual fluorescence of the Ca^{2+} indicator at low Ca_i. The other images are taken at times indicated. 10 ms after the onset of illumination a strong increase in fluorescence is visible in the region that corresponds to the rhabdomere. While the fluorescence signal in the rhabdomere starts to decline after 100 ms, it also spreads into the cell body. b) The same data as in a), but divided through the basal fluorescence level (average of the first 2 images taken) and re-scaled. These images show the fluorescence increase rather than the raw intensity.

ages in Figure 4.2b are based on the same data as the images in Figure 4.2a, but have been divided through the average of the first and the second image (the initial fluorescence level) and re-scaled. These images therefore show the fluorescence increase rather than the raw intensity.

A sizeable Ca^{2+} current flows into the photoreceptor cells during the steady state

The electrical response caused by bright illumination consists of a fast transient depolarization (on average 65 mV) that quickly decays to a steady state depolarization of about 30 mV (e.g. Chapter 2). During this steady state a continuous current flows through the light-activated channels which is counterbalanced by the strong, non-inactivating currents through voltage-dependent potassium channels (Weckström et al., 1991). The voltage-dependent potassium current at 30 mV depolarization is ∼3 nA (Weckström et al., 1991). This value can be used to estimate the Ca^{2+} current through the light-activated channels, as the current through the light-activated channels (I_L) needs to balance the currents through the voltage-dependent K^+ channels. Assuming the validity of the Goldman-Hodgkin-Katz theory (Hille, 1992, for application to fly photoreceptors see Gerster, 1997; Gerster et al., 1997; Postma et al., 1999) the current carried by Ca^{2+} ions (I_{Ca}) through the light-activated channels can be calculated as (Postma et al., 1999):

$$I_{\mathrm{Ca}} = I_L w_{\mathrm{Ca}} \frac{f_{\mathrm{Ca}}}{f_{\mathrm{Na}} + f_{\mathrm{K}} + f_{\mathrm{Ca}} + f_{\mathrm{Mg}}},$$

where f_q (the index q denotes the four cations considered) is given by:

$$f_q = {z_q}^2 w_q \frac{C_{q,\mathrm{i}} - C_{q,\mathrm{o}} e^{-z_q \beta V_m}}{1 - e^{-z_q \beta V_m}}, \text{ with } \beta = \frac{F}{RT}.$$

Here, z_q denotes the valence, $C_{q,\mathrm{i}}$ the intracellular and $C_{q,\mathrm{o}}$ the extracellular concentration of ion sort q. F is the Faraday constant, R the molar gas constant and $T = 293$ K denotes the temperature. The membrane potential (V_m) is taken to be -30 mV, the steady state value of strongly stimulated cells (Chapter 2). The relative permeabilities (w_q) of the light-activated channels have been measured in *Drosophila* photoreceptor cells (Hardie and Minke, 1992; Reuss et al., 1997); here we use $w_{\mathrm{Na}} = w_{\mathrm{K}} = 0.02$, $w_{\mathrm{Ca}} = 0.85$ and $w_{\mathrm{Mg}} = 0.11$, the values described for wild-type flies (Reuss et al., 1997, see also Postma et al., 1999). The following ion concentration are typically found in insect photoreceptor cells and retinas (in mM): $C_{\mathrm{Na,i}} = 10$, $C_{\mathrm{Na,o}} = 140$,

$C_{\mathrm{K,i}} = 120$, $C_{\mathrm{K,o}} = 4$, $C_{\mathrm{Mg,i}} = 4$, $C_{\mathrm{Mg,o}} = 2$ (Coles et al., 1985; Sandler and Kirschfeld, 1991). In strongly stimulated photoreceptor cells rather high values for the intracellular Ca^{2+} concentration ($C_{\mathrm{Ca,i}}$) have been reported (Hardie, 1996a; Chapter 2) and the extracellular Ca^{2+} concentration ($C_{\mathrm{Ca,o}}$) is probably reduced from its resting value of 1.4 mM (Sandler and Kirschfeld, 1991). Here we use $C_{\mathrm{Ca,i}} = \mathrm{Ca_i} = 20$ μM and $C_{\mathrm{Ca,o}} = \mathrm{Ca_o} = 1.2$ mM.

Using these values I_{Ca} works out to be 1.4 nA when I_L is assumed to be 3 nA. This value, however, might be an overestimate. It neglects the contribution of the Na^+/Ca^{2+} exchanger that can depolarize fly photoreceptor cells considerably due to its electrogenicity (Hochstrate, 1991; Gerster, 1997). Furthermore, the currents through the voltage-dependent K^+ channels might have been overestimated, as we neglected possible light-induced accumulation of K^+ in the extracellular space (Coles et al., 1985). In the following we take $I_{\mathrm{Ca}} = 0.7$ nA, in order not to overestimate the Ca^{2+} current through the light-activated channels.

Our previous measurements (Chapter 2) and the data presented in Figure 4.2 indicate that $\mathrm{Ca_i}$ does not increase substantially after approximately 200-500 ms of light stimulation. This shows that -during the steady state- Ca^{2+}-extruding mechanisms must generate a Ca^{2+} current of (at least) 0.7 nA Ca^{2+}, in order to balance the influx.

The steady state distribution of Ca_i contains information about the localization of Ca^{2+}-extruding proteins

The Ca^{2+} ions, flowing through the light-activated channels located in the rhabdomere, have to diffuse to the location of the Ca^{2+}-extruding proteins in order to be extruded. The subcellular location of the Ca^{2+}-extruding proteins therefore has a profound influence on the shape and size of the gradients that build up in the cytosol. This is illustrated in Figure 4.3 where we calculated distributions of $\mathrm{Ca_i}$ in the cross-section of a square model cell for four different locations of Ca^{2+}-extruding proteins, as indicated in Figure 4.3 (top panels). It was assumed that a continuous Ca^{2+} current (I_{Ca}) of 0.7 nA flows into the model cell at the center of one side, corresponding to the place where the rhabdomeric microvilli are attached. The influence of mobile Ca^{2+} buffers was initially neglected. When assuming that the Ca^{2+} extrusion takes place on the basolateral sides (Figure 4.3a), where the Na^+/K^+ pumps are located (Baumann et al., 1994), $\mathrm{Ca_i}$ in the rhabdomere should be as high as 97 μM, leveling off to reach 12-40 μM at the basolateral sides of the cell. Placing the Ca^{2+} extrusion to the apical side (except the rhabdomere),

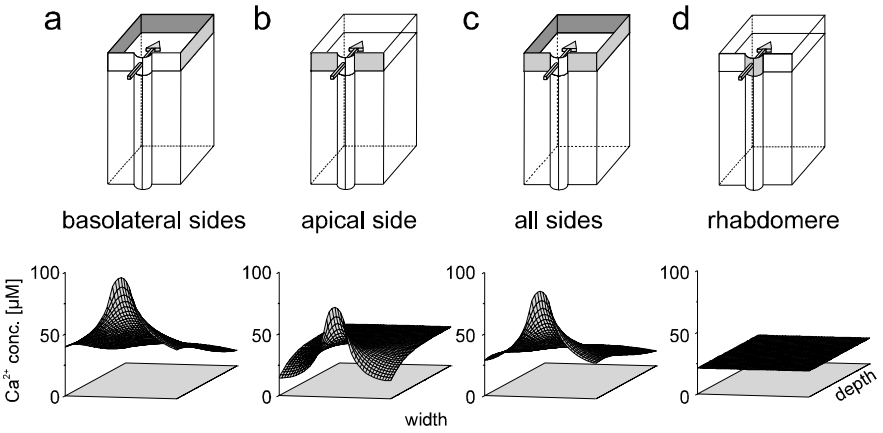

FIGURE 4.3: Calculated distribution of Ca_i in a cross-section of a square model cell. The continuous influx is assumed to occur at a 1.5 μm wide region of one side (arrow in the diagrams). Extrusion is modeled at different regions of the plasma membrane, as indicated in the diagrams by the gray shading. a) Ca^{2+} extrusion only at the basolateral sides. b) Ca^{2+} extrusion only at the apical side, the Ca^{2+} influx region (rhabdomere) excluded. c) Ca^{2+} extrusion at all sides, but the Ca^{2+} influx region excluded. d) Ca^{2+} extrusion only at the Ca^{2+} influx region. In a)-c), the resulting distribution of Ca_i shows large gradients, but not in d).

results in a much flatter distribution in the cell body (Figure 4.3b). Still, Ca_i in the rhabdomere would be at 73 μM and on the apical side as low as 14 μM. Modeling extrusion on all sides except the rhabdomere (Figure 4.3c) results in an intermediate situation between those found in Figure 4.3a and b. Only when the Ca^{2+} extrusion is modeled to take place exclusively at the location of Ca^{2+} influx, the rhabdomere, a homogeneous distribution of Ca_i is found throughout the cell (Figure 4.3d).

The gradients that can possibly be expected to be measured experimentally, however, are not as large as those depicted in Figure 4.3. The addition of fluorescent Ca^{2+} indicators, highly mobile Ca^{2+} buffers that are necessary for the measurements, will reduce those gradients (Neher and Augustine, 1992; Roberts, 1994). In order to estimate more realistically the measurable gradients, we repeated the calculations with varying concentrations of a highly mobile Ca^{2+} buffer (Figure 4.4). Increasing the buffer concentration flattens the expected distribution of Ca_i (Figure 4.4a, b). For the extreme case of 5.0 mM Ca^{2+} buffer (the concentration of the indicator in the record-

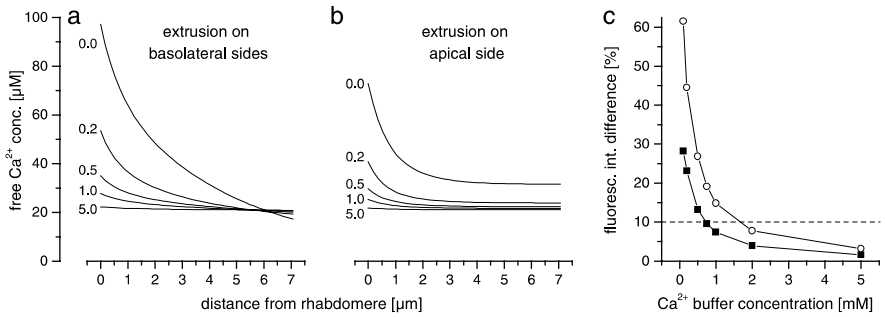

FIGURE 4.4: The concentration of the Ca^{2+} buffer strongly influences the modeled distribution of the free Ca^{2+} concentration. a) and b) The free Ca^{2+} concentration profile along a line through the cell body, from the Ca^{2+} influx region to the opposite side of the cell body, is plotted. The extrusion was assumed to take place only at basolateral sides (a; as in Figure 4.3a) or only at the apical side (b; as in Figure 4.3b). Increasing the buffer concentration (indicated by the numbers, in mM) reduces the size of the predicted gradients. c) The relative fluorescence intensity difference of a Ca^{2+} indicator with K_d = 20 μM between the Ca^{2+} influx region (x = 0 μm in a and b) and the opposite end of the cell body (x = 7.1 μm in a and b) is plotted as a function of the buffer concentration, when assuming extrusion on the basolateral sides (◯) or on the apical side (■). Below a buffer concentration of 750 μM, the fluorescence intensity between the two points differs by more than 10% (dashed line).

ing electrode), barely any gradients are discernible, no matter where the extrusion is assumed to take place (Figure 4.4a, b). From these calculated distributions of Ca_i we derived the fluorescence intensity, that would arise from the use of a Ca^{2+} indicator with $K_{d,B}$ = 20 μM. In Figure 4.4c, the expected difference in indicator fluorescence intensity between the rhabdomeric region and the side of the cell body opposite the rhabdomere is plotted as a function of the buffer concentration. It shows that even with buffer concentrations of 750 μM the intensity difference should be 18% if the Ca^{2+} extrusion is located at the basolateral sides. When the Ca^{2+} extrusion takes place on the apical side, the intensity difference should amount to 9%. For lower buffer concentrations, the fluorescence difference is predicted to be even larger. Importantly, no matter how large the buffer concentration, no gradient will arise if Ca^{2+} extrusion is confined to the place of Ca^{2+} influx, the rhabdomere (not shown). These considerations show that measurements of the Ca^{2+} gradients in the cell body can yield information about the location of Ca^{2+} extrusion, provided that the concentration of the Ca^{2+} indicator is not too high.

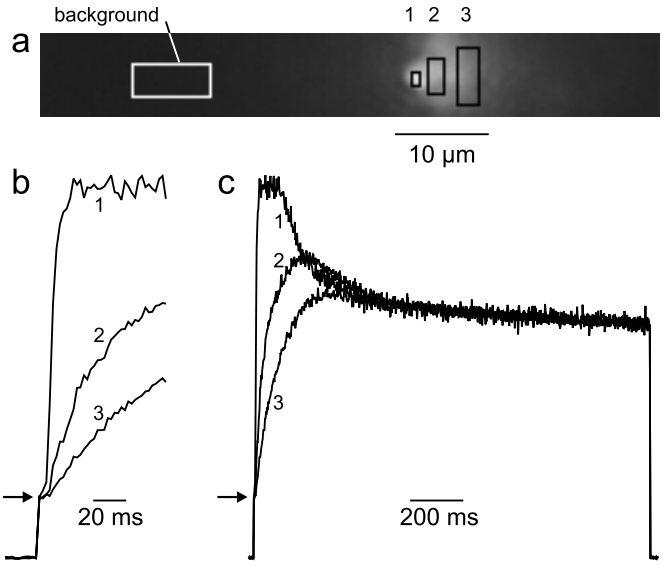

FIGURE 4.5: The steady state distribution of Ca_i in a cross-section of a photoreceptor cell is homogeneous. a) Raw intensity image (grayscale) of 100 successive images averaged during the steady state. The squares indicate the regions of interest quantitatively analyzed in b) and c); 1: rhabdomere; 2: center of cell; 3: side of cell opposite the rhabdomere. The background was measured outside the cell that was injected with the Ca^{2+} indicator. b), c) Normalized fluorescence traces (the first value obtained after turning on the light was used for normalization for the traces 1 and 2, and the first 3 values for the trace 3; see Results for details). The normalized fluorescence rises sharply in the rhabdomere (trace 1) and displays a large transient. After the decay of the transient, the normalized fluorescence shows the same values, independent of location of the region of interest. The distribution of Ca_i during the steady state thus is homogeneous. The traces are averages of 5 experiments.

The steady state distribution of Ca_i in a cross-section of the photoreceptor cells is homogeneous

Figure 4.5 shows the quantitative analysis of the data presented in Figure 4.2. In order to obtain a reasonable signal-to-noise ratio, we defined three regions of interest in the cross-section of the photoreceptor cell (Figure 4.5a). The regions correspond to the rhabdomere (region 1), the center of the cell body (region 2), and the side of the cell that lies opposite the rhabdomere (region 3). A fourth region was selected at least 10 μm away from the injected cell in order to measure the background signal. The raw intensity values

recorded are a superposition of a uniform background signal and the signal from the Ca^{2+} indicator. The signal from the Ca^{2+} indicator is shaped by the remaining optical properties of the tissue (waveguide properties of the rhabdomere and residual optical effects of the cornea and crystalline cone cells) and inhomogeneities in the distribution of the Ca^{2+} indicator. The distribution of intensity values during the latency period reflects these optical properties and inhomogeneities; it can therefore be used for normalization of the traces that have been background-subtracted. Hence, the intensity values in the regions of interest were averaged, background-subtracted, and subsequently normalized to the initial fluorescence level during the latency period (Figure 4.5b and c, arrows).

The intensity vs time plots of the normalized fluorescence (Figure 4.5b, c) are fully consistent with our earlier measurements (Chapters 2, 3). In the rhabdomere, very fast and large Ca^{2+} transients occur; 10 ms after the onset of the light stimulation, the normalized fluorescence in the rhabdomere has reached its maximum and stays at a plateau for about 100 ms before declining again. The plateau at the highest level of the normalized fluorescence is caused by the saturation of the Ca^{2+} indicator OG5N (Chapter 3). The further away from the rhabdomere the region of interest is chosen, the slower the increase of the normalized fluorescence is found to be. Also, the transient at light onset is much reduced in the cell body as compared to the rhabdomere. About 400 ms after the onset of light stimulation, however, the normalized fluorescence, and hence Ca_i, has reached the same value in all regions of interest, i.e. the distribution of Ca_i in the steady state is homogeneous. This observation argues that the Ca^{2+} extrusion is closely co-localized with the Ca^{2+} influx, assuming that the concentration of highly mobile Ca^{2+} buffers is below 750 μM (Figure 4.4). Evidence presented below shows that this condition is likely to be met in our experiments.

Ca^{2+} removal in the rhabdomere is faster than in the cell body

After turning off the light stimulation, Ca^{2+} influx through the light-activated channels ceases and Ca_i diminishes due to the on-going action of the Ca^{2+} extrusion mechanisms. When Ca^{2+} extrusion takes place only in the rhabdomere, it can be expected that Ca_i reduces faster in the rhabdomere than in the rest of the cell. In Figure 4.6, we stimulated a dark-adapted cell for 200 ms, turned off the light for 200, 400 or 600 ms, respectively, and then probed the change in Ca_i that occurred in darkness with a second period of illumination. Figure 4.6a shows that after 200 ms of darkness, the nor-

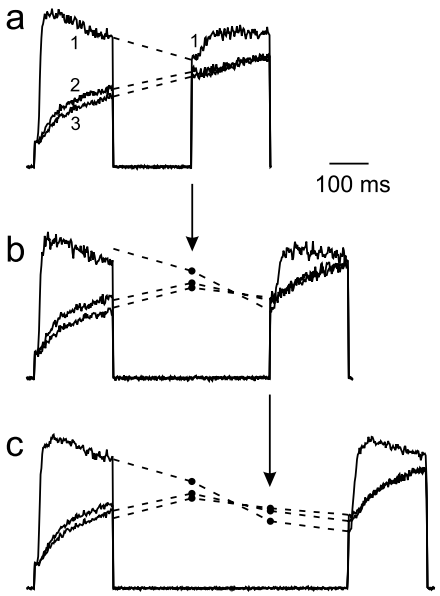

FIGURE 4.6: Ca^{2+} extrusion is faster in the rhabdomere than in the rest of the cell. The traces were obtained as in Figure 4.5, but come from a different cell. The cell was stimulated for 200 ms, the light was then turned off for 200 ms (a), 400 ms (b) or 600 ms (c) and turned on again (for 200 ms) to probe the change of fluorescence, and hence Ca_i, during the dark period. The dashed lines connect the recorded traces during the dark period. The dashed lines obtained in a) and b) are re-plotted in b) and c) (arrows), respectively, and connected to the new values obtained at the end of the dark period. a) During the first 200 ms of darkness, Ca_i in the rhabdomere (trace 1) diminishes, while it continues to rise in the cell body (traces 2 and 3). During the next 200 ms (b) to 400 ms (c) darkness, Ca_i also declines in the cell body, but in the rhabdomere it declines much faster, being lower than in the cell body. The traces were averaged 5 (a), 2 (b), and 6 times (c).

malized fluorescence, and therefore Ca_i, has diminished in the rhabdomere, while it has continued to rise in the cell body, consistent with Ca^{2+} being redistributed by diffusion. After 400 ms darkness (Figure 4.6b), Ca_i in the cell body has started to decline; by the same time Ca_i in the rhabdomere has fallen to a value lower than the one found in the cell body. The same is seen more clearly after 600 ms darkness (Figure 4.6c). This result cannot be explained by passive diffusion alone, but shows that some active components participate in the removal of Ca^{2+}. Equally, Ca_i in the cell body declines faster in the area closer to the rhabdomere (trace 2) compared to the area further away (trace 3). This indicates that during darkness Ca^{2+} diffuses from the cell body into the rhabdomere. In conclusion, we find that Ca^{2+} removal from the rhabdomere is faster than from the cell body, resulting in an inversion of the gradient of Ca^{2+}.

We cannot directly control or determine the indicator concentration employed in the experiments. However, the measurement shown in Figure 4.6 also shows that Ca^{2+} gradients can exist under our experimental conditions

after the Ca^{2+} transients in the rhabdomere at the onset of illumination has ceased. Therefore, the concentration of the Ca^{2+} indicator used in the experiments was not high enough to make it impossible to measure Ca^{2+} gradients. This argues that the homogeneous distribution of Ca_i in the steady state (Figure 4.5) cannot be explained solely with a high concentration of Ca^{2+} buffer but must indeed be caused by co-localization of Ca^{2+} influx and extrusion in or close to the rhabdomere (Figures 4.3, 4.4).

Discussion

An increase in Ca_i in fly photoreceptor cells is brought about by an influx of Ca^{2+} through the light-activated channels that are exclusively located in the rhabdomere (Ranganathan et al., 1994; Huber et al., 1996a; Niemeyer et al., 1996). Here we show that also Ca^{2+} extrusion takes place in or close to the rhabdomere. Ca^{2+} influx and Ca^{2+} extrusion are therefore co-localized.

Two independent arguments indicate that the homogeneous distribution of Ca_i we observe in the steady state is not due to a large, mobile Ca^{2+} buffer capacity. 1) Ca^{2+} gradients exist in the cell body during periods of dark-adaptation (Figure 4.6). High concentrations of a Ca^{2+} buffer would also strongly reduce these gradients, probably to a degree that makes it impossible to measure them. 2) Using blunt electrodes very easily overloads cells with the Ca^{2+} indicator. Recordings from those cells show profoundly modified kinetics of the membrane potential (Muijser, 1979) and the fluorescence (data not shown), and hence were discarded. Consequently, in not-overfilled cells the concentration of the indicator must have been much lower than 5 mM (the concentration of the indicator in the electrode). Therefore, our measurements exclude the possibility that Ca^{2+} extrusion is only located on the basolateral membranes (Figure 4.3a) and make it unlikely that Ca^{2+} extrusion takes place in the apical membrane excluding the rhabdomere (Figure 4.3b).

A new method for locating Ca^{2+} extrusion

Imaging of cells injected with fluorescent Ca^{2+} indicator dyes is an well-accepted method for demonstrating the location of channels permeable for Ca^{2+} (e.g. Ranganathan et al., 1994; Denk et al., 1995; Lumpkin and Hudspeth, 1995). Here we show that measuring spatial Ca^{2+} gradients, in combination with modeling, can be used for demonstrating the location of Ca^{2+} extrusion in living cells in vivo. As this method characterizes the location of Ca^{2+} extrusion by its very function, it is not necessary to know which type

of molecules causes Ca^{2+} to be extruded. It contrasts in this respect with more traditional, anatomical approaches, such as localization with antibodies. Additional problems of the immunohistochemical techniques are that not every protein detected by an antibody might be functional, and proteins might be regulated differentially depending on where they are located. The approach used in this Chapter therefore might provide a viable and quick alternative in systems, where data on Ca^{2+}-extruding proteins are absent (like in fly photoreceptor cells), and complement traditional approaches in other systems.

The identity of the Ca^{2+}-extruding mechanism

Ample evidence suggests that Na^+/Ca^{2+} exchanger proteins are present in fly photoreceptor cells (Armon and Minke, 1983; Hochstrate, 1991; Hardie, 1995a; Gerster, 1997; Schwarz and Benzer, 1997; Haug-Collet et al., 1999) and in photoreceptor cells of other invertebrates (bee: Minke and Tsacopoulos, 1986; *Limulus*: O'Day and Gray-Keller, 1989; Deckert and Stieve, 1991; squid: Bauer et al., 1999). Manipulating the function of the Na^+/Ca^{2+} exchanger has been shown to be capable of augmenting Ca_i in *Limulus* (O'Day and Gray-Keller, 1989) and has been shown to mimic the phenomena of light adaptation (Lisman and Brown, 1972), generally believed to be dependent on an increase in Ca_i (Lisman and Brown, 1972; Muijser, 1979). The Na^+/Ca^{2+} exchanger thus appears to be the main mechanism of Ca^{2+} extrusion in invertebrate photoreceptor cells. Probably, therefore, the Na^+/Ca^{2+} exchanger proteins contribute the largest part (or all) of the Ca^{2+} extrusion observed in our experiments. From the experiments presented here, it follows that the Na^+/Ca^{2+} exchanger proteins are located in or close to the rhabdomere of fly photoreceptor cells. This is in agreement with Bauer et al. (1999) who demonstrated Na^+/Ca^{2+} exchange in the rhabdomeres of squid photoreceptor cells. Since squids and flies do not belong to phylogenetically closely related groups, this raises the possibility that co-localization of Na^+/Ca^{2+} exchangers with the light-activated channels to the rhabdomeres is a general feature of invertebrate photoreceptor cells.

The close co-localization of Ca^{2+} influx and Ca^{2+} extrusion has important functional implications

Calcium ions directly regulates the light-activated channels (Hardie and Minke, 1994b; Hardie, 1995a), and either directly, or via calmodulin, many other proteins involved in phototransduction (rev.: Montell, 1999). Since most of

those proteins are located in or close to the rhabdomere (Montell, 1999), Ca_i in the rhabdomere rather than in the cell body may control the state of light adaptation. Rapid dark adaptation depends therefore on rapid removal of Ca^{2+} from the rhabdomere. Localizing Na^+/Ca^{2+} exchanger proteins to the rhabdomere thus helps achieving rapid dark-adaptation. Similarly, the co-localization of Ca^{2+} influx channels and Ca^{2+} extrusion mechanisms in small compartments observed in other cell types (Reuter and Porzig, 1995; Yamoah et al., 1998; Morgans et al., 1998; Krizaj and Copenhagen, 1998) might have the same functional significance, i.e. to increase the speed of Ca^{2+} removal in these compartments.

Co-localization of Ca^{2+} influx and extrusion results in a homogeneous distribution of Ca_i in the steady state throughout the cell body (Figure 4.5c). This ensures that structures located remotely from the Ca^{2+} influx are also exposed to the same levels of Ca_i. This is potentially important for the regulation of mitochondria that are located near the basolateral sides of fly photoreceptor cells (Walz, 1982) and are known to be regulated by Ca_i (Fein and Tsacopoulos, 1988).

5 Sodium/calcium exchange in *Drosophila* photoreceptor cells functions without potassium and tightly controls the activation of a calcium-activated potassium conductance

Abstract

The properties of the Na^+/Ca^{2+} exchange activity in *Drosophila* photoreceptor cell bodies was studied with the whole-cell patch-clamp technique in vivo. Rapid substitution of extracellular ions allowed to measure currents of up to 120 pA associated with the forward and the backward mode of operation. The Na^+/Ca^{2+} exchange operates in the absence of intra- and extracellular K^+. Operating the exchange current in reverse mode rapidly increases the intracellular free Ca^{2+} concentration, as witnessed by strong suppression of the response to light stimulation. This increase in free Ca^{2+} concentration activates a conductance that is highly permeable for Cs^+ and K^+, but not for Na^+ and Li^+ or divalent cations. The fast activation of the Ca^{2+}-activated conductance suggests that this conductance and the Na^+/Ca^{2+} exchange proteins are closely co-localized, most probably in the rhabdomere.

The research presented in this Chapter was conducted in collaboration with and in the laboratory of Dr. R.C. Hardie (Department of Anatomy, University of Cambridge, UK). It was partly financed by the Netherlands Organization for Scientific Research (NWO).

Introduction

Na^+/Ca^{2+} exchangers are highly efficient Ca^{2+} extrusion mechanisms that have been demonstrated in a great variety of tissues (rev.: Blaustein and Lederer, 1999). While most studies on Na^+/Ca^{2+} exchange have concentrated on the cardiac Na^+/Ca^{2+} exchanger, the exchanger also plays a crucial role in neurons to counterbalance Ca^{2+} influx. In sensory neurons, changes of the intracellular free Ca^{2+} concentration (Ca_i) often are functionally highly significant due to their effect on the adaptational state of the cell (rev.: Torre et al., 1995). Ca_i is therefore regulated rapidly and tightly in these cells; often Na^+/Ca^{2+} exchangers have been implicated in this process, for example in vertebrate rods (rev.: McNaughton, 1995), haircells (Ikeda et al., 1992; Boyer et al., 1999) and olfactory neurons (Jung et al., 1994; Reisert and Matthews, 1998).

In fly photoreceptor cells -a model system for PLC-mediated Ca^{2+} entry (revs: Minke and Selinger, 1996; Montell, 1997)- channels open when the cells are stimulated with light. The channels are highly permeable for Ca^{2+} (Hardie and Minke, 1992; Reuss et al., 1997) and located exclusively in the rhabdomere (Ranganathan et al., 1994; Huber et al., 1996a; Niemeyer et al., 1996). The rhabdomere consists of densely packed, tube-like protrusions of the plasma membrane, the microvilli (rev.: Hardie, 1985). The Ca^{2+} influx into the rhabdomere causes very high Ca^{2+} transients in the rhabdomere (Chapter 3; Postma et al., 1999), and the steady state Ca_i level reached throughout the cell can amount to more than 10 μM (Hardie, 1996a; Chapter 2). These high Ca^{2+} concentrations have a profound influence on the electrical response (Hardie, 1991a, 1995a) and are counterbalanced by efficient Na^+/Ca^{2+} exchange (Armon and Minke, 1983; Hochstrate, 1991; Hardie, 1995a, b; Gerster, 1997). Since the Na^+/Ca^{2+} exchanger proteins are most probably located in the rhabdomere (Chapter 4; Bauer et al., 1999), Ca^{2+} is removed faster from the rhabdomere than from the cell body. (Chapter 4). This might be functionally very important as most of the Ca^{2+}-dependent regulations of the phototransduction cascade are believed to take place in the rhabdomere.

CALX, a Na^+/Ca^{2+} exchanger homologous to the vertebrate cardiac Na^+/Ca^{2+} exchanger NCX1 has been cloned in *Drosophila* (Ruknudin et al., 1997; Schwarz and Benzer, 1997). Recently, a second gene, homologous to the vertebrate $Na^+/(Ca^{2+} + K^+)$ exchangers found in rods (Cervetto et al., 1989; Schnetkamp, 1989), has been identified (Haug-Collet et al., 1999) and termed NCKX30C. Both genes are expressed in the photoreceptor cells

of *Drosophila* (Schwarz and Benzer, 1997; Haug-Collet et al., 1999). We have therefore studied Na^+/Ca^{2+} exchange in *Drosophila* photoreceptor cell bodies in vivo and find that it does not require K^+, suggesting that at least part of the exchanger proteins are not encoded by NCKX30C. The exchanger proteins present in *Drosophila* photoreceptor cells functionally shield a Ca^{2+}-activated K^+ conductance, indicating that this conductance is co-localized with the exchangers to the rhabdomere.

Material and Methods

PREPARATION All experiments were carried out on isolated ommatidia of freshly emerged (less than 2 hours old) adult flies (*Drosophila melanogaster*). Usually, Oregon wild type animals were used, however, for some experiments the flies carried the *white* or the *trpl*/*white* double mutation. No differences between the different strains were found with respect to the studied phenomena. The preparation of the isolated ommatidia was carried out as described by Hardie (1991b). In short, eyes were dissected off the head while the head was immersed in dissecting solution (see below). The retinae then were carefully separated from the cornea. Subsequently, the ommatidia were isolated and stripped off the surrounding glial cells by gently triturating the retinae in chilled dissecting solution supplemented with 10% fetal calf serum. During this treatment, the photoreceptor cells lost their axon. The isolated ommatidia then were allowed to settle in the recording chamber mounted on an inverted microscope. Standard patch-clamping techniques were used to record whole-cell currents from single R1-6 photoreceptors, identified by their capacitance (50-70 pF; Hardie, 1991b); experiments were carried out at the physiological resting potential of -70 mV, except where indicated otherwise.

SOLUTIONS All solutions were made of chemicals obtained from Sigma. The dissecting solution contained (in mM): 120 NaCl, 5 KCl, 4 $MgCl_2$, 10 N-Tris (hydroxymethyl)-methyl-2-amino-ethanesulphonic acid (TES), 30 sucrose. The normal bath solution contained 120 NaCl, 5 KCl, 4 $MgCl_2$, 1.5 $CaCl_2$, 10 TES, 25 proline, and 5 arginine. This solution was varied as detailed in the text and figure legends by leaving away KCl or $CaCl_2$ (in this case 1 EGTA was added) or by replacing NaCl by LiCl or CsCl. However, all bath solutions were adjusted to a pH of 7.15 at 20°C (the temperature at which all experiments were carried out) with either HCl or the hydroxide of

the main monovalent cation. All bath solutions were also adjusted to an osmolarity of 282 mosm, by adding either H_2O or sucrose. When extracellular K^+ was present, a 5 s puls of bath solution containing 1 mM ouabain was puffed onto the cell (see below), to ensure that the Na^+/K^+ ATPase was blocked completely.

Intracellular (electrode) solutions were based on gluconate as the main anion to block a Cl^- conductance (Hardie and Mojet, 1995). A junction potential of 10 mV, resulting from the different intra- and extracellular anions, was corrected for. All intracellular solutions contained (in mM) 4 Mg-ATP, 0.4 Na_2-GTP, 1 NAD, 2 $MgCl_2$ and 10 TES and 130 mM of X-Glu, where X is a monovalent cation (or a combination of two monovalent cations, as indicated in text or legends). K^+-free intracellular solutions regularly contained 15 TEACl, to block the voltage dependent K^+ conductances (Hardie, 1991b); the concentration of X-Glu then was reduced accordingly. The pH of intracellular solutions was adjusted to 7.15 and the osmolarity to 276 mosm.

ION SUBSTITIONS Extracelllular solutions were changed by pressure-ejecting the substituting solution from a wide (diameter approximately 10 μm) puffer pipette, the mouth of which was positioned at a distance of $\sim$50 μm from the cell. Two puffer pipettes containing different solutions could be used in the same experiment. The bath solution was re-substituted by washing the whole recording chamber. Due to the geometry of the ommatidia (cylinders $\sim$100 μm long, 15 μm in diameter, with a central cavity; rev.: Hardie, 1985), the exchange of solutions was not fast (0.5-1 s); additionally, the timing of the solution exchange differs slightly between different recordings, as it was triggered by hand. The bars in the figures indicating the removal of Na_o, therefore, only roughly correspond to the period where the cells were exposed to a Na^+-free extracellular solution.

Results

The forward and reverse mode of operation of the Na^+/Ca^{2+} *exchanger are readily observed in* Drosophila *photoreceptor cell bodies in vivo*

All plasmalemmal Na^+/Ca^{2+} exchangers characterized so far transport one positive net-charge against each Ca^{2+} ion transported, independent of the direction of transport (rev.: Blaustein and Lederer, 1999). The transport of Ca^{2+} therefore is electrogenic, i.e. it gives rise to a current. Using typical intracellular ($Na_i = 20$ mM) and extracellular ($Ca_o = 1.5$ mM) solutions, the

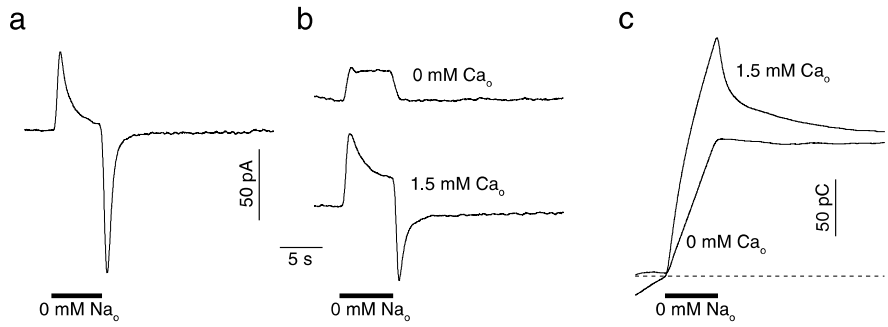

FIGURE 5.1: Manipulating extracellular Na^+ elicits currents from an electrogenic Na^+/Ca^{2+} exchanger in *Drosophila* photoreceptor cell bodies. a) Removing extracellular Na^+ (Na_o) elicits an outward current that inactivates with a time constant of a few seconds. Restoring Na_o then produces an inward current that equally inactivates. b) The inactivating outward and inward currents are dependent on the availability of extracellular Ca^{2+}. When extracellular Ca^{2+} was absent, an outward deflection of the current was seen that was caused by an inhibition of an inward current, as the resistance was increased in the absence of Na_o (not shown; see text for further details). c) The charge integral over the currents shown in b) was calculated and adjusted to yield zero (dotted line) at the beginning of Na_o removal. The charge integral over the inactivating currents is nearly zero, when the charge integral over the Ca^{2+}-independent current is subtracted. The patch electrode contained either 20 mM Na^+ and 110 mM K^+ (a) or 10 mM Na^+, 110 mM Li^+ and 10 mM TEA (b). Na_o was replaced by Li^+ in all panels; in a), the normal extracellular solution was used, while in b), the extracellular solution was K^+ free. The Ca^{2+}-free solution contained 1 mM EGTA.

reverse mode (i.e. uptake of Ca^{2+} into the cell) can be strongly favored by removing the extracellular Na^+ (Na_o) and replacing it with Li^+; this results in an outward current. When Na_o is resubstituted after a while, the forward mode (Ca^{2+} extrusion out of the cell) is favored, giving rise to an inward current. Figure 5.1a shows that these currents can readily be measured in *Drosophila* cell bodies. Current amplitudes of up to 120 pA have been measured (in the forward mode) using this paradigm.

Figure 5.1b shows that the inactivating currents attributed to the Na^+/Ca^{2+} exchanger are dependent on the presence of Ca_o, as must be expected for these currents. Figure 5.1b also shows a Ca^{2+}-independent component of the current that was often observed during ion substitution. This current was caused by inactivation of an inward current, as the resistance was increased in the absence of Na_o (data not shown). The charge integral (Figure 5.1c) of the currents shown in Figure 5.1b demonstrates that this conductance

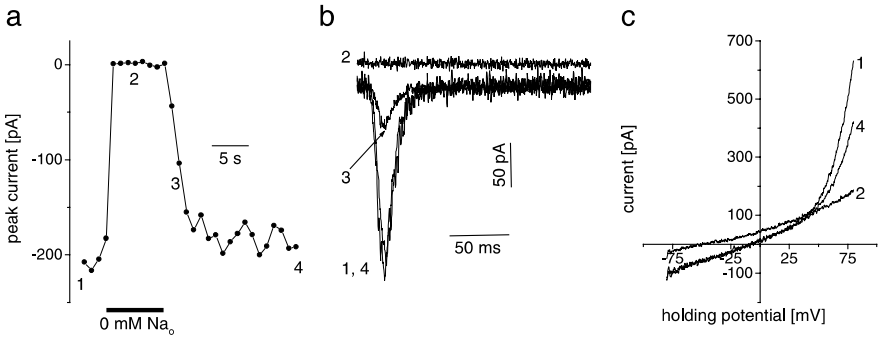

FIGURE 5.2: Removal of Na_o reversibly blocks the light response and the run-down current. a) The maximal current amplitude of the current induced by a 10 ms test flash given each second is plotted. When Na_o is removed, the light response is suppressed, but it recovers completely when Na_o is restored. b) Exemplary traces of the flash-induced current at times indicated in a). c) Voltage ramps show that the strongly outward-rectifying run-down current is suppressed during Na_o removal; when Na_o is present again, the run-down current recovers. The numbers indicate approximately when the voltage ramp was applied during a similar experiment as the one shown in a). The suppression of light response or run-down current cannot be explained by the removal of Na_o, but strongly indicates that Ca_i is increased during the absence of Na_o. The patch-electrode in a) and b) contained 20 mM Na^+ and 110 mM K^+, while in c) it contained 20 mM Na^+ and 110 mM Li^+. The extracellular solution in a) and b) contained 5 mM K^+, that was absent in c). Na_o was replaced by Li_o in all panels.

contributes equally to the current in the presence and the absence of Ca_o; it is therefore unlikely that it represents the so-called run-down current (see below) of light-activated channels (Hardie and Minke, 1994a). The Ca_o independent current reversed at +50 mV (data not shown). This, and its dependence on Na_o, argues against an unspecific leak current. However, this conductance was rather variable and we did not investigate it further.

The Na^+/Ca^{2+} exchanger operating in reverse mode should increase Ca_i. Increasing Ca_i strongly modulates the light response of *Drosophila* photoreceptor cells (Hardie, 1991a, 1995a). Monitoring the light response while manipulating the Na^+/Ca^{2+} exchanger therefore allows to demonstrate the increase in intracellular Ca^{2+} concentration caused by the exchanger. A corresponding experiment is shown in Figure 5.2a. The maximal current amplitude evoked by a 10 ms test flash (given every second) was measured during an ion substitution experiment similar to the one in Figure 5.1a. Removing Na_o quickly reduces the amplitude of the flash response. This cannot

be attributed to the removal of Na_o alone, since Li^+ also permeates the light-activated channels and the extracellular concentration of Ca^{2+}, which is the main permeant ion of the light-activated channels (Reuss et al., 1997), was not changed. The reduction of the flash response therefore has to be attributed to the increase in Ca_i. After resubstituting Na_o the flash response completely recovered, but with a slower time course. In Figure 5.2b, exemplary flash responses before (1) and during (2) Na_o removal and at the beginning (3) and at the end (4) of the recovery are shown.

Fly photoreceptors exhibit sometimes spontaneous activation of the channels that are normally opened only as a consequence of light stimulation; the current associated with the spontaneous activation of the light-activated channels has been termed run-down current (Hardie and Minke, 1994a, b). An increased intracellular Ca^{2+} concentration inhibits the run-down current (Hardie and Minke, 1994b). In Figure 5.2c, the current-voltage relationship was measured in a cell that showed the typically outward-rectifying run-down current (Hardie and Minke, 1994a) with voltage ramps. The outwardly rectifying current was strongly reduced when Na_o was removed and recovered after it was replaced. This demonstrates again that Ca_i is increased during the absence of Na_o.

The Na^+/Ca^{2+} exchanger in Drosophila *cell bodies does not require K^+*

Two genes encoding different types of Na^+/Ca^{2+} exchangers have been isolated from *Drosophila* and are expressed in the photoreceptor cells (Schwarz and Benzer, 1997; Haug-Collet et al., 1999). By analogy to the respective vertebrate homologues, it can be expected that CALX exchanges 3 Na^+ ions for 1 Ca^{2+} ion. NCKX30C is homologous to the exchanger in vertebrate rods (Haug-Collet et al., 1999), that exchanges 4 Na^+ ions against 1 Ca^{2+} ion and 1 K^+ ion (Cervetto et al., 1989; Schnetkamp et al., 1989). To determine which exchanger is expressed in the photoreceptor cell bodies of *Drosophila*, we investigated the K^+ dependency of the exchange currents. Figures 5.3a and b show that the currents attributable to the Na^+/Ca^{2+} exchanger were essentially unaffected by removing extracellular K^+. We can therefore conclude that Ca^{2+} uptake by the reverse mode of the exchanger does not require extracellular K^+.

Hardie (1995a) reported Na^+/Ca^{2+} exchange currents in the forward mode in the absence of intracellular K^+. In Figure 5.3c we confirm this finding and show that the exchanger in *Drosophila* cell bodies works without any K^+ present, intra- and extracellularly. The outcome of this experiment

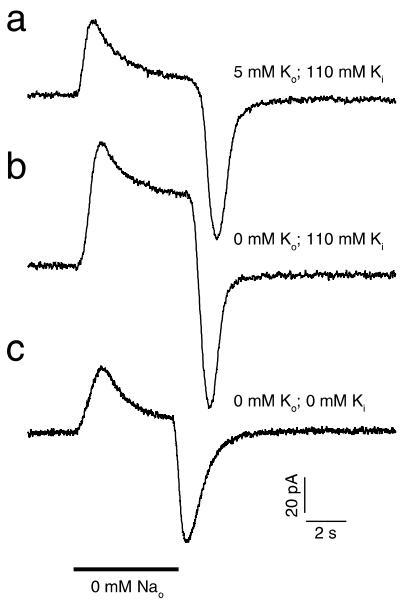

FIGURE 5.3: The Na^+/Ca^{2+} exchanger in *Drosophila* photoreceptor cell bodies does not require K^+. In a), the currents evoked by manipulating Na_o under physiological K^+ conditions are shown. In b), the solution replacing Na_o did not contain K^+. In c), no K^+ was present, neither intracellularly, nor in any of the extracellular solutions. The currents characteristic of an activation of the Na^+/Ca^{2+} exchanger are seen under all conditions. The recordings in a) and b) are from the same cell that was recorded with a patch electrode containing 110 mM K^+ and 20 mM Na^+. The recording in c) was done at a holding potential of -10 mV, to avoid currents through a Ca^{2+}-activated conductance (Figure 5.4); the patch-electrode therefore contained 96 mM Cs^+, 10 mM TEA and 26 mM Na^+. Na_o was replaced with Li_o in a) and b), but with Cs_o in c).

shows clearly that the exchange activity in *Drosophila* photoreceptor cells does not require K^+ on either side of the membrane. This result strongly argues that exchangers are present in *Drosophila* photoreceptor cell bodies homologous to the vertebrate NCX1-3 exchangers that do not require K^+ for transporting Ca^{2+}.

Ca^{2+} accumulation due to the reverse mode of the Na^+/Ca^{2+} exchanger rapidly activates a cationic conductance

Hardie (1995b) described a Ca^{2+}-activated conductance that required relatively high levels of Ca_i (threshold 5 μM) for activation and that could only be seen when the Na^+/Ca^{2+} exchanger was blocked. When substituting Cs_o for Na_o at -70 mV holding potential, a current was observed that differed markedly from the exchange currents observed normally (Figure 5.4a). Changing the holding potential proved that in addition to the exchange currents a conductance was activated that reversed around 0 mV. Measuring the current-voltage relationship with voltage ramps (Figure 5.4b) confirmed the reversal potential of $\sim$0 mV and showed that the conductance was inwardly rectifying. These properties indicate strongly that this conductance

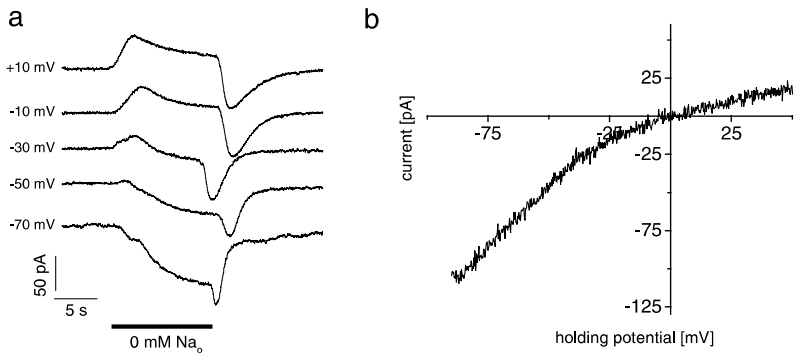

FIGURE 5.4: The Na^+/Ca^{2+} exchanger operating in the reverse mode readily activates a conductance. a) When Na_o is replaced by Cs_o, the resulting currents are strongly dependent on the holding potential. At negative holding potentials, an additional inward component is visible that becomes outward at positive holding potentials. b) The current-voltage relationship of the conductance activated during the absence of Na_o. Voltage ramps were applied before and during the absence of Na_o, and the obtained recordings subtracted. The resulting curve shows a reversal potential of ~0 mV, and inward rectification. The activation of the conductance by the reverse mode of operation of the Na^+/Ca^{2+} exchanger indicates that it is activated by an increase in Ca_i. To block the voltage activated K^+ conductances (Hardie, 1991a), the intracellular electrode contained 96 mM Cs^+, 26 mM Na^+ and 10 mM TEA. Extracellularly, K^+ was absent.

is identical to the conductance described by Hardie (1995b). In the experiments reported here, however, the reverse mode of the Na^+/Ca^{2+} exchanger was employed to increase Ca_i, and this leads to a relatively fast activation of the conductance. In contrast, when Ca_i was increased by perfusing the cell's interior with solutions containing high Ca^{2+} (Hardie, 1995b), the kinetics of activation were slower and activation did not occur at all as long as the exchangers could remove Ca^{2+} (Hardie, 1995b). Therefore, the Ca^{2+}-activated conductance probably is localized close to the exchanger, possibly even in a specialized compartment of the cytosol that is protected by the action of the Na^+/Ca^{2+} exchanger.

The Ca^{2+}-activated conductance is permeable for K^+ and Cs^+, but not for Na^+ and Li^+

The reversal potential of ~0 mV under the conditions of the experiment shown in Figure 5.4 indicates that the current was carried mainly by Cs^+, as the equilibrium potential for Cs^+ in this experiment was 7 mV. As the

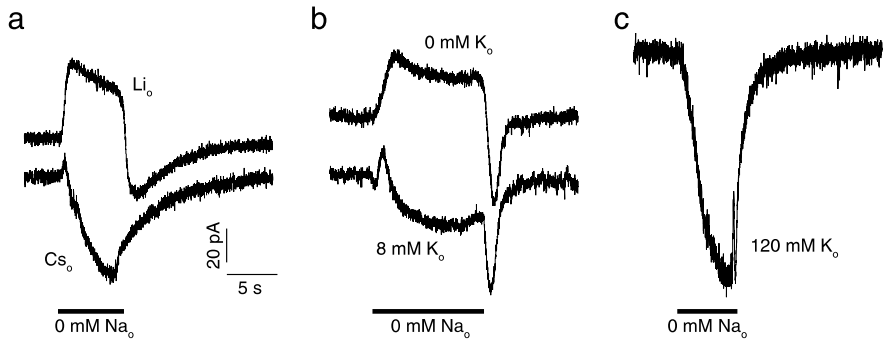

FIGURE 5.5: The Ca^{2+}-activated conductance is permeable for Cs^+ and K^+, but not for Li^+, Na^+ or Ca^{2+}. a) Depending on whether Li_o or Cs_o is used as substitute for Na_o, a large difference in the recorded currents is obtained. Only with Cs_o, a strong inward component is visible, indicating that Cs^+ but not Li^+ permeates the Ca^{2+}-activated conductance. These recordings also show that Ca^{2+}, which is present extracellularly, and Na^+, present intracellularly, did not permeate the Ca^{2+}-activated conductance substantially. b) A similar difference is observed when 8 mM K^+ is added to the Li^+-based extracellular solution used for substituting Na_o. This shows that K^+ permeates the Ca^{2+}-activated conductance as well. c) The permeation of K^+ through the Ca^{2+}-activated conductance can also be demonstrated with an extracellular solution entirely based on K^+. In a), the patch-electrode contained 120 mM Na^+ and 10 mM TEA, while extracellular K^+ was absent throughout the experiment. In b), the patch-electrode contained 120 mM Li^+, 2 mM Na^+ and 10 mM TEA, while in c) the patch-electrode was filled with a solution containing 110 mM K^+ and 20 mM Na^+.

equilibrium potentials for Na^+ and for Ca^{2+} were higher than +85 mV, these ions probably did not permeate to a significant extent through the Ca^{2+}-activated conductance. Furthermore, when substituting Na_o with Li_o, we did not observe this conductance (Figure 5.1). To confirm that Cs^+ permeates this conductance much better than Li^+, we compared these two ions directly in the same cell (Figure 5.5a). The reversal potentials for Cs^+ and Li^+ under the conditions of this experiment were similar (> 85 mV), but a large difference in the evoked currents was observed. Only with Cs_o as substitute for Na_o, an inward current was seen, confirming that Cs^+ permeates this conductance well, while Li^+ does not. Again, it can also be concluded that Na^+ did not permeate this conductance, as the strong outward gradient for Na^+ did not result in an outward current, when Li_o replaced Na_o.

Conductances permeable for Cs^+, but not for Li^+ and Na^+ are usually permeable for K^+ (Hille, 1992). We demonstrated this for the Ca^{2+}-activated

conductance by adding 8 mM K^+ to an Li^+-based extracellular solution (Figure 5.5b). The addition of extracellular K^+ resulted in an additional inward component of the cell, as expected from the inward gradient of K^+. Also, substituting Na_o with an extracellular solution entirely based on K^+ gave rise to an even larger inward current (Figure 5.5c), confirming that the Ca^{2+}-activated conductance is well permeated by K^+ ions. Altogether, these results demonstrate that the conductance investigated here has the properties of an inwardly rectifying, Ca^{2+}-activated K^+ conductance.

Discussion

In this study, the Na^+/Ca^{2+} exchanger proteins expressed in the cell bodies of *Drosophila* photoreceptors was investigated in vivo. The key findings are (1) that this exchanger does require K^+ on neither the extra- nor the intracellular side to function and (2) that the exchanger tighly controls the activation of a Ca^{2+}-activated K^+ conductance, suggesting that the exchanger and the Ca^{2+}-activated K^+ conductance are both located in the rhabdomere.

Na^+/Ca^{2+} exchange in Drosophila *photoreceptor cell bodies does not require K^+*

Removing extracellular Na^+, when millimolar intracellular Na^+ was present, resulted in an outward current that quickly inactivated; re-substituting the extracellular Na^+ evoked inward currents of up to 120 pA that quickly decayed to baseline as well. These currents are indicative of Ca^{2+} transport by an electrogenic Na^+/Ca^{2+} exchanger. Several control experiments support this interpretation: the currents are only observed when Ca^{2+} was present in the Na^+-free extracellular solution (Figure 5.1b). Additionally, the charge integral over the currents is zero (after the subtraction of the Ca^{2+}-independent components; Figure 5.1c), showing that the charge transported in reverse mode is identical to the charge subsequently transported during the forward mode of operation. This demonstrates that all the Ca^{2+} that was taken up during the removal of Na_o was extruded again when Na_o was restored. Finally, the reversible suppression of the light response and of the run-down current strongly indicates that Ca_i was increased during the absence of Na_o. In conclusion, these observations firmly establish that an electrogenic Na^+/Ca^{2+} exchanger is at the origin of the currents observed when manipulating Na_o.

The typical currents associated with the reverse and forward modes of operation were also observed in the absence of extracellular (Figure 5.2a) and intracellular K^+ (Figure 5.2b). This indicates that at least a part of the Na^+/Ca^{2+} exchangers expressed in the photoreceptor cell bodies of *Drosophila* are not encoded by the NCKX30C gene. In this respect the exchangers in the *Drosophila* photoreceptor cell bodies seem to be similar to the exchangers in the rhabdomeres of squids that also do not require K^+ (Bauer et al., 1999). This finding raises the question of where the K^+ dependent exchanger that are reportedly expressed by the same cells (Haug-Collet et al., 1999) are located. The present findings do not allow to rigorously rule out that a small population of $Na^+/(Ca^{2+} + K^+)$ exchangers is present in fly photoreceptor cell bodies. One possibility to explain why two different types of exchangers might be found in the same subcellular compartment is to assume that the $Na^+/(Ca^{2+} + K^+)$ exchangers only work in the submicromolar range of Ca^{2+} concentrations. It is not known if Ca^{2+} extrusion under these conditions is also confined to the rhabdomere. This hypothesis would imply that the two exchanger types have radically different Ca^{2+} affinities; the $Na^+/(Ca^{2+} + K^+)$ would thereby fulfill the "house-keeping" role traditionally assigned to plasma membrane Ca^{2+} ATPases (rev.: Blaustein and Lederer, 1999). An alternative possibility is that the axon terminals, which are known to host highly active synapses (Uusitalo et al., 1991) and that were absent from the investigated cells, possess Ca^{2+} extrusion proteins different from those found in the cell body.

In *Drosophila* photoreceptor cells, exchange currents of up to 120 pA were measured. Vertebrate exchangers have been reported to have maximal turn-over rates of ∼5000/s (Niggli and Lederer, 1991; Hilgemann, 1996), corresponding to a maximal current of ∼0.8 fA per molecule. Assuming that the exchangers in *Drosophila* photoreceptor cell bodies have similar turnover rates we can estimate that there are about 150,000 exchanger molecules in one cell. If they are all located in the rhabdomeric microvilli, this amounts to 5 molecules per microvillus, when assuming 30,000 microvilli in a *Drosophila* photoreceptor cell (rev.: Hardie, 1985).

A novel, Ca^{2+}-activated K^+ conductance

In Figure 5.4 we provide evidence that a Ca^{2+}-activated conductance previously described by Hardie (1995b) is a K^+ conductance under physiological ionic conditions. This conductance has unusual properties, because it is Ca^{2+}-activated and inwardly rectifying, and it has a very small single chan-

nel conductance ($<$ 0.5 pS; Hardie, 1995b). Furthermore, the Ca^{2+}-activated K^+ conductance in *Drosophila* cell bodies seems not to be blocked by TEA. These features do not fit with the two Ca^{2+}-activated K^+ conductances described in *Drosophila* (Gho and Mallart, 1986), and also do not fit with the traditional classification of Ca^{2+}-activated K^+ channels (Hille, 1992). It is therefore likely that the conductance investigated here represents a novel Ca^{2+}-activated K^+ conductance. The genetic potential of *Drosophila* should help to further investigate the genetic and molecular basis of this conductance.

The function of the Ca^{2+}-activated K^+ conductance is not clear. Its inward-rectifying current-voltage relationship raises questions about how much current flows through this conductance under physiological conditions, as the K^+ gradient in the insect retina only allows outward currents (Weckström et al., 1991). As discussed in Chapter 2, Ca_i continues to rise with increasing light intensity, even when the steady state membrane potential is already in saturation. This indicates that there is a further mechanism counteracting the depolarizing current through the light-activated channels, in addition to the voltage-gated K^+ currents. The Ca^{2+}-activated K^+ conductance might be a good candidate for this function, since its unusual high threshold of activation ($>$ 5 μM, Hardie, 1995b) coincides with the steady state intracellular Ca^{2+} concentration at the highest light intensity that does not saturate the steady state membrane potential (Chapter 2).

Na^+/Ca^{2+} exchangers and the Ca^{2+}-activated conductance are co-localized in the rhabdomere

The most striking property of the Ca^{2+}-activated K^+ conductance is its unusual behaviour when Ca_i is raised. Hardie (1995b) reports that this conductance can only be activated when the Na^+/Ca^{2+} exchanger is blocked by removing Na_o; even then, the time needed to activate the current was rather long and strongly dependent on the Ca^{2+} concentration inside the patch-electrode. Allowing the Na^+/Ca^{2+} exchanger to work in its reverse mode, and thereby raising Ca_i, activates the Ca^{2+}-activated K^+ conductance rather quickly (Figure 5.4). These observations strongly suggest that the Na^+/Ca^{2+} exchanger functionally shields the Ca^{2+}-activated K^+ conductance; only when the exchanger cannot reduce Ca_i in the vicinity of the Ca^{2+}-activated K^+ channels, or when it actually increases Ca_i at this location, the channels open. As the exchanger proteins in fly photoreceptor cell bodies are located in the microvilli of the rhabdomere (Chapter 4),

we conclude that the Ca^{2+}-activated K^+ conductance is also localized in the microvilli. In line with this, the very small single channel conductance (< 0.5 pS; Hardie, 1995b) allows that at least 1 channel of this conductance is located in each microvillus. Hardie (1995b) shows that at a holding potential of -80 mV (that also corresponds to an electromotive force of -80 mV under the specific conditions employed) a current of 700 pA flows through the Ca^{2+}-activated K^+ conductance. Assuming again 30,000 microvilli per photoreceptor cell (Hardie, 1985), a single channel conductance of 0.3 pS or smaller would be needed to have on average one open channel in each microvillus.

6 Modeling the calcium homeostasis of fly photoreceptor cells

Abstract

In neurons, Ca^{2+} influx from the extracellular space often occurs at highly specialized regions of the membrane. This localization can lead to large increases of the free Ca^{2+} concentration on the cytosolic side and to significant decreases on the extracellular side. In fly photoreceptors, the influx of Ca^{2+} ions is localized to a special compartment, the rhabdomere, where concentrations exceeding 200 μM have been measured. Based on the geometry and the electrical components of fly photoreceptor cells, a model is developed that predicts the membrane potential for a given time course of the rhabdomeric Ca^{2+} concentration. These calculated traces compare favorably with the measured membrane potential. Furthermore, the model is used to determine plausible ranges for the current generated by the Na^+/Ca^{2+} exchanger and the concentration of Ca^{2+} buffers.

Very low affinity fluorescent Ca^{2+} indicators are used to measure the changes of the extracellular Ca^{2+} concentration in the rhabdomere. With this technique, it is possible to show that the extracellular Ca^{2+} concentration in the rhabdomere decreases after the onset of light stimulation on the time scale of milliseconds. The model predicts changes in the extracellular Ca^{2+} concentration in the rhabdomere that are quantitatively similar to the measured traces. Together, the data presented here indicate that the model and its underlying assumptions adequately describe the Ca^{2+} homeostasis in the fly retina.

Introduction

A change in the intracellular free calcium concentration (Ca_i) is a very important signal for a wide variety of cellular processes in many cell types. Often, changes in Ca_i are constrained to specific regions of the cytosol of cells, allowing cells to utilize Ca^{2+} signals in different parts of the cell for different purposes. This restricted localization can be brought about by confining Ca^{2+} influx to a specific region of the plasma membrane. To further limit the spread of Ca^{2+} signals, proteins responsible for Ca^{2+} extrusion and Ca^{2+} buffers can be localized close to the location of influx. Also, the shape of cells can be modified to create geometrically defined small compartments that limit the diffusion of Ca^{2+}, such as spines of cortical neurons (Koch and Zador, 1993) or stereocilia of haircells (Lumpkin and Hudspeth, 1998).

Fly photoreceptor cells are a favorable system to study such a compartmentalization. They are highly polarized cells featuring a special cytosolic compartment, the rhabdomere, on the apical side. The rhabdomere consists of a densely packed stack of small, tube-like protrusions of the plasma membrane, the microvilli (rev.: Hardie, 1985). In its entirety, the rhabdomere acts as an optical waveguide, a property that can be exploited to quantitatively measure changes in Ca_i in this compartment (Chapter 3). The rhabdomeric microvilli contain the majority of proteins that have been implicated in the phototransduction, including the light activated channels (Ranganathan et al., 1994; Huber et al., 1996a; Niemeyer et al., 1996; rev.: Montell, 1999). These channels open upon light stimulation and are highly permeable for Ca^{2+} (Hardie and Minke, 1992; Reuss et al., 1997). Due to the small dimensions of the rhabdomeric microvilli, light stimulation leads to rapid increases in Ca_i that exceed 200 μM (Chapter 3; Postma et al., 1999). Ca^{2+} ions then diffuse from the rhabdomere into the cell body (Ranganathan et al., 1994; Chapter 4), where changes in Ca^{2+} concentrations are more modest, but nevertheless amount to tens of micromolar (Hardie, 1996a; Chapter 2). To counteract the Ca^{2+} influx, strong Na^+/Ca^{2+} exchanger proteins are located in or close to the microvilli (Bauer et al., 1999; Chapters 4, 5), and high concentrations of calmodulin, a Ca^{2+}-binding protein, have been shown to exist in the rhabdomere (Porter et al., 1993).

To resolve the Ca^{2+} dynamics in the small subcellular compartments the resolution of optical measurements often is unsatisfactory, and hence modeling approaches are taken (e.g. Koch and Zador, 1993; De Schutter and Smolen, 1998; Lumpkin and Hudspeth, 1998; Postma et al., 1999). Here, I present a model that integrates the known geometry of fly photoreceptor

cells with the mechanisms responsible for ion in- or effluxes. Using suitable parameters, this model allows to show that the membrane potential can be calculated from the Ca^{2+} concentration with reasonable accuracy; this shows that the measured time course of Ca_{rh} is consistent with the measured membrane potential. The model also allows determining a range for parameters that are otherwise difficult to measure, as the concentration of Ca^{2+} buffers and the size of the current generated by the Na^+/Ca^{2+} exchanger proteins. Furthermore it predicts changes in extracellular Ca^{2+} and K^+ concentrations that compare favorably with measurements.

Material and Methods

MEASURING THE INTRACELLULAR Ca^{2+} CONCENTRATION IN THE RHABDOMERE The preparation and all experimental details were as described previously (Chapter 3). Only recordings were used in which both the Ca_{rh} and the membrane potential could be measured simultaneously.

MEASURING THE EXTRACELLULAR Ca^{2+} CONCENTRATION IN THE RHABDOMERE After setting up the fly (female *Calliphora vicina*, mutant *chalky*) as described previously (Chapters 2, 3), an electrode with the tip broken to a diameter of $\sim$20 μm was inserted into a small hole, which was cut into the dorsal part of the cornea and sealed with silicon grease. The electrode was filled with fly Ringer solution made of (in mM) 120 NaCl, 4 KCl, 1.4 $CaCl_2$, 4 $MgCl_2$ and 10 HEPES, adjusted to pH 7.1 and supplemented with 0.5 mM of the very low affinity Ca^{2+} indicator X-rhod-5N (XR5N; obtained from Molecular Probes, Oregon). XR5N has a reported K_d of 350 μM and does not fluoresce in the absence of free Ca^{2+}. The addition of XR5N is calculated to have reduced the free Ca^{2+} concentration in the Ringer solution to 1.03 mM; in the eye, the Ca^{2+} concentration in the extracellular space probably was closer to the physiological value of 1.4 mM (Sandler and Kirschfeld, 1991), because the injected dye-containing Ringer was diluted. A drop of the solution in the electrode was injected into the eye by applying pressure to the back of the electrode. As the injected volume is unknown it is not possible to calculate the final concentration of the Ca^{2+} indicator. Furthermore, the fluorescence intensity due to the Ca^{2+} indicator diminished during the duration of an experiment to almost background values. This was surprising as Weyrauther et al. (1989) reported that fluorescence of Lucifer Yellow that was injected into the retina reduced with a time course of $\sim$1 h. This

indicates that XR5N is either taken up by cells in the retina or otherwise removed from the retina much faster than Lucifer Yellow.

After the injection of the dye, the fluorescence was recorded (by using a 580 nm fluorescence cube) from the deep pseudopupil (Franceschini and Kirschfeld, 1971) in the ventral part of the eye, as there was no damage from the injection in that area. By recording from the deep pseudopupil the contribution of the light originating from the rhabdomeres is maximized (see also Figure 6.9a).

The fluorescence intensity (F) measured from the deep pseudopupil can be converted into free Ca^{2+} concentration. For this conversion it was assumed that the Ca^{2+} concentration in the dark-adapted rhabdomere (Ca_o) is 1.4 mM (Sandler and Kirschfeld, 1991). The fluorescence intensity during the latency period (F_{lat}) corresponds to this concentration. Furthermore, the autofluorescence of the tissue at the applied excitation wavelengths can be neglected, as can the fluorescence of XR5N at low Ca^{2+} concentrations. Therefore, the output of the photomultiplier in darkness can be taken as the minimum fluorescence (F_{min}). The free Ca^{2+} concentration in the extracellular rhabdomere ($Ca_{rh,ex}$) is given by:

$$Ca_{rh,ex} = K_d Ca_o \frac{F - F_{min}}{Ca_o (F_{lat} - F) + K_d (F_{lat} - F_{min})}$$

The Model

The model is based on the known geometry and electrical components of *Calliphora vicina* R1-6 photoreceptor cells. The central assumption is that the three-dimensional geometry of a photoreceptor cell can be reduced to two dimensions. This assumption is likely to be valid because only very high light intensities were used for stimulating the cells. The intensities were such that every rhodopsin molecule was photoconverted at least once in 10 ms. This implies that also microvilli at the proximal base of the photoreceptor cells, close to the basal membrane, absorb enough light to activate all transduction units. No attempt was made to account for the tapering of both, the rhabdomere and the photoreceptor cells (Boschek, 1971) over the depth of the retina.

A related, but additional assumption made throughout this Chapter is that the Ca^{2+} concentration in all microvilli is similar. While this assumption might well hold for the first 60 to 100 ms, the duration of a single bump (Hardie and Minke, 1995), it might break down for longer periods of

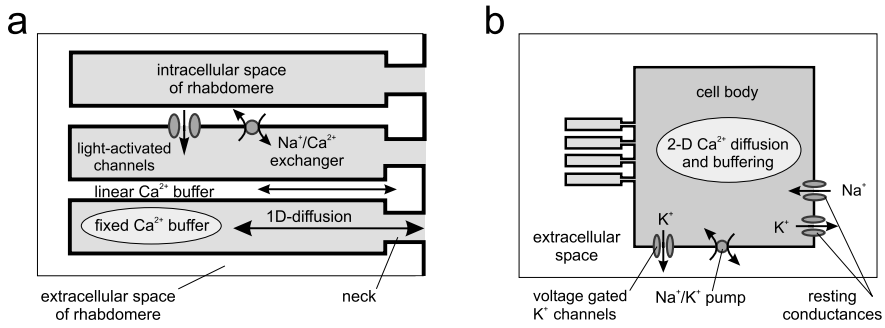

FIGURE 6.1: Schematic representation of the elements of the model (not to scale). a) The rhabdomeric microvilli contain the light-activated channels (Huber et al., 1996a; Niemeyer et al., 1996) and the Na^+/Ca^{2+} exchangers (Bauer et al., 1999; Chapters 4, 5). The activity of both types of molecules is supposed to be homogeneously distributed in the membrane of the microvilli. A fixed Ca^{2+} buffer buffers the Ca^{2+} ions in the microvilli. The lipids in the membrane are modeled to act as a fixed, linear Ca^{2+} buffer in the extracellular space of the rhabdomere. All cations (Na^+, K^+, Ca^{2+}, Mg^{2+}) diffuse in one dimension in both, the extracellular and the intracellular compartment of the rhabdomere. The microvilli are connected to the cell body by narrow necks (Boschek, 1971). b) The membrane of the cell body hosts the voltage-gated K^+ channels (Hardie, 1991b; Weckström et al., 1991), the Na^+/K^+ pump (Baumann et al., 1994) and the resting Na^+ and K^+ conductances. Ca^{2+} ions are buffered by a mobile Ca^{2+} buffer to which the fluorescent Ca^{2+} indicators contribute. The 2-dimensional diffusion in the cell body is calculated only for free and bound Ca^{2+} ions, but not for the other cations. For dimensions and further explanation, see text.

illumination. It has been established that the macroscopic light response is composed of many superimposing quantum bumps, and a bump-producing transduction unit might have a refractory period before being able to produce another bump (Hochstrate and Hamdorf, 1990; Scott and Zuker, 1998). This could imply that the Ca^{2+} concentration in a given microvillus fluctuates even under constant illumination. Due to the large number of microvilli, these fluctuations would not be visible in measured traces of Ca_{rh}. While the consequences of these fluctuations in specific microvilli have not been explored quantitatively, it can be argued that the error introduced is small as long as the fluctuations in the microvilli are small. This condition seems to be met, as the Ca^{2+} transients in strongly light-adapted photoreceptor cells have been shown to be small (Chapter 3).

GEOMETRY Figure 6.1 gives a schematic overview of the main components of the model. The cross-section of the cell body was modeled as a two-dimensional square, with a side length of 7.1 μm; the surface of this cross-section is equivalent to a circle with a radius of 4 μm. The length of the model photoreceptor cell was taken to be 211 μm. This yields a total volume of $1.1 \cdot 10^{-14}$ m^3 for the cell body. The surface of the cell body is $6.1 \cdot 10^{-9}$ m^2.

The microvilli were assumed to have a length of 1.1 μm, and an outer diameter of 60 nm (Suzuki et al., 1993). Because membranes have a thickness of 5 nm, the inner diameter of the microvilli was assumed to be 50 nm. 20 microvilli were assumed to be located in a cross-section of the rhabdomere (El-Gammal et al., 1987), and their centers to be separated by 75 nm (Suzuki et al., 1993). The width of the rhabdomere therefore amounts to 1.5 μm. The difference in length of microvilli being situated in different positions in a given cross-section of the rhabdomere was not taken into account. The neck connecting the microvilli to the cell body was modeled as a cylinder with a length of 60 nm and an inner diameter of 35 nm (Boschek, 1971). Actin filaments, found along the length of microvilli and the neck (Arikawa et al., 1990), might further reduce the inner volume of microvilli, especially in the neck region; however, their contribution was neglected. The volume of a microvillus, including the neck, then works out to be $2.2 \cdot 10^{-21}$ m^3, and its surface equals $2.0 \cdot 10^{-13}$ m^2.

Assuming that the microvilli are densely packed (Suzuki et al., 1993), the total number of microvilli that fit in a rhabdomere of 211 μm length is 90,000. The rhabdomere then has a total internal volume of $2.0 \cdot 10^{-16}$ m^3 and a surface of $1.8 \cdot 10^{-8}$ m^2. The total volume of the model cell then equals $1.1 \cdot 10^{-14}$ m^3 and the total surface of the cell amounts to $2.38 \cdot 10^{-8}$ m^2. With the specific membrane capacitance $c_m = 0.01$ F/m^2, the capacitance of the model cell equals 238 pF. This value is higher than previous measurements (130-160 pF; Jansonius, 1990; Anderson and Hardie, 1996), but further reducing the cell surface (by reducing the length of microvilli, as this is the most important parameter determining the cell surface) is incompatible with the published anatomy.

The extracellular space was divided in a compartment representing the large intraommatidial cavity found in the fly retina and a compartment corresponding to the extracellular space of the rhabdomere. The volume of the extracellular space of the rhabdomere can be calculated by subtracting the volume of all microvilli ($2.0 \cdot 10^{-16}$ m^3 including the neck) from the total volume of the rhabdomere (length of microvilli plus neck times width of rhabdomere times length of rhabdomere = $3.7 \cdot 10^{-16}$ m^3). The extracellular

Description	*Symbol*	*Value*
Length of microvillus	l_{mv}	1.1 μm
Inner diameter of microvillus	d_{mv}	50 nm
Length of neck	l_n	60 nm
Inner diameter of neck	d_n	35 nm
Volume of microvillus (incl. neck)	v_{mv}	$2.2{\cdot}10^{-21}$ m^3
Surface of microvillus (incl. neck)	S_{mv}	$1.7{\cdot}10^{-13}$ m^2
Number of microvilli per cell	N_{mv}	90,000
Volume of rhabdomere	v_{rh}	$2.0{\cdot}10^{-16}$ m^3
Surface of rhabdomere	S_{rh}	$1.8{\cdot}10^{-8}$ m^2
Length of photoreceptor cell	l_{pr}	211 μm
Length of one side of the cell body	l_{cb}	7.1 μm
Volume of cell body	v_{cb}	$1.1{\cdot}10^{-14}$ m^3
Surface of cell body	S_{cb}	$6.1{\cdot}10^{-9}$ m^2
Volume of total cell	v_{tot}	$1.1{\cdot}10^{-14}$ m^3
Surface of total cell	S_{tot}	$2.38{\cdot}10^{-8}$ m^2
Volume of extracellular rhabdomere	$v_{\mathrm{rh,ex}}$	$7.8{\cdot}10^{-17}$ m^3
Volume of intraommatidial cavity (per cell)	v_{ic}	$1.6{\cdot}10^{-15}$ m^3

TABLE 6.1: Geometrical values used in the model. These values are derived from the known anatomy of the blowfly retina and were not varied throughout this Chapter.

volume of the rhabdomere then amounts to $7.8 \cdot 10^{-17}$ m^3, while the volume of the membranes in the rhabdomere equals $8.9 \cdot 10^{-17}$ m^3. The total volume of the extracellular space (rhabdomere and intraommatidial cavity) was set to be 6.3 times smaller than the volume of the photoreceptor cell (Hamdorf, cited in Sandler and Kirschfeld, 1991), and therefore equals $1.7 \cdot 10^{-15}$ m^3 for each photoreceptor cell. The volume of the part of the intraommatidial cavity that "belongs" to a single peripheral photoreceptor cell therefore amounts to $1.6 \cdot 10^{-15}$ m^3. Table 6.1 summarizes the geometrical parameters.

IN- AND EFFLUX OF CATIONS Immunohistochemical studies have shown that the light-activated channels are homogeneously distributed throughout the rhabdomere (Huber et al., 1996a; Niemeyer et al., 1996). In the calculations presented here, the activity of the light-activated channels was therefore assumed to be homogeneously distributed throughout the rhabdomere.

Drosophila photoreceptors express two types of Na^+/Ca^{2+} exchanger proteins (Haug-Collet, 1999), one of which is dependent on K^+ on the same side as Ca^{2+} to function. The evidence presented in Chapter 5 indicates that the exchanger in the cell bodies of *Drosophila* is not dependent on K^+ on both sides of the plasma membrane. Accordingly, the exchanger was modeled

here to transport 3 Na^+ ions against 1 Ca^{2+} ion. Equally, there is evidence (Bauer et al., 1999; Chapters 4, 5) that the exchanger proteins are located close to or even in the rhabdomere. In the absence of any ultrastructural data the Na^+/Ca^{2+} exchange activity was modeled as being homogeneously distributed in the membranes of the rhabdomeric microvilli. The activity of the Na^+/Ca^{2+} exchanger proteins was assumed to follow a simple Hill-function with Hill-coefficient 1 (rev.: Blaustein and Lederer, 1999). Hardie (1995a) determined that the exchanger current in *Drosophila* photoreceptor cell bodies is 10 times stronger when $Ca_i \approx 20$ μM compared to $Ca_i \approx 1$ μM. As a starting point in the simulations, the K_d of the Ca^{2+} binding to the transport site of the exchanger proteins was thus taken to be 18 μM. Note, however, that this value is unusually high compared to values determined in other preparations (rev.: Blaustein and Lederer, 1999). The voltage dependence of the exchanger (e.g. Hardie, 1995a) was ignored.

The membrane of the cell body was assumed to contain fast and slow voltage-gated K^+ channels (Weckström et al., 1991). The kinetics of the voltage-gated channels was modeled as described by Gerster et al. (1997). Additionally, non-neglible Na^+ and K^+ resting conductances and the Na^+/K^+ pump proteins were assumed to be located in the plasma membrane of the cell body (Baumann et al., 1994).

All membrane channels were modeled according to the Goldman-Hodgkin-Katz theory (Hille, 1992; for application of this theory on fly photoreceptor cells: Gerster et al., 1997; Gerster, 1997; Postma et al., 1999). The light-activated channels are permeable for all physiologically relevant cations (Na^+, K^+, Ca^{2+}, Mg^{2+}) and were assumed to have the relative permeability ratios (w) reported by Reuss et al. (1997) for the *trp*-dependent channels ($w_{Na} = 0.01$; $w_K = 0.01$; $w_{Ca} = 0.88$; $w_{Mg} = 0.1$; see also Postma et al., 1999).

The photoreceptor cells of flies possess an axon that makes synaptic contacts with interneurons in the lamina. On the presynaptic side, voltage dependent Ca^{2+} channels are present that presumably are important for regulating the release of neurotransmitter. A small part of the electrical activity of these channels can be measured when recording in the soma. It is visible as a minor but distinct shoulder on the membrane potential trace when the photoreceptor cell depolarizes quickly (Weckström et al., 1992; see Figure 6.7). The contribution of these channels to the membrane potential was not taken into account.

Description	*Symbol*	*Value*	*Reference*
Extracellular Na^+	Na_o	140 mM	Sandler and Kirschfeld (1991)
Intracellular Na^+	Na_i	10 mM	Coles et al. (1985)
Extracellular K^+	K_o	140 mM	Weckström et al. (1991)
Intracellular K^+	K_i	120 mM	Coles et al. (1985)
Extracellular Ca^{2+}	Ca_o	1.4 mM	Sandler and Kirschfeld (1991)
Intracellular Ca^{2+}	Ca_i	160 nM	Hardie (1996a)
Extracellular Mg^{2+}	Mg_o	4.0 mM	see text
Intracellular Mg^{2+}	Mg_i	2.0 mM	see text

TABLE 6.2: The ionic concentrations assumed in the model for the resting, dark-adapted condition. The extracellular concentrations of Na^+ and K^+ have been determined in the retinae of honey bee drones.

THE RESTING CONDITIONS The ionic conditions were chosen to yield a resting potential of -60 mV. Since the reversal potential of the *trp*-dependent channels is at $+11$ mV (Reuss et al., 1997), the photoreceptor cell can maximally depolarize 71 mV, a value that corresponds closely to the maximal depolarization observed in the recordings (e.g. Figure 6.2). The resting intra- and extracellular ion concentrations were chosen as in Gerster et al. (1997; see also Table 6.2 for references). The concentrations of extracellular or intracellular Mg^{2+} are not known for fly retinas. Available estimates of the intracellular total Mg^{2+} concentration in photoreceptors of the bee drone amount to $\sim$10 mM (Coles and Rick, 1985; Baumann et al., 1989). This value is almost certainly an overestimate, as Mg^{2+} can be chelated by other molecules, most notably ATP. Here, 2 mM is assumed for Mg_i, and 4 mM for Mg_o, a value typically used for Ringer solutions. The Nernst potential for K^+ has been reported to be -85 mV (Weckström et al., 1991), consistent with the resting membrane potential of glial cells (see Results). This is consistent with the values chosen ($K_i = 120$ mM; $K_o = 4$ mM). Estimates in the drone retina, however, indicate that K_o might have been underestimated (Cardinaud et al., 1994).

The maximal permeability for both, the fast and the slow component of the voltage-gated K^+ channels, was taken to be to $1.9 \cdot 10^{-8}$ m/s. The constant "resting" Na^+ conductance was assumed to have a permeability of $2.7 \cdot 10^{-9}$ m/s. In order to maintain the resting membrane potential at -60 mV, an additional resting K^+ conductance had to be assumed, with permeability $2.9 \cdot 10^{-8}$ m/s. The currents calculated from these permeability values are only assumed to flow across the surface of the cell body ($S_{cb} = 6.1 \cdot 10^{-9}$ m^2). Note that Gerster et al. (1997) expressed the permeability

values relative to the total surface of the cell ($S_{\mathrm{cb}} = 1.6 \cdot 10^{-9}$ m^2 in their model). Accounting for this difference in membrane surface, the values used here represent a reduction of the current through the voltage dependent K^+ channels by a factor of ~8 compared to the currents calculated by Gerster et al. (1997). The current generated by the Na^+/K^+ pump was set to be I_P = 0.19 nA. This pump current balances the Na^+ and K^+ fluxes at a resting potential of −60 mV, as long as the current due to the Na^+/Ca^{2+} exchanger is neglected. Since only the first 500 ms of illumination were investigated, the pump current was assumed to be constant.

The parameter set used here represents considerable changes compared to the values used by Gerster et al. (1997) and Gerster (1997). It was chosen because it yields a higher input resistance of the modeled cell. The input resistance is calculated to be 30.5 MΩ (Oberwinkler and Vanhoutte, unpublished), a value that agrees well with the experimental data (e.g. Anderson and Hardie, 1996).

Ca^{2+} BUFFERING Often differences between changes in the total amount of Ca^{2+} and changes in the free Ca^{2+} concentration are measured (e.g. Hardie, 1996a). These differences are usually well explained by the presence of substances that bind Ca^{2+}, thus lowering the free Ca^{2+} concentration. An important aspect thereby is whether the Ca^{2+}-binding substance (the Ca^{2+} buffer) can diffuse itself or not (e.g. Roberts, 1994; revs: Neher, 1998, De Schutter and Smolen, 1998). Importantly, fluorescent Ca^{2+} indicators bind Ca^{2+} and can have fairly high diffusion constants (rev.: De Schutter and Smolen, 1998). In fly photoreceptors, the concentration of the Ca^{2+}-binding protein calmodulin is known to be high in the rhabdomere (Porter et al., 1993). Furthermore, the rhabdomere is a structure rich in membranes, that are known to bind Ca^{2+}, although with low affinity (McLaughlin et al., 1981). In the model, we assume that the Ca^{2+} buffer in the cell body is mobile and has the same diffusion constant as Ca^{2+}, i.e. $D_B = 220$ μm^2/s, in order not to underestimate the diffusion constant of the mobile Ca^{2+} buffer. Values as high as 200 μm^2/s have been reported for the diffusion coefficient of Ca^{2+} indicators in vivo (Hall et al., 1997, rev.: De Schutter and Smolen, 1998). In the rhabdomere we assume that the Ca^{2+} buffer does not diffuse on the time scale of our measurements, due to the smallness of the compartment. All intracellular Ca^{2+} buffers have been assumed to have a K_d of 20 μM, which roughly corresponds to the K_d of the Ca^{2+} indicator Oregon Green 5N (OG5N; Haugland, 1996; Dabdoub and Payne, 1999) and the two low

affinity binding sites of calmodulin (Maune et al., 1992). The binding reactions between Ca^{2+} and the buffers were assumed to be always in equilibrium (instantaneous buffer assumption).

In the extracellular space of the rhabdomere, Ca^{2+} buffering is assumed to be solely due to Ca^{2+} binding to the lipid membranes. As the K_d of the phospholipids for Ca^{2+} is much higher than the concentrations of extracellular Ca^{2+}, the buffering reactions can be approximated with a linear function (Neher, 1998). Taking the surface of membranes in the rhabdomere to be $1.8 \cdot 10^{-8}$ m^2, and the volume of the extracellular space in the rhabdomere to be $7.8 \cdot 10^{-17}$ m^3 the effective concentration of all phospholipids can be calculated to be 547 mM by assuming that a single phospholipid molecule occupies $0.7 \cdot 10^{-18}$ m^2 (McLaughlin and Brown, 1981). Zinkler et al. (1985) showed that 6.25% of all phospholipids in rhabdomeric membranes of flies are phosphatidylserines (PS), and the remaining main phospholipids are phosphatidylcholines (PC) or phosphatidylethanolamines (PE). The reported K_d's for Ca^{2+}-binding of these phospholipids (McLaughlin et al., 1981) were divided by 1.5 to account for the effects of the surface potential (Postma et al., 1999). Using an effective K_d of 55.5 mM for PS and 222 mM for PC and PE, the ratio of bound Ca^{2+} to free Ca^{2+} works out to be 2.9 in the extracellular space of the rhabdomere. Therefore, a fixed, instantaneous, linear Ca^{2+} buffer with a buffering ratio of 2.9 was included when modeling the changes of extracellular Ca^{2+} in the rhabdomere. No Ca^{2+} buffer was assumed to be present in the intraommatidial cavity.

DIFFUSION Diffusion in the microvilli was modeled in only one dimension as described previously (Postma et al., 1999). However, to keep the simulation time within reasonable bounds, a coarser resolution was chosen. Typically, the microvillus was split up in 6 compartments and the concentrations were calculated at the boundaries of each compartment. The diffusional profiles of all four cations considered were calculated.

Both free Ca^{2+} ions and Ca^{2+} bound to buffer were modeled to diffuse in two dimensions in the cell body. Typically, the cell body was divided in a grid yielding 11×11 compartments, and the concentration was calculated at the crossing points of the grid. Higher resolutions yielded very similar results but considerably increased the time for calculation. The diffusion of free and bound Ca^{2+} ions was assumed to take place along the grid-lines. The concentration of the three other cations (Na^+, K^+, Mg^{2+}) was calculated as the average concentration of the ion inside the cell body, as the relative

changes in their concentration were much smaller than the relative changes of Ca_i.

The models describing the diffusion in the rhabdomere and in the cell body were connected to each other by calculating the ion flux over the microvillar neck for all four cations and updating the concentrations in the rhabdomere and the cell body accordingly. The influx region of the cell body was located in the middle of one side, on a length of 1.5 μm, which is equal to the width of the rhabdomere.

The diffusion of the cations on the extracellular side of the rhabdomere, was treated in a manner identical to the calculations of the intracellular side. Only the 1-dimensional diffusion along the length of the microvilli was considered, and the possible diffusion in a perpendicular direction at the base of the microvilli was neglected. The intraommatidial cavity was treated as one large compartment with a homogeneous distribution of all ion concentrations.

CALCULATING THE MEMBRANE POTENTIAL FROM THE FREE Ca^{2+} CONCENTRATION IN THE RHABDOMERE Using intracellular recordings and exploiting the natural optics of fly eyes, the membrane potential and the free Ca^{2+} concentration in the rhabdomere, Ca_{rh}, can be measured simultaneously (Chapter 3). Due to the waveguide properties of the rhabdomere (van Hateren, 1989), the strongest fluorescence signal comes from the central part of the rhabdomere when measuring Ca_{rh}. In this Chapter it is assumed that the quantified Ca_{rh} values represent the concentration at the midpoint of the modeled microvilli, being 0.55 μm away from both the distal tip and the neck.

Ca_{rh} increases shortly after the onset of the illumination, due to Ca^{2+} influx. Using the model outlined above, the Ca^{2+} influx through the light-activated channels was calculated from the changes in Ca_{rh}. All changes in the Ca^{2+} concentration due to diffusion, Ca^{2+} removal by the exchanger and buffering have been taken into account. Following the approach of Postma et al. (1999), the calculated Ca^{2+} influx is then converted into a light-induced permeability value. From the known ratios of relative permeabilities of the Na^+, K^+ and Mg^{2+} ions (Reuss et al., 1997) the fluxes of these ions can be calculated as well. The time course of the total current, I_{tot}, then follows as the current through the light-activated channels plus the other currents produced by the Na^+/Ca^{2+} exchanger, the Na^+/K^+ pump, the resting conductances and the voltage dependent K^+ channels. The total current I_{tot}

then allows to calculate the change in membrane potential that can subsequently be compared with the measured membrane potential. The formulae for implementing this model are given in the Appendix.

The chosen approach is the reverse of that taken by Gerster (1997) who derives the changes in ion concentrations from the membrane potential, via a calculation of the light-induced permeability. Initial trials quickly showed that this alternative approach is not feasible, as the membrane potential in the recordings used here approaches the equilibrium potential of the light-induced current, making it impossible to calculate meaningful values for the light-induced permeability under these conditions.

Results

Calculating the membrane potential from the time course of Ca^{2+} concentrations in the rhabdomere

The first aim of this study was to establish that the model can be used to calculate the membrane potential from the Ca^{2+} concentration in the rhabdomere, without making it necessary to choose unlikely values for some of the parameters. It was reasoned that this test is useful, as a failure of the model to reproduce the measured membrane potential would immediately indicate that the model is inadequate. Figure 6.2 shows that a reasonable fit between the calculated and the measured membrane potential can indeed be obtained. The starting point is the measured Ca^{2+} concentration at the midpoint of the microvilli (Figure 6.2a). Ca_{rh} values that exceed 200 μM are not well characterized, due to the saturation of OG5N. Therefore, these values were replaced by a linear increase to a peak at 300 μM, reached 20 ms after the onset of illumination, and a subsequent linear decrease. This time course of Ca_{rh} closely follows the fluorescence traces obtained with the non-saturating Ca^{2+} indicator Fluo5N (Chapter 3). Figure 6.2b shows the calculated currents through the light-activated channels in the rhabdomere. The currents through the other channels and the current generated by the Na^+/Ca^{2+} exchanger are plotted in Figure 6.2c. Together, these currents (Figure 6.2b, c) cause the ion concentrations to change in the rhabdomere and the cell body. Figure 6.2d shows the resulting Ca^{2+} concentrations in 3 places in the rhabdomere and in the cell body; note that the Ca^{2+} concentration in the midpoint of the microvilli is identical to the Ca^{2+} concentration used as the starting point of the calculations (Figure 6.2a). The currents across the membrane (Figure 6.2b, c) also cause a change in the membrane potential (Figure 6.2e). The reasonable match between the calculated and the mea-

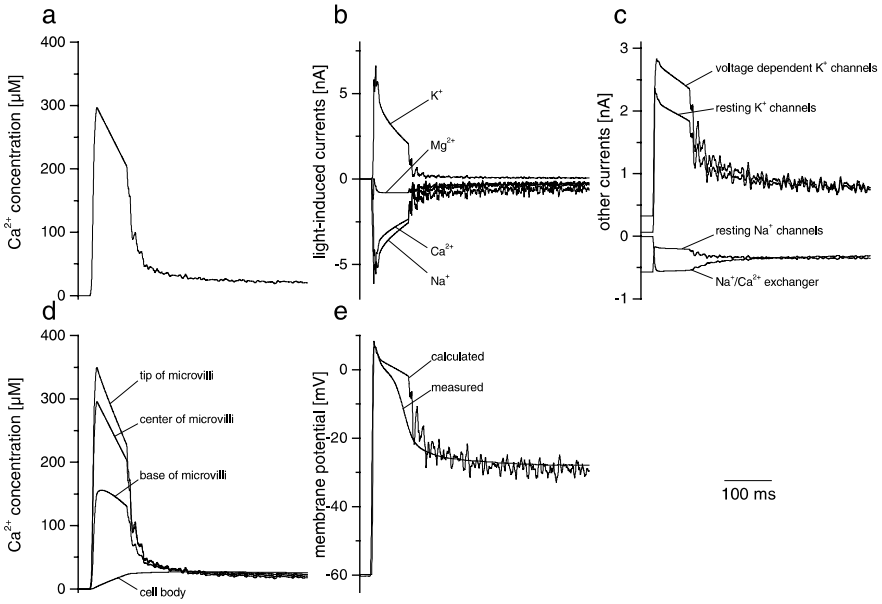

FIGURE 6.2: The model can accurately predict the membrane potential from the time course of Ca_{rh} (a), when the parameters are chosen appropriately. The Ca^{2+} concentration that has been measured in the rhabdomere is taken in modified form (see Results) to represent the free Ca^{2+} concentration in the center of the modeled microvillus (a). In order to achieve this Ca^{2+} concentration during the calculations, the light-activated permeability needs to be varied. This results in cation currents through the light-activated channels (b). Other currents, due to the K^+ and Na^+ channels and the Na^+/Ca^{2+} exchanger also contribute to the total net current that flows across the membrane (c). The ionic currents change the ion concentrations in the rhabdomere and the cell body. The changes in the free Ca^{2+} concentration at the tip of the modeled microvillus, its center and its base, close to the neck is shown in (d), together with the spatially averaged free Ca^{2+} concentration in the cell body. The total net current changes the membrane potential. The calculated membrane potential can be compared with the measured traces (e). The buffer concentration in the rhabdomere for this calculation was 500 μM, and in the cell body 100 μM. The activity of the exchanger was modeled with K_d = 18 μM and $I_{X,\max}$ = -0.55 nA. The trace for Ca_{rh} (a) was smoothed by averaging over a 5 ms time window.

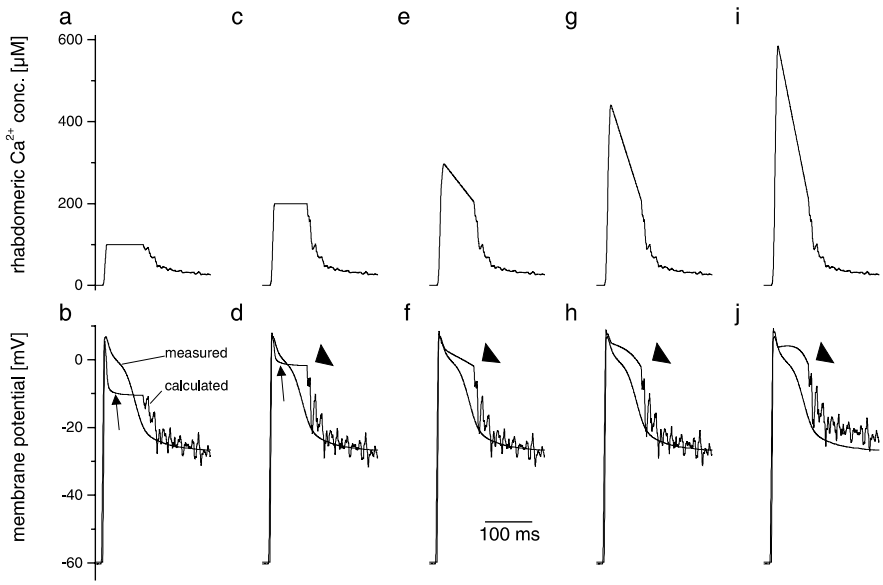

FIGURE 6.3: Only when the Ca^{2+} concentration in the central part of the rhabdomeric microvilli rises to values above 200 μM, the initial part of the calculated and the measured membrane potential fit. The peak Ca^{2+} concentration in the center of the microvillus was varied as shown in the upper row panels. From these traces the membrane potential traces were calculated (lower row panels). In a) and c) the values exceeding 100 μM or 200 μM were set to 100 μM or 200 μM, respectively. The calculated membrane potentials repolarize faster than the measured trace (b, d, arrows). In the other panels, peak values of 300 μM (e, f); 450 μM (g, h) and 600 μM (i, j) were assumed. The calculated membrane potentials repolarize slower than the measured membrane potential (arrow heads). This does, however, not allow to conclude that the Ca^{2+} concentration in the rhabdomere does not reach values that high, as other explanations can be found (see Discussion, Figure 6.11). The parameters of all calculations were identical to those used in Figure 6.2.

sured membrane potential indicates that the model and the parameter set can be used as a working hypothesis and a basis for further investigations. However, the parameter set used in this calculation is not a unique set of parameters that produces acceptable fits between the measured and the calculated membrane potential. In the following, the consequences of varying some of the parameters are explored.

The Ca^{2+} concentration in the rhabdomeric microvilli during the initial transients

Ca_{rh} rises to very high concentrations shortly after the onset of bright illumination, in dark-adapted photoreceptor cells. The Ca^{2+} indicator OG5N, but not the lower affinity indicator Fluo5N, becomes saturated under these conditions (Chapter 3). This finding was interpreted as to indicate that the peak values for Ca_{rh} exceed 200 μM (taking the K_d of OG5N to be 20 μM; Haugland, 1996; Dabdoub and Payne, 1999). This conclusion was tested by modeling the changes of the membrane potential and using time courses for Ca_{rh} that were modified to have lower peak values. In Figure 6.3a, all values of Ca_{rh} exceeding 100 μM were set to 100 μM. The resulting calculated membrane potential remains at values lower than the measured membrane potential during the peak of Ca_{rh} (Figure 6.3b, arrow). In Figure 6.3c, the threshold for the maximal values of Ca_{rh} was set to 200 μM. Again, the calculated membrane potential declines faster (Figure 6.3d. arrow) than the measured membrane potential, and it goes through a stable plateau that is also not seen in the measured trace.

In the remaining panels of Figure 6.3, the time course of Ca_{rh} was modified as described for Figure 6.2a (see above). The peak values were chosen to be 300 μM (Figure 6.3c), 450 μM (Figure 6.3d) and 600 μM (Figure 6.3d). The membrane potential traces calculated from these time courses for Ca_{rh} are shown in Figures 6.3f, h, j. Their initial phase fits the measured membrane potential better than the calculated traces in Figures 6.3b and d (arrows). However, they all show an overestimation of the depolarization after about 100 ms of illumination (arrowheads). This indicates that the necessary influx of Ca^{2+} was overestimated. It is, however, not possible to conclude that this overestimation is caused by assuming too high concentrations for Ca_{rh}, as this can also be explained by an overestimation of Ca^{2+} extrusion via the Na^+/Ca^{2+} exchanger or an overestimation of the diffusion through the neck (see Discussion). Overall, these calculations confirm that the peak concentrations of Ca_{rh} exceed 200 μM.

Properties of the Na^+/Ca^{2+} exchanger

The activity of the Na^+/Ca^{2+} exchanger is modeled to be solely dependent on the local Ca^{2+} concentration with a simple Hill-relationship (rev.: Blaustein and Lederer, 1999). In this relation two parameters, the dissociation constant ($K_{d,X}$) and the maximal current ($I_{X,\max}$), need to be specified. Figure 6.4 shows that $I_{X,\max}$ critically determines the calculated membrane

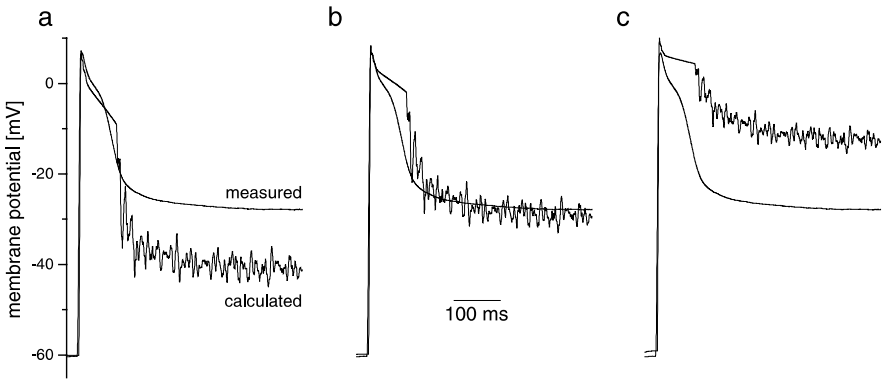

FIGURE 6.4: The current generated by the Na^+/Ca^{2+} exchanger critically determines the quality of the fit between the calculated and the measured membrane potential. Underestimating (a) or overestimating (c) the current generated by the Na^+/Ca^{2+} exchanger changes the calculated membrane potential. The exchanger current in (b) was modeled with a $K_{d,X}$ of 18 μM and a maximal current $I_{X,\max} = -0.55$ nA. In a) $I_{X,\max}$ was reduced to -0.27 nA and in c) increased to -1.1 nA. Other parameters of the calculation were as in Figure 6.2.

potential after the cessation of the initial transients, i.e. after 300-500 ms of illumination. There is no net uptake of Ca^{2+} then, and consequently, an amount equal to the extruded Ca^{2+} must flow in. Setting the current generated by exchanger to half (Figure 6.4a) or twice (Figure 6.4c) its original value (Figure 6.4b) yields membrane potentials that are quite incompatible with the measured membrane potential. For 6 cells investigated, on average a current of -0.35 nA ($\pm$ 0.09 nA SD) generated by the exchanger 500 ms after the onset of illumination produced good fits. The average Ca^{2+} concentration in the rhabdomere was 23 μM ($\pm$ 6 μM SD). When taking the dissociation constant to be $K_{d,X} = 18$ μM (Hardie, 1995a; see above), the corresponding maximal current ($I_{X,\max}$) then is -0.62 nA.

The affinity of the exchanger's transport site for Ca^{2+}, expressed as $K_{d,X}$, on the other hand can be largely varied without much deterioration of the fits. Figure 6.5a shows that reducing the $K_{d,X}$ to 2 μM does not visibly improve the fit between the calculated and the measured membrane potentials. Increasing the $K_{d,X}$ to 50 μM deteriorates the fit somewhat at the transition between peak and plateau of the membrane potential (Figure 6.5c, arrow). These calculations show that a K_d for the exchanger as high as 18 μM is

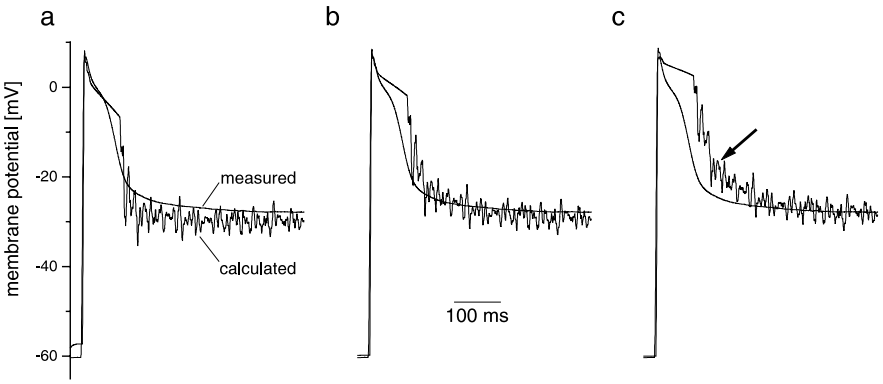

FIGURE 6.5: Low affinities between Ca^{2+} ions and the Ca^{2+} transport site of the Na^+/Ca^{2+} exchanger are consistent with the data. Changing the Ca^{2+} affinity of the exchanger ($K_{d,X}$) from 2 μM (a) to 18 μM (b) or to 50 μM (c) changes the calculated membrane potential only slightly. The only discernible effect is that the calculated membrane potential repolarizes somewhat slower when the dissociation constant ($K_{d,X}$) of the Na^+/Ca^{2+} exchanger is high (c, arrow). Panel b) is identical to Figure 6.4b and is reproduced for comparison. $I_{X,\max}$ was adjusted to roughly yield the same depolarization after 500 ms of illumination (a: $I_{X,\max} = -0.31$ nA; b: $I_{X,\max} = -0.55$ nA; c: $I_{X,\max} = -1.0$ nA); other parameters were as in Figure 6.2.

consistent with the available data. The current generated by the exchanger after 500 ms of illumination has to be -0.35 nA in order to extrude all the Ca^{2+} flowing in at that moment. This corresponds to a Ca^{2+} influx through the light activated channels of -0.7 nA.

The concentration of Ca^{2+} buffers in cell body

The amount of Ca^{2+} buffering in photoreceptor cells is an important question for understanding the Ca^{2+} homeostasis in these cells, since this value has important consequences for the distribution of the Ca^{2+} concentration in the cell body (Chapter 4). It was therefore attempted to estimate an upper bound for the concentration of the Ca^{2+} buffer in the cell body. Using high buffer concentrations (> 1 mM) depleted the extracellular space in the rhabdomere within 50 ms of illumination (data not shown), causing the physically impossible situation where more Ca^{2+} influx was required for reaching the measured value of Ca_{rh} than could be provided from the extracellular space. This implies that the concentration of intracellular Ca^{2+} buffer cannot be higher than 1 mM in all cells of the retina.

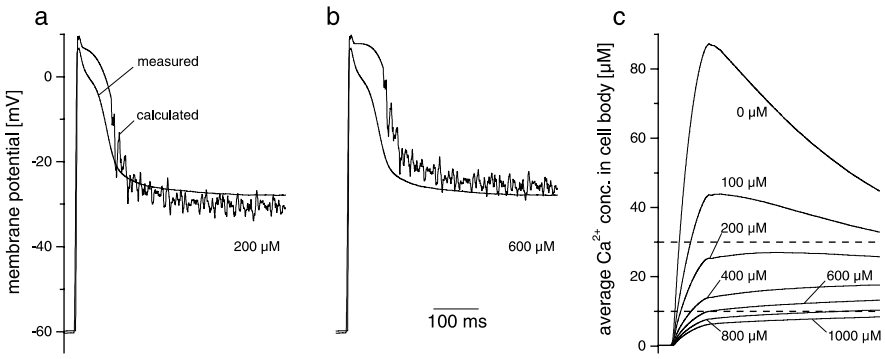

FIGURE 6.6: The effects of different concentrations of Ca^{2+} buffer in the cell body. Varying the buffer concentration in the cell body from 200 μM (a) to 600 μM (b) changes the calculated membrane potential, but not in a way that can be distinguished from varying other parameters (Figures 6.3, 6.4, 6.11). However, the calculated spatially averaged free Ca^{2+} concentration in the cell body (c) is strongly dependent on the assumed buffer concentration. The dashed lines indicate the range of values that are compatible with earlier measurements (Chapters 2-4). This allows to conclude that the buffer concentration in the cell body does not exceed 800 μM. Buffer concentrations lower than 200 μM can however be consistent with the available data (see Discussion, Figure 6.11). The parameters of the calculations were as in Figure 6.3i and j, except that the extracellular Ca^{2+} concentration was kept constant at 1.4 mM.

This, however, does not rule out the possibility that the concentration of Ca^{2+} buffers is higher in the investigated cell compared to the other cells in the retina, due to the added Ca^{2+} indicator. In order to estimate an upper bound for the buffer concentration in the cell that was injected with indicator, the peak of Ca_{rh} was set to 600 μM (as in Figure 6.3i), in order to maximize the diffusional influx into the cell body. It was further assumed that the Ca^{2+} concentration in the extracellular space of the rhabdomere does not change. Figures 6.6a and b show that the influence of the Ca^{2+} buffer on the calculated membrane potential is not very large. It is therefore not possible to determine the concentrations of the buffer by comparing the calculated and the measured membrane potential. However, the concentration of the buffer has a profound influence on the free Ca^{2+} concentration in the cell body. Figure 6.6c shows the spatially averaged concentration for different concentrations of Ca^{2+} buffer. At buffer concentrations of 100 μM or less, the Ca^{2+} concentration in the cell body rises very quickly, in the first 100 ms of illumination to peak at more than 40 μM. During the subsequent

decline Ca^{2+} ions diffuse in the reverse direction, from the cell body into the rhabdomere where they are extruded by the exchanger. At buffer concentrations above 800 μM, the free Ca^{2+} concentration in the cell body only rises monotonically, not reaching even 10 μM after 500 ms of illumination. These calculated data can be compared with measurements of Ca^{2+} induced fluorescence obtained from the whole cell (Chapters 2, 3) and from different locations across the cell body (Chapter 4). From these measurements, it can be concluded that the Ca^{2+} concentration in the cell body reaches more than 10 μM in less than 500 ms. This indicates that the buffer concentration in the cell body, including the artificially added Ca^{2+} indicator, does not exceed 800 μM. With these data it is not possible to obtain an estimate for the lower bound of the concentration of the Ca^{2+} buffer in the cell body, as (1) the free Ca^{2+} concentration in the rhabdomere might have been overestimated (Figure 6.3) and (2) the diffusion across the neck might be more restricted than assumed here (see Discussion).

The concentration of Ca^{2+} buffer in the rhabdomere

In *Drosophila*, calmodulin was found to be present at 0.5 mM in the rhabdomeres (Porter et al., 1993). With 4 Ca^{2+}-binding sites per calmodulin molecule this indicates the presence of 2.0 mM Ca^{2+}-binding sites, being a considerable Ca^{2+} buffer. In order to investigate how much Ca^{2+} buffer is present in the rhabdomeres of *Calliphora* photoreceptors, the membrane potential was calculated from the measured time course of Ca_{rh} as before (Figures 6.2 - 6.6) and the assumed concentration of Ca^{2+} buffer in the rhabdomere was varied (Figure 6.7). The higher the assumed concentration of the buffer, the faster the membrane potential depolarizes. This can be readily understood considering that the buffer must first be filled before the Ca^{2+} concentrations can rise to values higher than 200 μM. The extra Ca^{2+} influx for filling the buffer depolarizes the membrane more rapidly. When comparing the calculated traces with the measured membrane potential, it is immediately apparent that the measured membrane potential depolarizes 2-3 ms earlier than the calculated traces. This delay between the measured and calculated membrane potential is caused by the delayed onset of the increase of the fluorescence intensity described in Chapter 3 (see also Hardie, 1996a; Walz et al., 1994). The cause of this delay is not well understood (see Discussion in Chapter 3), but it is accentuated by the influence of the voltage-gated Ca^{2+} channels in the synaptic terminals (Weckström et al., 1992). These channels depolarize the membrane potential more rapidly and

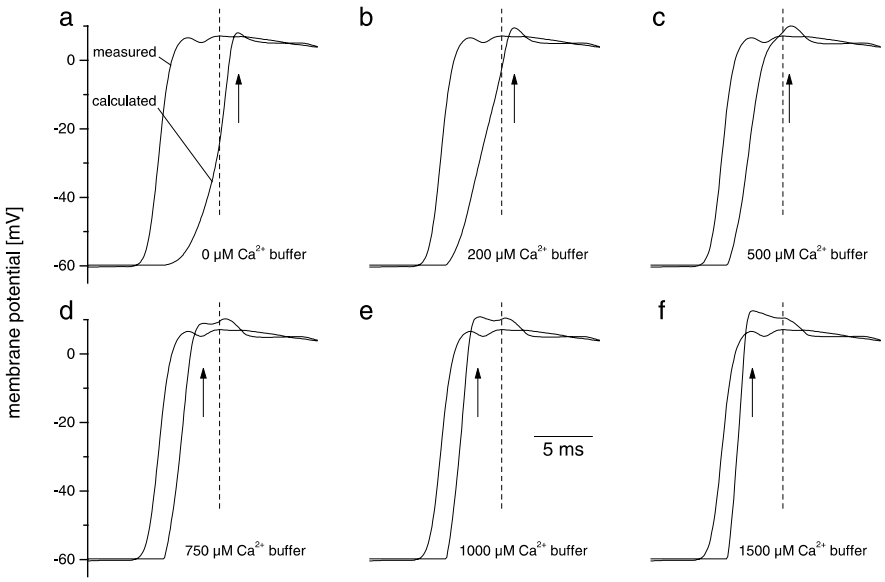

FIGURE 6.7: The concentration of Ca^{2+} buffer in the rhabdomere determines the speed of depolarization of the membrane potential at the onset of the light stimulus. The concentration of the Ca^{2+} buffer in the rhabdomere was varied as indicated in the figures. The time to peak in the calculated membrane potential (arrows) shortens as the buffer concentration increases. Comparing these traces with the measured membrane potential is complicated by 2 factors: 1. The measured membrane potential is distorted by voltage-gated Ca^{2+} channels in the axon terminals (Weckström et al., 1992). This produces the double peak, the second peak (dashed lines) being caused by the light induced currents. 2. The measured membrane potential depolarizes 2-3 ms earlier than the fluorescence signal from the Ca^{2+} indicator increases (Chapter 3). This causes the delay between the measured and calculated membrane potential. It can be concluded that the concentration of the Ca^{2+} buffer in the rhabdomere is higher than 500 μM and does not exceed 1000 μM (see Results for details). The parameters of the calculations were as in Figure 6.2, except that Ca_{rh} was smoothed by averaging over a 1 ms time window.

cause the double peak of the membrane potential visible in Figure 6.7. The first peak is thought to be caused by the voltage-dependent Ca^{2+} channels in the presynaptic terminal (Weckström et al., 1992); the peak of the membrane potential that can be attributed to the light-induced current occurs $\sim$3 ms later (Figure 6.7, dashed lines). The peak of the calculated membrane potential occurs around the same time as the second peak (dashed line) when assuming that 500-750 μM Ca^{2+} buffer is present in the rhabdomere (Fig-

ure 6.7c, d), while it takes substantially more (or less) time when assuming less (or more) Ca^{2+} buffer, respectively (Figure 6.7). This indicates that in the rhabdomere 500-750 μM Ca^{2+} buffer is present. The 2-3 ms delay at the onset of depolarization does not significantly corrupt this conclusion. For short periods, the change of Ca_{rh} is an integral of the fraction of the light-activated current that is carried by Ca^{2+}, while the change of the membrane potential is proportional to the integral of the total light-activated current. It is therefore not critical how long it takes to reach the peak of the membrane potential or that of Ca_{rh}. In other words: if there was more Ca^{2+} buffer in the rhabdomere, the peak of the membrane potential that is caused by the light-activated current, would need to occur earlier than is observed. This argument neglects the contribution of the voltage dependent K^+ channels during the period where the measured membrane potential is higher than the calculated value. It can, however, be estimated that the current through the voltage dependent K^+ channels is less than 30% of the Ca^{2+} current through the light-activated channels during the 6 ms before the calculated membrane potential reaches similar values as the measured traces. It seems therefore likely that the concentration of Ca^{2+} buffer in the rhabdomere is below 1 mM; the best fits are obtained with values between 500 and 750 μM.

It could be argued that additional Ca^{2+} buffers with slower binding kinetics are present. However, the binding kinetics of calmodulin are fast enough to justify the assumption of instantaneous buffering (Martin et al., 1992; see also Postma et al., 1999). Equally, the kinetics of the indicator OG5N, which might contribute to the Ca^{2+} buffer in the rhabdomere, is likely to be fast, since the structurally very similar calcium indicator Calcium Orange 5N has been shown to have very fast binding kinetics (Escobar et al., 1995).

Changes in the free Ca^{2+} concentration in the extracellular rhabdomere

The large changes in free Ca^{2+} concentration in the rhabdomeric microvilli (Chapter 3; Postma et al., 1999) are partly due to the very small internal volume of these structures. The extracellular space in the rhabdomere, however, is still smaller, and therefore considerable changes of the free Ca^{2+} concentration in the extracellular space of the rhabdomere can be expected. In order to quantitatively assess these changes, the very low affinity Ca^{2+} indicator XR5N (K_d = 350 μM) was applied to the extracellular space of the fly retina. Injecting this indicator gives a faint red fluorescence that is strongest in the deep pseudopupil. Figure 6.8a shows that the intensity of the fluorescence from the deep pseudopupil of a dark-adapted fly decreases

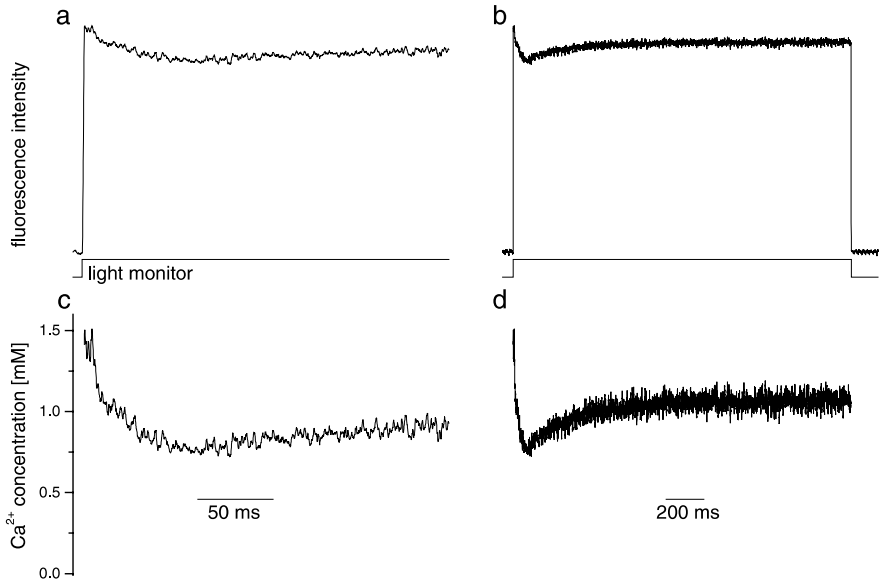

FIGURE 6.8: The Ca^{2+} concentration in the extracellular space of the rhabdomere decreases quickly after the onset of light stimulation. The fluorescence intensity of the very low affinity Ca^{2+} indicator XR5N was measured from the deep-pseudopupil, after XR5N was injected into the extracellular space of the eye (a, b). From this trace, the change in Ca^{2+} concentration can be calculated (c, d; see text for details). Shortly after light onset, the Ca^{2+} concentration decreases from 1.4 mM to 0.8 mM after ~70 ms and then recovers to 1.1 mM. The sampling rate was 10 kHz and the data were subsequently smoothed by averaging over a 1 ms time window (10 consecutive values).

shortly after the onset of the light. It reaches a minimum ~70 ms later and then partially recovers (Figure 6.8b). Recordings obtained from similar experiments showed similar time courses but were quantitatively different. The recording in Figure 6.8a and b was chosen because it showed the largest modulation of fluorescence intensity. Figure 6.8c and d shows the free Ca^{2+} concentrations that have been calculated from the fluorescence intensity values (Figure 6.8a and b) as detailed in Material and Methods.

The measured time course of the extracellular Ca^{2+} concentration in the rhabdomere can be compared with traces that have been calculated with the model. Similar as for the intracellular Ca_{rh} (see Materials and Methods), most of the signal from the rhabdomere should come from its central part.

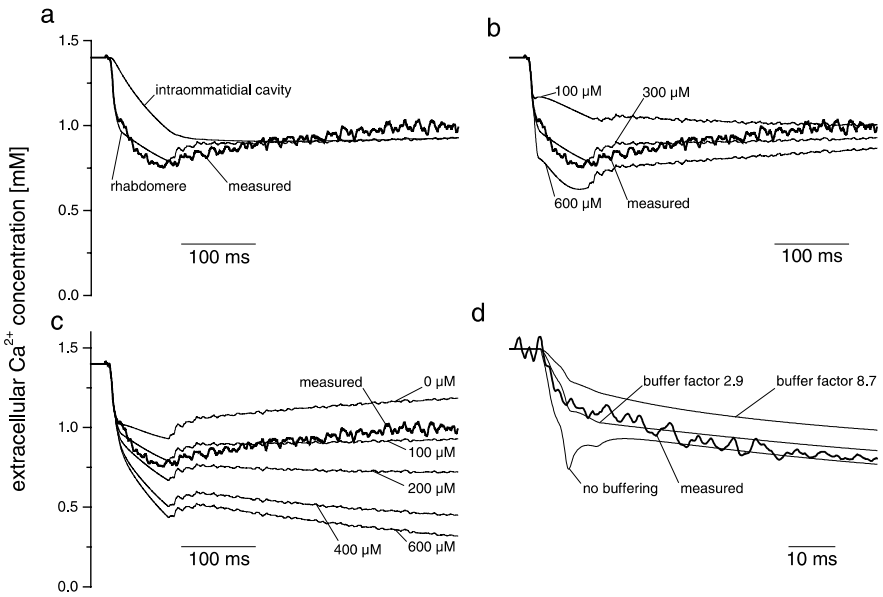

FIGURE 6.9: Comparison between the predictions of the model and the measured time course of the extracellular Ca^{2+} concentration in the rhabdomere (thick line in all panels). The calculations in this figure were performed with the parameters used in Figure 6.2; in the panels b)-d), one of these parameters was changed as described below. a) The predicted time course for the Ca^{2+} concentration in the center of the rhabdomere fits the experimental data better than the predicted time course for the Ca^{2+} concentration in the intraommatidial cavity. This indicates that a large part of the signal measured in Figure 6.8 indeed originates from the rhabdomeres. b) The assumed peak concentration of the Ca^{2+} concentration in the rhabdomeric microvilli (traces as in Figure 6.2a, e, i) influences the predicted change in extracellular Ca^{2+} concentration in the rhabdomere. The best fit is obtained with peak values of $\sim$300 μM for the intramicrovillar Ca^{2+} concentration. c) The concentration of Ca^{2+} buffer in the cell body strongly influences the changes calculated for the extracellular Ca^{2+} concentration in the rhabdomere. High Ca^{2+} buffer concentrations in the cell body reduce the extracellular concentration present after 500 ms illuminations. The calculations that best fit the measured trace are obtained assuming 100 μM Ca^{2+} buffer concentrations in the cell body. d) The amount of extracellular buffering determines the speed of decrease of the Ca^{2+} concentration in the extracellular rhabdomere. Assuming no buffering leads to calculated time courses that show a minimum $\sim$7 ms after light onset. Such a peak is not seen in the measured trace. Conversely, assuming buffering to be 3 times more effective than what is predicted from the properties of the phospholipid membranes (see text), slows down the decrease of the Ca^{2+} concentration in the extracellular rhabdomere. In panels a)-c) Ca_{rh} was smoothed by averaging over a 5 ms time window, in d) with a 1 ms time window.

This conclusion is supported by the calculations shown in Figure 6.9a. Using the same parameter set as in Figure 6.2 a reasonable fit can be obtained also for the extracellular Ca^{2+} concentration in the rhabdomere. The calculated change in the intraommatidial cavity, on the other hand, displays distinctly slower kinetics. Therefore, a large part of the fluorescence signal stems from the extracellular region within the rhabdomere.

The peak concentration assumed for Ca_{rh} has a profound effect on the calculated changes of the extracellular Ca^{2+} concentration in the rhabdomere (Figure 6.9b). There, the best fit was obtained when assuming that Ca_{rh} rises to values between 300 and 450 μM. It is however conceivable that the diffusion through the neck was overestimated in these calculations, and reducing the diffusion through the neck could allow for higher peak values of Ca_{rh} (see Discussion). Equally, the calculated change in the extracellular rhabdomeric Ca^{2+} concentration strongly depends on the assumed concentration of Ca^{2+} buffers in the cell body (Figure 6.9c); the best fits are obtained with $\sim$100 μM Ca^{2+} buffer in the cell body. The Ca^{2+} buffer in the extracellular space of the rhabdomere is taken to be linear and instantaneous with a buffering ratio of 2.9 (see above). Figure 6.9d shows that this value is reasonable, as neglecting this buffer makes the calculations show a negative peak shortly after light onset. Equally, increasing the buffering ratio by a factor of 3 makes the decrease in extracellular Ca^{2+} concentration to be considerably slower than the measured trace. In these calculations, however, the effect of the Ca^{2+} indicator was not taken into account, as its effective concentration is not known.

Changes in the extracellular K^+ concentration

Potassium ions leave the photoreceptor cells during light stimulation through the light activated channels, as they also are permeable for K^+ (Reuss et al., 1997). Mainly however, they leave the photoreceptor cells through the voltage-dependent channels and possibly through a resting, voltage-independent potassium conductance, as modeled here. Because the extracellular space is considerably smaller than the intracellular space (Sandler and Kirschfeld, 1991) and the resting extracellular K^+ concentration is low, a considerable increase in the extracellular K^+ concentration can be expected. Measurements with ion-selective electrodes have indeed shown that illumination causes K^+ to accumulate in the extracellular space of the retina (Sandler and Kirschfeld, 1991; Coles et al., 1985). Besides photoreceptor cells, the fly retina contains glial cells, the so-called secondary pigment cells.

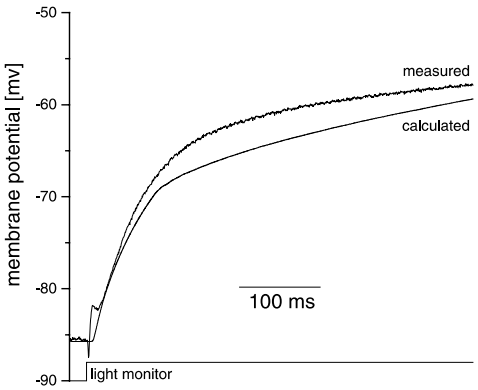

FIGURE 6.10: The membrane potential of the glial cells follows the calculated change of the K^+ Nernst potential. The eye was stimulated with bright light that passed through a NAL 575 nm filter, and the change of the membrane potential of a glial cell was measured. The K^+ Nernst potential was calculated with the K^+ concentration in the intraommatidial cavity and assuming the intracellular K^+ concentration in the glial cells to be constant at 120 mM. The parameters used for the calculation were identical to those used in Figure 6.2.

Upon illumination of the eye, these cells show a much slower and smaller depolarization compared to the photoreceptor cells (Hochstrate, 1989). The resting potential in these cells is $\sim$25 mV lower than in the photoreceptor cells, which yields an absolute potential of -85 mV. This in excellent agreement with the assumed potassium Nernst potential $E_K = -86$ mV (K_o = 4 mM; $K_i = 140$ mM; Weckström et al., 1991), indicating that the membrane potential of the glial cells is determined by E_K. In order to assess the change of E_K induced by light stimulation, the membrane potential of glial cells was recorded. In Figure 6.10 the membrane potential of a glial cell during strong illumination is compared with E_K calculated by taking the calculated changes of the extracellular K^+ concentration in the intraommatidial cavity and assuming a constant intracellular K^+ concentration of 120 mM. The time courses of the two curves match reasonably well. This can be taken as an indication that the assumed values for the ratio of intra- to extracellular volume of 6.3 (Hamdorf, cited in Sandler and Kirschfeld, 1991) and for the K^+ currents through the ion channels are not unrealistic.

Discussion

In this Chapter, a model based on the physiology of fly photoreceptor cells is developed. It takes into account the geometry of the cells and the known mechanisms that allow ions to enter or leave the cells. Generally, an advantage of such a model is that it allows to investigate the validity of the underlying assumptions and to predict the time course of physical parameters

that are difficult to measure directly. Accordingly, the main result of this Chapter is that the model can, despite its limitations and simplifications, calculate the change of the membrane potential with reasonable accuracy, starting from the Ca^{2+} concentration in the rhabdomere, thus confirming that the underlying assumptions are consistent. Furthermore, the model seems to reproduce reasonably well the measured changes in extracellular Ca^{2+} concentration in the rhabdomere (Figures 6.8, 6.9) and the K^+ Nernst potential (Figure 6.10). By varying the relevant parameters of the model, it was possible to constrain the range of the concentration of Ca^{2+} buffers to 0.5-1 mM in the rhabdomere, and to less than 800 μM in the cell body of cells that were injected with the Ca^{2+} indicator OG5N.

The diffusion from the microvilli through the neck into the cell body

The connection between the microvilli and the cell body is formed by a narrow neck that was modeled here as a cylinder that is 60 nm long and 35 nm in diameter (Postma et al., 1999). In anatomical pictures, however, the neck sometimes appears to be narrower (e.g. Walz, 1982). It furthermore contains an actin filament and the dense, membranous subrhabdomeric cisternae (SRC) are located at its mouth on the side of the cell body (Walz, 1982; Arikawa et al., 1990; Suzuki et al., 1993). Hence, diffusion through the neck might be more restricted than was assumed in the calculations presented above.

When running the model with reduced diffusion through the neck, the calculated membrane potential did not change substantially (Figure 6.11). Even reducing the diffusion to 14% of its original value did not compromise the quality of the fit. Reducing the diffusion further to 7% of its original value, however, induces visible deviations (data not shown). The relative stability of the calculations with respect to the diffusion through the neck can be explained by considering that under conditions where diffusion through the neck is assumed to be fast, a high Ca^{2+} concentration builds up in the region of the cell body where the rhabdomeric microvilli are connected. This Ca^{2+} accumulation then diminishes the diffusion through the neck in a similar way as occurs when reducing the speed of diffusion geometrically. Reducing the diffusion through the neck, however, puts more stringent constraints on the concentration of the Ca^{2+} buffer in the cell body. In order to achieve a spatially averaged concentration of 10 μM after 500 ms (see above; Figure 6.6) with the diffusion through the neck reduced to 14% of the original value, the concentration of Ca^{2+} buffer in the cell body must not exceed 300 μM (data

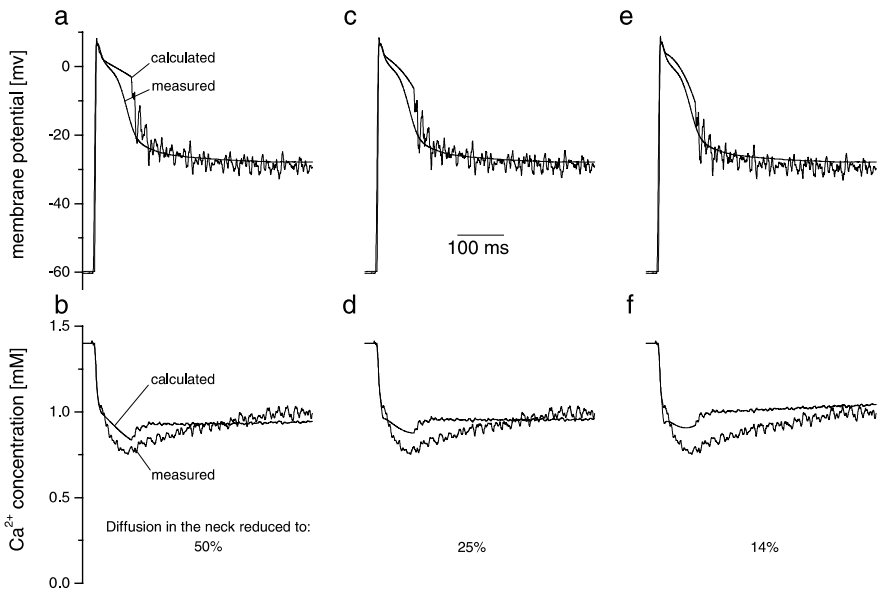

FIGURE 6.11: The effect of reducing the diffusion rate through the neck on the calculated membrane potential and Ca^{2+} concentration in the extracellular space of the rhabdomere. The diffusion through the neck was reduced to 50% (a, b), 25% (c, d) or 14% (e, f) of the value used in all previous Figures. The calculations were performed assuming the peak Ca^{2+} concentration in the rhabdomeric microvilli to reach 300 μM (a, b; same trace for Ca_{rh} as in Figure 6.3e), 450 μM (c, d; same trace for Ca_{rh} as in Figure 6.3g), or 600 μM (e, f; same trace for Ca_{rh} as in Figure 6.3i). Ca^{2+} buffer in the cell body was assumed to be 100 μM (a-d) or 50 μM (e, f). All other parameters were as in Figure 6.2. Reducing the diffusion through the neck does not deteriorate the fit between the calculated and the measured membrane potential. This also demonstrates that Ca^{2+} concentrations in the microvilli as high as 600 μM are not incompatible with the measured data (Figure 6.3; see text). Reduced diffusion through the neck, however, results in worse fits between the calculated and measured Ca^{2+} concentration in the extracellular rhabdomere (d, f).

not shown). Figure 6.11 also shows that the time course of the extracellular Ca^{2+} concentration in the rhabdomere is strongly dependent on the assumed diffusion through the neck. Judging from the extracellular Ca^{2+} concentration data, a reduction in diffusion to 14% seems to be too much, with values between 33% and 100% (no reduction in diffusion) giving better fits.

The concentration of Ca^{2+} buffers in different compartments of the photoreceptor cell

A previous study in *Drosophila* indicated that less than 1% of the inflowing Ca^{2+} appears in the cell body as free Ca^{2+}, the rest being buffered or extruded (Hardie, 1996a). In *Calliphora* photoreceptor cells, comparing the intracellular increase in free Ca^{2+} with the extracellular decrease under similar illumination conditions (Sandler and Kirschfeld, 1988) led to the conclusion that much less Ca^{2+} buffering takes place (Chapter 2). The results presented here indicate that as much as 600 μM of endogenous buffer could be present in the photoreceptor cells without totally depleting the extracellular Ca^{2+}. However, such high Ca^{2+} concentrations are not compatible with the measurements of the extracellular Ca^{2+} concentration in the rhabdomere. These measurements indicate that the endogenous intracellular Ca^{2+} buffer concentration does not exceed 100 μM (Figure 6.9c). The latter estimate, however, does not take into account that the proteins present in the intraommatidial matrix might represent a significant Ca^{2+} buffer. Additional Ca^{2+} buffering in the intraommatidial matrix would allow for higher concentrations of Ca^{2+} buffers in the cell body.

Filling the photoreceptor cells with a fluorescent Ca^{2+} indicator increases the amount of Ca^{2+} buffers. Comparing the increases in the average Ca^{2+} concentration in the cell body with measured data (Chapters 2, 4) indicates that the total concentration of buffers, endogenous plus the added indicator, does not exceed 800 μM.

The concentration of Ca^{2+} buffers in the rhabdomere could be estimated to be between 500 and 1000 μM. This estimate, being obtained from *Calliphora* photoreceptor cells, is slightly lower than one can expect from the 2.0 mM Ca^{2+}-binding sites of calmodulin that have been reported for *Drosophila* rhabdomeres (Porter et al., 1993). It is unclear, how much of the buffer capacity estimated in this Chapter is endogenous. Taking the buffer concentration in the cell body to be 800 μM, only 100 μM of which is endogenous, as much as 700 μM of the buffer in the rhabdomere could arise from the added Ca^{2+} indicator. On the other hand, it is conceivable that the concentration of the Ca^{2+} indicator in the rhabdomere is much lower than in the cell body, due to restricted diffusion at the neck. In this scenario, almost all of the buffer in the rhabdomere could be endogenous.

Changes in extracellular ion concentrations

While it has long been appreciated that changes in intracellular Ca^{2+} concentration can carry important signals, the same could be true for changes in extracellular Ca^{2+} concentration, as has been suggested on the basis of theoretical considerations (Edelman and Montague, 1999). Recently, experimental evidence has been provided that depletion in extracellular Ca^{2+} in the narrow synaptic cleft can be a factor determining the transmission efficiency of synapses (Borst et al., 1999). In the limited extracellular space of insect photoreceptors, changes in the free Ca^{2+} concentration have been reported repeatedly (Sandler and Kirschfeld, 1988, 1991; Ziegler and Walz, 1989; Peretz et al., 1994a). However, the geometry of the rhabdomere suggests that Ca^{2+} concentration changes in the extracellular space surrounding the microvilli might be more pronounced. Furthermore, the changes might occur on a time scale that cannot be resolved with ion-selective electrodes, the preferred means of measuring extracellular Ca^{2+} previously. Employing very low affinity fluorescent Ca^{2+} indicators, such fast changes are demonstrated here (Figure 6.8). The time course of the measured changes and the changes predicted by the model match well (Figure 6.9). While both modeling and experiment show the existence of fast and pronounced changes in the extracellular Ca^{2+} concentration in the rhabdomere, it must remain open whether these changes have a physiological significance, for example in limiting the current through the light-activated channels and thereby enhancing light adaptation.

The changes in the extracellular K^+ concentration predicted by the model compare reasonably with the measured changes in the membrane potential of glial cells, provided that the membrane potential of these cells is governed by the potassium Nernst potential E_K (Figure 6.10). This finding supports the values that have been assumed for the volume of the extracellular space and the strength of the potassium currents. It also lends credibility to the estimates calculated with the model for changes in the concentration of other ions. For example, the model predicts that the extracellular Na^+ concentration changes only in small amounts, in the intraommatidial cavity and in the rhabdomere. After 500 ms of illumination, the extracellular Na^+ concentration decreases (for the calculation shown in Figure 6.3i, j) only by 14 mM, from 140 mM to 126 mM. The corresponding rise in intracellular Na^+ is even more modest, from 10 mM to 12 mM. This indicates that, at least for illuminations as short as 500 ms, the Na^+ Nernst potential does not collapse; it remains sufficiently high for driving a Na^+/Ca^{2+} exchanger with a

3:1 stoichiometry. For estimating the Na^+ concentration during longer light stimulation, it would be necessary to take into account the activation of the Na^+/K^+ pump (Gerster et al., 1997) that has been neglected here.

Conclusion

The model presented here integrates the current knowledge about the electrical components of *Calliphora* photoreceptor cells. It shows that the assumptions are quantitatively consistent, and it allows to make predictions about parameter values that have not been determined. Equally important, it shows where the present knowledge is not yet sufficient, as exemplified by the equivocal results that can be obtained with largely differing values for the speed of diffusion in the neck. It is hoped that this model provides a framework for testing hypotheses and interpreting future results. It may even help designing future experiments in order to better understand the functioning of this cell type.

Appendix

In the following, the formulae used for implementing the model are given. The forward Euler method was used for time integration. The time step typically was chosen to be $\Delta t = 10\ \mu$s; smaller time steps did not change the result of the calculations.

Diffusion in the microvillus

Diffusion in the microvillus is modeled as described by Postma et al. (1999). The microvillus is divided in n_{mv} compartments of equal length (typically, $n_{\mathrm{mv}} = 6$). The concentration of ions is determined at the borders of the compartments, thus on $n_{\mathrm{mv}} + 1$ points. The volume associated with point x, v^x_{mv}, is given by the volume of the microvillus divided by n_{mv}, for $1 < x < n_{\mathrm{mv}} + 1$. The volume associated with the point located at the tip of the microvillus, v^1_{mv}, is half the value of other compartments. Also, the volume associated with the point that is closest to the neck, $v^{n_{\mathrm{mv}}+1}_{\mathrm{mv}}$, is assumed to be the same as v^1_{mv} plus the volume of the entire neck. The diffusional fluxes in the microvillus can be expressed for each ion type q as currents $I_{q,D}$:

$$I_{q,D}^{x,t} = \begin{cases} \rho_{q,\mathrm{mv}} O_{\mathrm{mv}} \left(C_{q,f}^{x+1,t} - C_{q,f}^{x,t} \right) & \text{for } x = 1 \\ \rho_{q,\mathrm{mv}} O_{\mathrm{mv}} \left(C_{q,f}^{x+1,t} + C_{q,f}^{x-1,t} - 2C_{q,f}^{x,t} \right) & \text{for } 1 < x \leq n_{\mathrm{mv}} \\ \rho_{q.\mathrm{mv}} O_{\mathrm{mv}} \left(C_{q,f}^{x-1,t} - C_{q,f}^{x,t} \right) & \text{for } x = n_{\mathrm{mv}} + 1 \end{cases}$$

$C_{q,f}$ indicates the free concentration of ion type q, O_{mv} the surface of the cross-section of the microvillus, and $\rho_{q,\mathrm{mv}} = -D_q z_q F / \Delta x_{\mathrm{mv}}$; F denotes the Faraday constant, Δx_{mv} the length of one compartment of the microvillus and z_q the valence of ion type q.

Diffusion in the extracellular space of the rhabdomere

The extracellular space that surrounds the modeled microvillus is subdivided in an equal amount of compartments (n_{mv}) as the microvillus. Equally, the ion concentrations are calculated on the borders of these compartments, yielding $n_{\mathrm{mv}} + 1$ points. However, the ion concentration at the first point, located at the tip of the microvillus, is also thought to represent the concentration in the larger intraommatidial cavity. Therefore, the volume that is associated with this point (v_{ex}^{1}) is the volume of the intraommatidial cavity plus half of the volume of an extracellular rhabdomeric compartment. Similarly, the point that is closest to the neck has an associated volume ($v_{\mathrm{ex}}^{n_{\mathrm{mv}}+1}$) given by the sum of half of the volume of an extracellular rhabdomeric compartment plus the extracellular volume of the neck region. The formulae for calculating the currents due to extracellular diffusion are given by:

$$I_{q,\mathrm{ex},D}^{x,t} = \begin{cases} \rho_{q,\mathrm{mv}} O_{\mathrm{ex},\mathrm{mv}} \left(C_{q,\mathrm{ex},f}^{x+1,t} - C_{q,\mathrm{ex},f}^{x,t} \right) & \text{for } x = 1 \\ \rho_{q,\mathrm{mv}} O_{\mathrm{ex},\mathrm{mv}} \left(C_{q,\mathrm{ex},f}^{x+1,t} + C_{q,\mathrm{ex},f}^{x-1,t} - 2C_{q,\mathrm{ex},f}^{x,t} \right) & \text{for } 1 < x \leq n_{\mathrm{mv}} \\ \rho_{q,\mathrm{mv}} O_{\mathrm{ex},\mathrm{mv}} \left(C_{q,\mathrm{ex},f}^{x-1,t} - C_{q,\mathrm{ex},f}^{x,t} \right) & \text{for } x = n_{\mathrm{mv}} + 1 \end{cases}$$

The index ex indicates that the symbol represents an extracellular value.

Diffusion in the cell body

Diffusion in the cell body is calculated in two dimensions for the free (index f) and the bound (index b) Ca^{2+} ions. Diffusion is supposed to take place along the x- and the y-axis. The two-dimensional plane is divided in n_{cb} compartments along each axis, with n_{cb} typically equaling 11. This results

in $(n_{\mathrm{cb}}+1)^2$ grid points for each of which the concentration of free and bound Ca^{2+} is calculated. The difference scheme employed assigns a volume to each point that corresponds to the volume of the cell body divided by n_{cb}^2. Points on the border of the modeled cell body are assigned half of this volume, and points in the corner a quarter. Furthermore, the surface through which diffusion takes place is given by $O_{\mathrm{cb}} = (L_{\mathrm{cb}}/n_{\mathrm{cb}})\, L_{\mathrm{pr}}$, where $L_{\mathrm{cb}} = 7.1\ \mu$m is the length of one side and $L_{\mathrm{pr}} = 211\ \mu$m the length of the modeled photoreceptor cell. The distance between two grid-points, Δx_{cb}, is given by L_{cb} divided by n_{cb}. Defining $\rho_{Ca,\mathrm{cb}} = -D_{\mathrm{Ca},g} z_{Ca} F/\Delta x_{\mathrm{cb}}$, the currents due to diffusion (I_D) are given by:

$$I_{D,g}^{x,y,t} = \rho_{\mathrm{Ca,cb}} O_{\mathrm{cb}} \left(C_{\mathrm{Ca},g}^{x,y-1,t} + C_{\mathrm{Ca},g}^{x,y+1,t} + C_{\mathrm{Ca},g}^{x-1,y,t} + C_{\mathrm{Ca},g}^{x+1,y,t} - 4C_{\mathrm{Ca},g}^{x,y,t} \right)$$

for the points defined by x and y that are not on a border of the modeled cell body;

$$I_{D,g}^{x,y,t} = \rho_{\mathrm{Ca,cb}} O_{\mathrm{cb}} \left(\tfrac{1}{2} C_{\mathrm{Ca},g}^{x,y-1,t} + \tfrac{1}{2} C_{\mathrm{Ca},g}^{x,y+1,t} + C_{\mathrm{Ca},g}^{x+1,y,t} - 2C_{\mathrm{Ca},g}^{x,y,t} \right)$$

for points on the border that is defined by $x = 1$. For the other borders, this formula needs to be adjusted by appropriately changing the x- and y-values;

$$I_{D,g}^{x,y,t} = \rho_{\mathrm{Ca,cb}} O_{\mathrm{cb}} \left(\tfrac{1}{2} C_{\mathrm{Ca},g}^{x,y+1,t} + \tfrac{1}{2} C_{\mathrm{Ca},g}^{x+1,y,t} - C_{\mathrm{Ca},g}^{x,y,t} \right)$$

for the point in the corner defined by $x = y = 1$. Again, for the other corners, the indices need to be adjusted. In all cases, the index g can stand for f or b, indicating free or bound Ca^{2+}.

Diffusion across the neck

For the three ion types, Na^+, K^+ and Mg^{2+}, the currents due to diffusion across the neck are given by:

$$I_{q,n}^{t} = \frac{-D_q z_q F}{L_n} O_n N_{\mathrm{mv}} \left(C_q^{x,t} - C_{q,\mathrm{cb}}^{t} \right)$$

where q only represents Na^+, K^+ and Mg^{2+} and $x = n_{\mathrm{mv}} + 1$. $L_n = 60$ nm is the length of the neck, O_n is the surface of a cross-section through the neck and N_{mv} is number of microvilli. Because the free Ca^{2+} concentration can be spatially inhomogeneous, the free Ca^{2+} concentration at the mouth

($C^M_{\mathrm{Ca},f}$) of the neck needs to be taken into account. $C^M_{\mathrm{Ca},f}$ represents the concentration at the center of one side of the modeled cell body:

$$C^{M,t}_{\mathrm{Ca},f} = C^{1,(n_{\mathrm{cb}}+1)/2}_{\mathrm{Ca},f,\mathrm{cb}}$$

Taking again $x = n_{\mathrm{mv}} + 1$, the Ca^{2+} current due to diffusion through the neck ($I_{\mathrm{Ca},n}$) is:

$$I^t_{\mathrm{Ca},n} = \frac{-D_{\mathrm{Ca}} z_{\mathrm{Ca}} F}{L_n} O_n N_{\mathrm{mv}} \left(C^{x,t}_{\mathrm{Ca},f} - C^{M,t}_{\mathrm{Ca},f} \right)$$

Note that these currents are expressed for the whole rhabdomere, as the currents through individual necks are multiplied with the number of microvilli (N_{mv} = 90,000).

The currents across the membrane of the rhabdomeric microvilli

The concentration of free Ca^{2+} in the center of the microvillus (c_{mv}), is assumed to be given by the measured trace $\mathrm{Ca_{rh}}$ (Figures 6.2a, 6.3a, c, e, g, i). The Ca^{2+} influx through the light-activated channels ($I_{\mathrm{Ca},L}$) at the center of the microvillus is adjusted in order to reach the value given by $\mathrm{Ca_{rh}}$ at each time step. $I_{Ca,L}$ can be broken down into three components: the Ca^{2+} current caused by the changing Ca^{2+} concentration ($I_{\Delta\mathrm{Ca}}$), the Ca^{2+} current caused by the exchanger (I_X) and the Ca^{2+} current caused by diffusion (I_D). With $x = c_{\mathrm{mv}}$, this can be written as:

$$I^{x,t}_{\mathrm{Ca},L} = I^{x,t}_{\Delta\mathrm{Ca}} + 2I^{x,t}_X - I^{x,t}_{\mathrm{Ca}.D}$$

where

$$\begin{aligned}
I^{x,t}_{\Delta\mathrm{Ca}} &= \frac{F z_{\mathrm{Ca}} v^x_{\mathrm{mv}}}{\Delta t} \left(C^{x,t}_{\mathrm{Ca,tot}} - C^{x,t+1}_{\mathrm{Ca,tot}} \right) \\
I^{x,t}_X &= \frac{1}{n_{\mathrm{mv}} N_{\mathrm{mv}}} I_{X,\max} \frac{C^{x,t}_{\mathrm{Ca},f}}{C^{x,t}_{\mathrm{Ca},f} + K_{d,X}} \\
I^{x,t}_{\mathrm{Ca},D} &= \frac{-D_{\mathrm{Ca}} z_{\mathrm{Ca}} F}{\Delta x_{\mathrm{mv}}} O_{\mathrm{mv}} \left(C^{x-1,t}_{\mathrm{Ca},f} + C^{x+1,t}_{\mathrm{Ca},f} - 2C^{x,t}_{\mathrm{Ca},f} \right)
\end{aligned}$$

$C_{\mathrm{Ca,tot}}$ is the total Ca^{2+} concentration, calculated as the sum of free ($C_{\mathrm{Ca},f}$) and bound ($C_{\mathrm{Ca},b}$) Ca^{2+} concentrations. $I_{X,\max}$ is the maximal current the exchanger molecules in the cell can generate, and $K_{d,X}$ is the dissociation constant for Ca^{2+} binding to the exchanger. Note that the exchanger always

produces an inward current, and that therefore $I_{X,\max}$ always has negative values.

The light-activated Ca^{2+} current at the center of the microvillus now allows to calculate the light-induced permeability P_L of the light-activated channels (Gerster, 1997; Postma et al., 1999). For these calculations, the Goldman-Hodgkin-Katz equation (Hille, 1992) is assumed to be valid. Again taking $x = c_{\mathrm{mv}}$, P_L is given by:

$$P_L^t = I_{\mathrm{Ca},L}^{x,t} \frac{1 - e^{\beta_{\mathrm{Ca}}^t}}{S_{\mathrm{mv}}^x z_{\mathrm{Ca}} w_{\mathrm{Ca}} \beta_{\mathrm{Ca}}^t F \left(C_{\mathrm{Ca,ex},f}^{x,t} e^{\beta_{\mathrm{Ca}}^t} - C_{\mathrm{Ca},f}^{x,t} \right)}$$

where

$$\beta_{\mathrm{Ca}}^t = \frac{-V_m^t z_{\mathrm{Ca}} F}{RT}$$

S_{mv}^x denotes the microvillar membrane surface associated with point x, V_m the membrane potential, R the molar gas constant and $T = 293$ K the temperature. w_{Ca} (always assumed to be 0.88, the value determined for the *trp*-dependent channels; Reuss et al., 1997) is the relative permeability of the light activated channels for Ca^{2+} (Postma et al., 1999). When Ca_{rh} is very noisy, it can happen that this formalism produces negative values for P_L. In this case, P_L was set to 0.

The light-induced permeability P_L is assumed to be the same along the length of each microvillus (Postma et al., 1999). Therefore, the currents through the light-activated channels $I_{L,q}$ can be obtained for each ion-type q.

$$I_{q,L}^t = \frac{N_{\mathrm{mv}}}{1 - e^{\beta_q^t}} P_L^t z_q w_q \beta_q^t F \sum_{x=1}^{n_{\mathrm{mv}}+1} S_{\mathrm{mv}}^x \left(C_{q,\mathrm{ex},f}^{x,t} e^{\beta_q^t} - C_{q,f}^{x,t} \right)$$

The total light-activated current I_L is the sum of the current carried by each ion-type q:

$$I_L^t = \sum_q I_{q,L}^t = I_{\mathrm{Na},L}^t + I_{\mathrm{K},L}^t + I_{\mathrm{Ca},L}^t + I_{\mathrm{Mg},L}^t$$

Likewise, the total current generated by the exchanger I_X can be obtained by integrating spatially over the length of the microvillus:

$$I_X^t = I_{\mathrm{X,max}} \sum_{x=1}^{n_{\mathrm{mv}}+1} \left(\frac{C_{\mathrm{Ca,f}}^{x,t}}{C_{\mathrm{Ca,f}}^{x,t} + K_{\mathrm{d,X}}} \frac{S_{\mathrm{mv}}^x}{S_{\mathrm{mv}}} \right)$$

The currents across the membrane of the cell body

The concentration of ion type q in the intraommatidial cavity ($C_{q,\mathrm{ic}}$) is assumed identical to the ion concentration at the distal tip of the extracellular part of the rhabdomere:

$$C^t_{q,\mathrm{ic}} = C^{1,t}_{q,\mathrm{ex}}$$

The resting Na^+ and K^+ currents ($I_{\mathrm{Na},R}$ and $I_{\mathrm{K},R}$) are thus given by:

$$I^t_{q,R} = P_{q,R} S_{\mathrm{cb}} z_q \beta^t_q F \frac{C^t_{q,\mathrm{ic}} e^{\beta^t_q} - C^t_{q,\mathrm{cb}}}{1 - e^{\beta^t_q}}$$

where q only represents Na^+ and K^+. $P_{q,R}$ is the permeability of the resting conductance for ion type q. The current through the voltage-gated K^+ channels ($I_{\mathrm{K},V}$), accordingly, is calculated as:

$$I^t_{\mathrm{K},V} = \left(P^t_{\mathrm{K},V,f} + P^t_{\mathrm{K},V,s}\right) S_{\mathrm{cb}} z_{\mathrm{K}} \beta^t_{\mathrm{K}} F \frac{C^t_{\mathrm{K,ic}} e^{\beta^t_{\mathrm{K}}} - C^t_{\mathrm{K,cb}}}{1 - e^{\beta^t_{\mathrm{K}}}}$$

where the permeability for the fast and the slow component ($P_{\mathrm{K},V,f}$ and $P_{\mathrm{K},V,s}$) are calculated as described by Gerster et al. (1997), except for the different values for the maximal permeabilities (see main text). $S_{\mathrm{cb}} = 6.1 \cdot 10^{-9}$ m^2 is the surface of the cell body.

Calculating changes of the membrane potential and of the ion concentrations

I_{tot}, the total current, is calculated as:

$$I^t_{\mathrm{tot}} = I^t_L + I^t_X + I^t_{\mathrm{K},V} + I^t_{\mathrm{K},R} + I^t_{\mathrm{Na},R} + I_P$$

where $I_P = -0.19$ nA is the current generated by the Na^+/K^+ pump. The change in membrane potential is obtained as:

$$\Delta V^t_m = \frac{-1}{c_m S_{\mathrm{tot}}} I^t_{\mathrm{tot}} \Delta t$$

with $c_m = 0.01$ F/m^2 being the specific capacitance and $S_{\mathrm{tot}} = 2.38 \cdot 10^{-8}$ m^2 the total surface of the cell membrane.

Defining $\tau^x_{q,\mathrm{mv}} = \Delta t / (z_q F v^x_{\mathrm{mv}})$, where v^x_{mv} is the volume that is associated with point x in the microvillus, the changes of the concentration of each ion type in the microvillus are calculated with the following equations:

$$
\begin{aligned}
\Delta C^{x,t}_{\mathrm{Na}} &= -\tau^{x}_{\mathrm{Na,mv}} \left(I^{x,t}_{\mathrm{Na},D} + 3I^{x,t}_{X} + I^{x,t}_{\mathrm{Na},L} - \kappa^{x,t}_{\mathrm{Na}} \right) \\
\Delta C^{x,t}_{\mathrm{K}} &= -\tau^{x}_{\mathrm{K,mv}} \left(I^{x,t}_{\mathrm{K},D} + I^{x,t}_{\mathrm{K},L} - \kappa^{x,t}_{\mathrm{K}} \right) \\
\Delta C^{x,t}_{\mathrm{Ca,tot}} &= -\tau^{x}_{\mathrm{Ca,mv}} \left(I^{x,t}_{\mathrm{Ca},D} - 2I^{x,t}_{X} + I^{x,t}_{\mathrm{Ca},L} - \kappa^{x,t}_{\mathrm{Ca}} \right) \\
\Delta C^{x,t}_{\mathrm{Mg}} &= -\tau^{x}_{\mathrm{Mg,mv}} \left(I^{x,t}_{\mathrm{Mg},D} + I^{x,t}_{\mathrm{Mg},L} - \kappa^{x,t}_{\mathrm{Mg}} \right)
\end{aligned}
$$

where

$$
\kappa^{x,t}_{q} = \begin{cases} 0 & \text{for } 1 \leq x < n_{\mathrm{mv}} + 1 \\ I^{t}_{q,n}/N_{\mathrm{mv}} & \text{for } x = n_{\mathrm{mv}} + 1 \end{cases}
$$

As before, the index D indicates currents due to diffusion, the index n the currents due to diffusion through the neck, the index X the current generated by the exchanger and the index L the current through the light-activated channels.

Taking $\tau_{q,\mathrm{cb}} = \Delta t / (z_q F v_{\mathrm{cb}})$, where v_{cb} indicates the total volume of the cell body, the changes of the ionic concentrations in the cell body are calculated as:

$$
\begin{aligned}
\Delta C^{t}_{\mathrm{Na,cb}} &= -\tau_{\mathrm{Na,cb}} \left(I^{t}_{\mathrm{Na},n} + I^{t}_{\mathrm{Na},R} - 3I_P \right) \\
\Delta C^{t}_{\mathrm{K,cb}} &= -\tau_{\mathrm{K,cb}} \left(I^{t}_{\mathrm{K},n} + I^{t}_{\mathrm{K},R} + I^{t}_{\mathrm{K},V} + 2I_P \right) \\
\Delta C^{t}_{\mathrm{Mg,cb}} &= -\tau_{\mathrm{Mg,cb}} I^{t}_{\mathrm{Mg},n}
\end{aligned}
$$

The change of the total Ca^{2+} concentration in the cell body is calculated for each point defined by the indices x and y. v_{cb} therefore becomes $v^{x,y}_{\mathrm{cb}}$ to indicate the volume associated with a point given by x and y; consequently, $\tau_{\mathrm{Ca,cb}}$ becomes $\tau^{x,y}_{\mathrm{Ca,cb}}$:

$$
\Delta C^{x,y,t}_{\mathrm{Ca,tot,cb}} = -\tau^{x,y}_{\mathrm{Ca,cb}} \left(I^{x,y,t}_{D,f} + I^{x,y,t}_{D,b} \right)
$$

For the points that represent the region where the neck of the microvilli connects to the cell body, the current due to diffusion through the neck is added to the currents of the above formula.

For calculating the changes of extracellular ion concentrations, $\tau^{x}_{q,\mathrm{ex}}$ was analogously defined as $\tau^{x}_{q,\mathrm{ex}} = \Delta t / (z_q F v^{x}_{\mathrm{ex}})$, for each point x in the extracellular rhabdomere. The changes in extracellular ion concentrations are consequently (for the entire rhabdomere) given by:

$$\begin{aligned}
\Delta C^{x,t}_{\mathrm{Na,ex}} &= \tau^{x}_{\mathrm{Na,ex}} \left(-I^{x,t}_{\mathrm{Na,ex},D} + 3N_{\mathrm{mv}} I^{x,t}_{X} + N_{\mathrm{mv}} I^{x,t}_{\mathrm{Na},L} + \lambda^{x,t}_{\mathrm{Na}} \right) \\
\Delta C^{x,t}_{\mathrm{K,ex}} &= \tau^{x}_{\mathrm{K,ex}} \left(-I^{x,t}_{\mathrm{K,ex},D} + N_{\mathrm{mv}} I^{x,t}_{\mathrm{K},L} + \lambda^{x,t}_{\mathrm{K}} \right) \\
\Delta C^{x,t}_{\mathrm{Ca,ex,tot}} &= \tau^{x}_{\mathrm{Ca,ex}} \left(-I^{x,t}_{\mathrm{Ca,ex},D} - 2N_{\mathrm{mv}} I^{x,t}_{X} + N_{\mathrm{mv}} I^{x,t}_{\mathrm{Ca},L} \right) \\
\Delta C^{x,t}_{\mathrm{Mg,ex}} &= \tau^{x}_{\mathrm{Mg,ex}} \left(-I^{x,t}_{\mathrm{Mg,ex},D} + N_{\mathrm{mv}} I^{x,t}_{\mathrm{Mg},L} \right)
\end{aligned}$$

with

$$\lambda^{x,t}_{\mathrm{Na}} = \begin{cases} I^{t}_{\mathrm{Na},R} - 3I_P & \text{for } x = 1 \\ 0 & \text{for } 1 < x \leq n_{\mathrm{mv}} + 1 \end{cases}$$

and

$$\lambda^{x,t}_{\mathrm{K}} = \begin{cases} I^{t}_{\mathrm{K},R} + I^{t}_{\mathrm{K},V} + 2I_P & \text{for } x = 1 \\ 0 & \text{for } 1 < x \leq n_{\mathrm{mv}} + 1 \end{cases}$$

Calculating the free Ca^{2+} concentration

The newly calculated values for the total Ca^{2+} concentration in the microvilli and the cell body can now be converted into new values for the free Ca^{2+} concentration. Assuming instantaneous buffering by a single buffer with concentration B and dissociation constant $K_{d,B} = 20\ \mu$M, the relation between $C_{\mathrm{Ca,tot}}$ and $C_{\mathrm{Ca},f}$ is given by (the spatial and temporal indices being omitted):

$$C_{\mathrm{Ca,tot}} = C_{\mathrm{Ca},f} + C_{\mathrm{Ca},b} = C_{\mathrm{Ca},f} + B \frac{C_{\mathrm{Ca},f}}{C_{\mathrm{Ca},f} + K_{d,B}}$$

Transforming this equation to isolate $C_{\mathrm{Ca},f}$ yields:

$$C_{\mathrm{Ca},f} = \frac{1}{2} \left(C_{\mathrm{Ca,tot}} - K_{d,B} - B + \sqrt{(C_{\mathrm{Ca,tot}} - K_{d,B} - B)^2 + 4K_{d,B} C_{\mathrm{Ca,tot}}} \right)$$

Due to the linear Ca^{2+} buffering in the extracelluar rhabdomere, $C_{\mathrm{Ca,ex},f}$ is given by:

$$C_{\mathrm{Ca,ex},f} = C_{\mathrm{Ca,ex,tot}} / (1 + f_{B,\mathrm{ex}})$$

The extracellular buffering factor, $f_{B,\mathrm{ex}}$, was typically set to 2.9 in the rhabdomere, and to 0 in the intraommatidial cavity.

Bibliography

1. Allbritton NL, Meyer T, Stryer L (1992) Range of messenger action of calcium and inositol 1,4,5-trisphosphate. Science 258:1812-1815.
2. Alloway PG, Dolph PJ (1999) A role for the light-dependent phosphorylation of visual arrestin. Proc Natl Acad Sci USA 96:6072-6077.
3. Anderson J, Hardie RC (1996) Different photoreceptors within the same retina express unique combinations of potassium channels. J Comp Physiol 178:513-522.
4. Arikawa K, Hicks JL, Williams DS (1990) Identification of actin filaments in the rhabdomeral microvilli of *Drosophila* photoreceptors. J Cell Biol 110:1993-1998.
5. Armon E, Minke B (1983) Light activated electrogenic Na^{+}-Ca^{2+} exchange in fly photoreceptors: modulation by Na^{+}/K^{+}-pump activity. Biophys Struct Mech 9:349-357.
6. Augustine GJ, Neher E (1992) Neuronal Ca^{2+} signalling takes the local route. Curr Opin Neurobiol 2:302-307.
7. Autrum H (1979) Light and dark adaptation in invertebrates. In: Handbook of sensory physiology, Vol. VII/6A. (Autrum H, ed), pp 1-91. Berlin: Springer.
8. Babcock DF, Herrington J, Goodwin PC, Park YB, Hille B (1997) Mitochondrial participation in the intracellular Ca^{2+} network. J Cell Biol 136:833-844.
9. Bader CR, Baumann F, Bertrand D (1976) Role of intracellular calcium and sodium in light adaptation in the retina of the honeybee drone (*Apis mellifera*, L). J Gen Physiol 67:475-491.
10. Bauer PJ, Schauf H, Schwarzer A, Brown JE (1999) Direct evidence of Na^{+}/Ca^{2+} exchange in squid rhabdomeric membranes. Am J Physiol, 276:C558-C565.
11. Baumann O, Walz B, Somlyo AV, Somlyo AP (1991) Electron probe microanalysis of calcium release and magnesium uptake by endoplasmic reticulum in bee photoreceptors. Proc Natl Acad Sci USA 88:741-744.
12. Baumann O, Lautenschläger B, Takeyasu K (1994) Immunolocalization of Na,K-ATPase in blowfly photoreceptor cells. Cell Tissue Res 275:225-234.
13. Bernardi P (1999) Mitochondrial transport of cations: channels, exchangers, and permeability transition. Physiol Rev 79:1127-1155.
14. Berridge MJ (1995) Capacitative calcium entry. Biochem J 312:1-11.
15. Blaustein MP, Lederer WJ (1999) Sodium/calcium exchange: its physiological implications. Physiol Rev 79:763-854.
16. Borst JG, Sakmann B (1999) Depletion of calcium in the synaptic cleft of a calyx-type synapse in the rat brainstem. J Physiol (Lond) 521:123-133.

17. Boschek CB (1971) On the fine structure of the peripheral retina and lamina ganglionaris of the fly, Musca domestica. Z Zellforsch 118:369-409.
18. Boyer C, Sans A, Vautrin J, Chabbert C, Lehouelleur J (1999) K^+-dependence of Na^+- Ca^{2+} exchange in type I vestibular sensory cells of guinea-pig. Eur J Neurosci 11:1955-1959.
19. Cardinaud B, Coles JA, Perrottet P, Spencer AJ, Osborne MP, Tsacopoulos M (1994) The composition of the interstitial fluid in the retina of the honeybee drone: implications for the supply of substrates of energy metabolism from blood to neurons. Proc R Soc Lond B 257:49-58.
20. Cervetto L, Lagnado L, Perry RJ, Robinson DW, McNaughton PA (1989) Extrusion of calcium from rod outer segments is driven by both sodium and potassium gradients. Nature 317, 740-743.
21. Chevesich J, Kreuz AJ, Montell C (1997) Requirement for the PDZ domain protein, INAD, for localization of TRP store-operated channel to a signaling complex. Neuron 18:95-105.
22. Chyb S, Raghu P, Hardie RC (1999) Polyunsaturated fatty acids activate the *Drosophila* light-sensitive channels TRP and TRPL. Nature 397:255-259.
23. Coles JA, Orkand RK (1985) Changes in sodium activity during light stimulation in photoreceptors, glia and extracellular space in drone retina. J Physiol (Lond) 362:515- 435.
24. Coles JA, Rick R (1985) An electron microprobe analysis of photoreceptors and outer pigment cells in the retina of the honeybee drone. J Comp Physiol A 156:213-222.
25. Coles JA, Orkand RK, Yamate CL, Tsacopoulos M (1985) Free concentrations of Na, K, and Cl in the retina of the honeybee drone: stimulus-induced redistribution and homeostasis. Ann NY Acad Sci 481:303-317.
26. Cook B, Minke B (1999) TRP and calcium stores in *Drosophila* phototransduction. Cell Calcium 25:161-171.
27. Dabdoub A, Payne R (1999) Protein kinase C activators inhibit the visual cascade in *Limulus* ventral photoreceptors at an early stage. J Neurosci 19:10262-10269.
28. Deckert A, Stieve H (1991) Electrogenic Na^+-Ca^{2+} exchanger, the link between intra- and extracellular calcium in the *Limulus* ventral photoreceptor. J Physiol (Lond) 443:467-482.
29. Denk W, Holt JR, Shepherd GMG, Corey DP (1995) Calcium imaging of single stereocilia in hair cells: localization of transduction channels at both ends of tip links. Neuron 15:1311-1321.
30. De Schutter E, Smolen P (1998) Calcium dynamics in large neuronal models. In: Methods in neuronal modeling: from ions to networks, Ed 2 (Koch C, Segev I, eds) pp 211-250.
31. Edelman DM, Montague PR (1999) Calcium dynamics in the extracellular space of mammalian neural tissue. Biophys J 76:1856-1867.
32. El-Gammal S, Hamdorf K, Henning U (1987) The paracrystalline structure of an insect rhabdomere (*Calliphora vicina*). Cell Tissue Res 248:511-518.
33. Escobar AL, Cifuentes F, Vergara JL (1995) Detection of Ca^{2+}-transients elicited by flash photolysis of DM-nitrophen with a fast calcium indicator. FEBS Lett 364:335-

338.

34. Fein A, Tsacopoulos M (1988) Activation of mitochondrial oxidative metabolism by calcium ions in *Limulus* ventral photoreceptor. Nature 331:437-440.
35. Franceschini N, Kirschfeld K (1971) Les phénomènes de pseudopupille dans l'œil composé de *Drosophila*. Kybernetik 9:159-182.
36. Gerster U (1997) A quantitative estimate of flash-induced Ca^{2+}- and Na^{+}- influx and Na^{+}/Ca^{2+}-exchange in blowfly *Calliphora* photoreceptors. Vision Res 37:2477-2485.
37. Gerster U, Stavenga DG, Backhaus W (1997) Na^{+}/K^{+}-pump activity in photoreceptors of the blowfly *Calliphora*: a model analysis based on membrane potential measurements. J Comp Physiol A 180:113-122.
38. Gho M, Mallart A (1986) Two distinct calcium-activated potassium currents in larval muscle fibers of *Drosophila melanogaster*. Pflügers Arch 407:526-533.
39. Grynkiewicz G, Poenie M, Tsien RY (1985) A new generation of Ca^{2+} indicators with greatly improved fluorescence properties. J Biol Chem 260:3440-3450.
40. Hall JD, Betarbet S, Jarmillo F (1997) Endogenous buffers limit the spread of free calcium in hair cells. Biophys J 73:1243-1252.
41. Hardie RC (1985) Functional organization of the fly retina. In: Progress in sensory physiology, Vol. 5 (Ottoson D, ed), pp 1-79. Berlin: Springer.
42. Hardie RC (1991a) Whole-cell recordings of the light induced current in dissociated *Drosophila* photoreceptors: evidence for feedback by calcium permeating the light-sensitive channels. Proc R Soc Lond B Biol Sci 245:203-210.
43. Hardie, RC (1991b) Voltage-sensitive potassium channels in *Drosophila* photoreceptors. J Neurosci 11:3079-3095.
44. Hardie RC (1995a) Photolysis of caged Ca^{2+} facilitates and inactivates but does not directly excite light-sensitive channels in *Drosophila* photoreceptors. J Neurosci 15:889-902.
45. Hardie RC (1995b) Effects of intracellular Ca^{2+} chelation on the light response in *Drosophila* photoreceptors. J Comp Physiol A 177:707-721.
46. Hardie RC (1996a) INDO-1 measurements of absolute resting and light-induced Ca^{2+} concentration in *Drosophila* photoreceptors. J Neurosci 16:2924-2933.
47. Hardie RC (1996b) Excitation of *Drosophila* photoreceptors by BAPTA and ionomycin: evidence for capacitative Ca^{2+} entry? Cell Calcium 20:315-327.
48. Hardie RC, Minke B (1992) The trp gene is essential for a light-activated Ca^{2+} channel in *Drosophila* photoreceptors. Neuron 8:643-651.
49. Hardie RC, Minke B (1993) Novel Ca^{2+} channels underlying transduction in *Drosophila* photoreceptors: implications for phosphoinositide-mediated Ca^{2+} mobilization. Trends Neurosci 16:371-376.
50. Hardie RC, Minke B (1994a) Spontaneous activation of light-sensitive channels in *Drosophila* photoreceptors. J Gen Physiol 103:389-407.
51. Hardie RC, Minke B (1994b) Calcium-dependent inactivation of light-sensitive channels in *Drosophila* photoreceptors. J Gen Physiol 103:409-427.
52. Hardie RC, Minke B (1995) Phosphoinositide-mediated phototransduction in *Drosophila* photoreceptors: the role of Ca^{2+} and trp. Cell Calcium 18:256-274.

53. Hardie RC, Mojet MH (1995) Mg^{2+} dependent block of the light-activated and trp dependent conductance in *Drosophila* photoreceptors. J Neurophysiol 74:2590-2599.
54. Hardie RC, Peretz A, Suss-Toby E, Rom-Glas A, Bishop SA, Selinger Z, Minke B (1993) Protein kinase C is required for light adaptation in *Drosophila* photoreceptors. Nature 363:634-637.
55. Hardie RC, Reuss H, Lansdell SJ, Millar NS (1997) Functional equivalence of native light-sensitive channels in the *Drosophila* trp^{301} mutant and TRPL cation channels expressed in a stably transfected *Drosophila* cell line. Cell Calcium 21:431-440.
56. Haug-Collet K, Pearson B, Webel R, Szerencsei RT, Winkfein RJ, Schnetkamp PP, Colley NJ (1999) Cloning and characterization of a potassium-dependent sodium/calcium exchanger in *Drosophila*. J Cell Biol 147:659-770.
57. Haugland RP (1996) Handbook of fluorescent probes and research chemicals, Ed 6. Eugene, OR: Molecular Probes
58. Hilgemann, DW (1996) Unitary cardiac Na^{+}, Ca^{2+} exchange current magnitudes determined from channel-like noise and charge movements of ion transport. Biophys J 71:759-768.
59. Hille B (1992) Ionic channels of excitable membranes, Ed 2. Sunderland, MA: Sinauer.
60. Hochstrate P (1989) Photoresponses from cells in the fly's eye which are not visual cells. Z Naturforsch 44c:867-875.
61. Hochstrate P (1991) Electrogenic Na^{+}-Ca^{2+} exchange contributes to the light response of fly photoreceptors. Zeitschr für Naturforsch 46c:451-460.
62. Hochstrate P, Hamdorf K (1990) Microvillar components of light adaptation in blowflies. J Gen Physiol 95:891-910.
63. Hochstrate P, Juse A (1991) Intracellular free calcium concentration in the blowfly retina studied by fura-2. Cell Calcium 12:695-712.
64. Hofstee CA, Stavenga DG (1996) Calcium homeostasis in photoreceptor cells of *Drosophila* mutants inaC and trp studied with the pupil mechanism. Vis Neurosci 13:257-263.
65. Howard J (1984) Calcium enables photoreceptor pigment migration in a mutant fly. J Exp Biol 113:471-475.
66. Howard J, Blakeslee B, Laughlin SB (1987) The intracellular pupil mechanism and photoreceptor signal:noise ratios in the fly Lucilia cuprina. Proc R Soc Lond B Biol Sci 231:415-435.
67. Huber A, Sander P, Gobert A, Bähner M, Hermann R, Paulsen R (1996a). The transient receptor potential protein (Trp), a putative store-operated Ca^{2+} channel essential for phosphoinositide-mediated photoreception, forms a signaling complex with NorpA, InaC and InaD. EMBO J 15:7036-7045.
68. Huber A, Sander P, Paulsen R (1996b) Phosphorylation of the InaD gene product, a photoreceptor membrane protein required for recovery of visual excitation. J Biol Chem 271:11710-11717.
69. Huber A, Sander P, Bähner M, Paulsen R (1998) The TRP Ca^{2+} channel assembled in a signaling complex by the PDZ domain protein INAD is phosphorylated through the interaction with protein kinase C (ePKC). FEBS Lett 425:317-322.

70. Ikeda K, Saito Y, Nishiyama A, Takasaka T (1992) Na^{+}-Ca^{2+} exchange in the isolated cochlear outer hair cells of the guinea-pig studied by fluorescence image microscopy. Pflügers Arch 420:493-499.
71. Jansonius NM (1990) Properties of the sodium pump in the blowfly photoreceptor cell. J Comp Physiol A 167:461-468.
72. Jaramillo F (1995) Signal transduction in hair cells and its regulation by calcium. Neuron 15:1227-1230.
73. Jung A, Lischka FW, Engel J, Schild D (1994) Sodium/calcium exchanger in olfactory receptor neurones of Xenopus laevis. Neuroreport 5:1741-1744.
74. Kirschfeld K, Franceschini N (1969) Ein Mechanismus zur Steuerung des Lichtflusses in den Rhabdomeren des Komplexauges von Musca. Kybernetik 6:13-22.
75. Kirschfeld K, Vogt K (1980) Calcium ions and pigment migration in fly photoreceptors. Naturwissenschaften 67:516-517.
76. Koch C, Zador A (1993) The function of dendritic spines: devices subserving biochemical rather than electrical compartmentalization. J Neurosci 13:413-422.
77. Krizaj D, Copenhagen DR (1998) Compartmentalization of calcium extrusion mechanisms in the outer and inner segments of photoreceptors. Neuron 21:249-256.
78. Laughlin SB (1981) Neural principles in the peripheral visual systems of invertebrates. In: Handbook of sensory physiology, Vol. VII/6B. (Autrum H, ed), pp 133-280. Berlin: Springer.
79. Laughlin SB (1989) The role of sensory adaptation in the retina. J Exp Biol 146:39-62.
80. Laughlin SB, Hardie RC (1978) Common strategies for light adaptation in the peripheral visual systems of fly and dragonfly. J Comp Physiol 128:319-340.
81. Lenzi D, Roberts WM (1994) Calcium signalling in hair cells: multiple roles in a compact cell. Curr Opin Neurobiol 4:496-502.
82. Lisman JE, Brown JE (1972) The effects of intracellular iontophoretic injection of calcium and sodium ions on the light response of *Limulus* ventral photoreceptors. J Gen Physiol 59:701-719.
83. Lisman JE, Brown JE (1975) Effects of intracellular injection of calcium buffers on light adaptation in *Limulus* ventral photoreceptors. J Gen Physiol 66:489-506.
84. Llinás R, Sugimori M, Silver RB (1992) Microdomains of high calcium concentration in a presynaptic terminal. Science 256:677-679.
85. Llinás R, Sugimori M, Silver RB (1995) The concept of calcium concentration microdomains in synaptic transmission. Neuropharmacology 34:1443-1451.
86. Lumpkin EA, Hudspeth AJ (1995) Detection of Ca^{2+} entry through mechanosensitive channels localizes the site of mechanoelectrical transduction in hair cells. Proc Natl Acad Sci USA 92:10297-10301.
87. Lumpkin EA, Hudspeth AJ (1998) Regulation of free Ca^{2+} concentration in hair-cell stereocilia. J Neurosci 18:6300-6318.
88. Martin SR, Maune JF, Beckingham K, Bayley PM (1992) Stopped-flow studies of calcium dissociation from calcium-binding-site mutants of *Drosophila melanogaster* calmodulin. Eur J Biochem 205:1107-1114.

89. Matić T, Laughlin SB (1981) Changes in the intensity-response function of an insect's photoreceptors due to light adaptation. J Comp Physiol 145:169-177.
90. Maune JF, Klee CB, Beckingham K (1992) Ca^{2+} binding and conformational change in two series of point mutation to the individual Ca^{2+} binding sites of calmodulin. J Biol Chem 8:5286-5295.
91. McLaughlin S, Brown JE (1981) Diffusion of calcium ions in retinal rods. A theoretical calculation. J Gen Physiol 77:475-487.
92. McLaughlin S, Mulrine N, Gresalfi T, Vaio G, McLaughlin A (1981) Adsorption of divalent cations to bilayer membranes containing phosphatidylserine. J Gen Physiol 77:445-473.
93. McNaughton PA (1995) Rods, cones and calcium. Cell Calcium 18:275-284.
94. Menini A (1999) Calcium signalling and regulation in olfactory neurons. Curr Opin Neurobiol 9:419-426.
95. Minke B, Selinger Z (1996) The roles or trp and calcium in regulating photoreceptor function in *Drosophila*. Curr Opin Neurobiol 6:459-466.
96. Minke B, Tsacopoulos M (1986) Light induced sodium dependent accumulation of calcium and potassium in the extracellular space of bee retina. Vision Res 26:679-690.
97. Miyata H, Silverman HS, Sollott SJ, Lakatta EG, Stern MD, Hansford RG (1991) Measurement of mitochondrial free Ca^{2+} concentration in living single rat cardiac myocytes. Heart Circ Physiol 30:H1123-H1134.
98. Mojet MH, Tinbergen J, Stavenga DG (1991) Receptor potential and light-induced mitochondrial activation in blowfly photoreceptors mutant. J Comp Physiol A 168:305- 312.
99. Montell C (1997) New light on TRP and TRPL. Mol Pharmacol 52:755-763.
100. Montell C (1998) TRP trapped in fly signalling web. Curr Opin Neurobiol 8:389-397.
101. Montell C (1999) Visual transduction in *Drosophila*. Annu Rev Cell Dev Biol 15:231-268.
102. Morgans CW, El Far O, Berntson A, Wässle H, Taylor WR (1998) Calcium extrusion from mammalian photoreceptor terminals. J Neurosci 18:2467-2474.
103. Muijser H (1979) The receptor potential of retinular cells of the blowfly *Calliphora*: the role of sodium, potassium and calcium ions. J Comp Physiol 132:87-95.
104. Neher E (1995) The use of fura-2 for estimating Ca buffers and Ca fluxes. Neuropharmacology 34:1423-1442.
105. Neher E (1998) Usefulness and limitations of linear approximations to the understanding of Ca^{++} signals. Cell Calcium 24:345-357.
106. Neher E, Augustine GJ (1992) Calcium gradients and buffers in bovine chromaffin cells. J Physiol (Lond) 450:273-301.
107. Niemeyer BA, Suzuki E, Scott K, Jalink K, Zuker CS (1996) The *Drosophila* light-activated conductance is composed of the two channels TRP and TRPL. Cell 85:651-659.
108. Niggli E, Lederer WJ (1991) Molecular operations of the sodium-calcium exchanger revealed by conformation currents. Nature 349:621-624.

109. Obukhov AG , Schultz G, Lückhoff A (1998) Regulation of heterologously expressed transient receptor potential-like channels by calcium ions. Neuroscience 85:487-495.

110. O'Day PM, Gray-Keller MP (1989) Evidence for electrogenic Na^+/Ca^{2+} exchange in *Limulus* ventral photoreceptors. J Gen Physiol 93:473-492.

111. Orkand RK, Dietzel I, Coles JA (1984). Light-induced changes in extracellular volume in the retina of the drone, *Apis mellifera*. Neurosci Lett 45:273-278.

112. Peretz A, Sandler C, Kirschfeld K, Hardie RC, Minke B (1994a) Genetic dissection of light-induced Ca^{2+} influx into *Drosophila* photoreceptors. J Gen Physiol 104:1057-1077.

113. Peretz A, Suss-Toby E, Rom-Glas A, Arnon A, Payne R, Minke B (1994b) The light response of *Drosophila* photoreceptors is accompanied by an increase in cellular calcium: effects of specific mutations. Neuron 12:1257-1267.

114. Petrozzino JJ, Pozzo Miller LD, Connor JA (1995) Micromolar Ca^{2+} transients in dendritic spines of hippocampal pyramidal neurons in brain slice. Neuron 14:1223-1231.

115. Phillips AM, Bull A, Kelly LE (1992) Identification of a *Drosophila* gene encoding a calmodulin-binding protein with homology to the trp phototransduction gene. Neuron 8:631-642.

116. Porter JA, Yu M, Doberstein SK, Pollard TD, Montell C (1993) Dependence of calmodulin localization in the retina on the NinaC unconventional myosin. Science 262:1038-1042.

117. Postma M, Oberwinkler J, Stavenga DG (1999) Does Ca^{2+} reach millimolar concentrations after single photon absorption in *Drosophila* photoreceptor microvilli? Biophys J 77:1811-1823.

118. Ranganathan R, Harris GL, Stevens CF, Zuker CS (1991) A *Drosophila* mutant defective in extracellular calcium-dependent photoreceptor deactivation and rapid desensitization. Nature 354:230-232.

119. Ranganathan, R, Bacskai BJ, Tsien RY, Zuker CS (1994) Cytosolic calcium transients: spatial localization and role in *Drosophila* photoreceptor cell function. Neuron 13:837-848.

120. Reisert J, Matthews HR (1998) Na^+-dependent Ca^{2+} extrusion governs response recovery in frog olfactory receptor cells. J Gen Physiol 112:529-525.

121. Reuss H, Mojet MH, Chyb S, Hardie RC (1997) In vivo analysis of the *Drosophila* light-sensitive channels, TRP and TRPL. Neuron 19:1249-1259.

122. Reuter H, Porzig H (1995) Localization and functional significance of the Na^+/Ca^{2+} exchanger in presynaptic boutons of hippocampal cells in culture. Neuron 15:1077-1084.

123. Richard EA, Ghosh S, Lowenstein JM, Lisman JE (1997) Ca^{2+}/calmodulin-binding peptides block phototransduction in *Limulus* ventral photoreceptors: evidence for direct inhibition of phospholipase C. Proc Natl Acad Sci USA 94:14095-14099

124. Roberts WM (1994) Localization of calcium signals by a mobile calcium buffer in frog saccular hair cells. J Neurosci 14:3246-3262.

125. Roebroek JGH, Stavenga DG (1990) Insect pupil mechanisms. IV. Spectral characteristics and light intensity dependence in the blowfly, *Calliphora erythrocephala*. J Comp Physiol A 166:537-543.

126. Rom-Glas A, Sandler C, Kirschfeld K, Minke B (1992) The nss mutation or lanthanum inhibits light-induced Ca^{2+} influx into fly photoreceptors. J Gen Physiol 100:767-781.

127. Ruknudin A, Valdivia C, Kofuji P, Lederer WJ, Schulze DH (1997) Na^{+}/Ca^{2+} exchanger in *Drosophila*: cloning, expression, and transport differences. Am J Physiol 273:C257-C265.

128. Running Deer JL, Hurley JB, Yarfitz SL (1995) G protein control of *Drosophila* photoreceptor phospholipase C. J Biol Chem 270:12623-12628.

129. Sandler C, Kirschfeld K (1988) Light intensity controls extracellular Ca^{2+} concentration in the blowfly retina. Naturwissenschaften 75:256-258.

130. Sandler C, Kirschfeld K (1991) Light-induced extracellular calcium and sodium concentration changes in the retina of *Calliphora*: involvement in the mechanism of light adaptation. J Comp Physiol A 169:299-311.

131. Sandler C, Kirschfeld K (1992) Light-induced changes in extracellular calcium concentration in the compound eye of *Calliphora*, *Locusta* and *Apis*. J Comp Physiol A 171:573-581.

132. Schnetkamp PPM, Szerencsei RT, Basu DK (1989) Na^{+}-Ca^{2+}-exchange in bovine rod outer segments requires and transports K^{+}. Am J Physiol 257, C153-C157.

133. Scholes JH (1964) Discrete subthreshold potentials from the dimly lit insect eye. Nature 202:572-573.

134. Schwarz EM, Benzer S (1997) Calx, a Na-Ca exchanger gene of *Drosophila melanogaster*. Proc Natl Acad Sci USA 94:10249-10254.

135. Scott K, Zuker CS (1998) Assembly of the *Drosophila* phototransduction cascade into a signalling complex shapes elementary responses. Nature 395:805-808.

136. Scott K, Sun Y, Beckingham K, Zuker CS (1997) Calmodulin regulation of *Drosophila* light-activated channels and receptor function mediates termination of the light response in vivo. Cell 91:375-383.

137. Selinger Z, Doza YN, Minke B (1993) Mechanisms and genetics of photoreceptors desensitization in *Drosophila* flies. Biochim Biophys Acta 1179:283-299.

138. Snyder AW (1979) The physics of vision in compound eyes. In: Handbook of sensory physiology, Vol. VII/6A (Autrum H, ed), pp 225-313. Berlin: Springer.

139. Stavenga DG (1983) Fluorescence of blowfly metarhodopsin. Biophys Struct Mech 9:309-317.

140. Stavenga DG, Tinbergen J (1983) Light dependence of oxidative metabolism in fly compound eyes studied in vivo by microspectrofluorometry. Naturwissenschaften 70:618-620.

141. Stavenga DG, Franceschini N, Kirschfeld K (1984) Fluorescence of housefly visual pigment. Photochem Photobiol 40:653-659.

142. Suzuki E, Katayama E, Hirosawa K (1993) Structure of photoreceptive membranes of *Drosophila* compound eyes as studied by quick-freezing electron microscopy. J Electron Microsc 42:178-184.

143. Torre V, Ashmore JF, Lamb TD, Menini A (1995) Transduction and adaptation in sensory receptor cells. J Neurosci 15:7757-7768.

144. Tsukahara Y (1980) Effect of intracellular injection of EGTA and tetraethylammonium chloride on the receptor potential of locust photoreceptors. Photochem Photobiol 32:509-514.

145. Ukhanov K, Payne R (1995) Light activated calcium release in *Limulus* ventral photoreceptors as revealed by laser confocal microscopy. Cell Calcium 18:301-313.

146. Ukhanov KY, Flores TM, Hsiao HS, Mohapatra P, Pitts CH, Payne R (1995) Measurement of cytosolic Ca^{2+} concentration in *Limulus* ventral photoreceptors using fluorescent dyes. J Gen Physiol 105:95-116.

147. Uusitalo RO, Juusola M, Kouvalainen E, Weckström M (1995) Tonic transmitter release in a graded potential synapse. J Neurophysiol 74:1-7.

148. van Hateren JH (1984) Waveguide theory applied to optically measured angular sensitivities of fly photoreceptors. J Comp Physiol A 154:761-771.

149. van Hateren JH (1989) Photoreceptor optics, theory and practice. In: Facets of vision (Stavenga DG, Hardie RC, eds), pp 74-89. Berlin: Springer.

150. Walz B (1982) Calcium-sequestering smooth endoplasmic reticulum in retinula cells of the blowfly. J Ultrastruct Res 81:240-248.

151. Walz B (1992) Enhancement of sensitivity in photoreceptors of the honey bee drone by light and by Ca^{2+}. J Comp Physiol A 170:605-513.

152. Walz B, Zimmermann B, Seidl S (1994) Intracellular Ca^{2+} concentration and latency of light-induced Ca^{2+} changes in photoreceptors of the honey bee drone. J Comp Physiol A 174:421-431.

153. Walz B, Baumann O, Zimmermann B, Ciriacy-Wantrup EV (1995) Caffeine- and ryanodine-sensitive Ca^{2+}-induced Ca^{2+} release from the endoplasmic reticulum in honeybee photoreceptors. J Gen Physiol 105:537-567.

154. Warr CG, Kelly LE (1996) Identification and characterization of two distinct calmodulin-binding sites in the Trpl ion-channel protein of *Drosophila melanogaster*. Biochem J 314:497-503.

155. Weckström M (1989) Light and dark adaptation in fly photoreceptors: Duration and time integral of the impulse response. Vision Res 29:1309-1317.

156. Weckström M, Hardie RC, Laughlin SB (1991) Voltage-activated potassium channels in blowfly photoreceptors and their role in light adaptation. J Physiol (Lond) 440:635- 657.

157. Weckström M, Juusola M, Laughlin SB (1992) Presynaptic enhancement of signal transients in photoreceptor terminals in the compound eye. Proc R Soc Lond B 250:83-89.

158. Weyrauther E, Roebroek JGH, Stavenga DG (1989) Dye transport across the retinal basement membrane of the blowfly *Calliphora erythrocephala*. J Exp Biol 141:47-59.

159. Wu CF, Pak WL (1978) Light-induced voltage noise in the photoreceptor of *Drosophila melanogaster*. J Gen Physiol 71:249-268.

160. Xu X-ZS, Li H-S, Guggino WB, Montell C (1997) Coassembly of TRP and TRPL produces a distinct store-operated conductance. Cell 89:1155-1164.

161. Yamoah EN, Lumpkin EA, Dumont RA, Smith PJ, Hudspeth AJ, Gillespie PG (1998) Plasma membrane Ca^{2+}-ATPase extrudes Ca^{2+} from hair cell stereocilia. J Neurosci 18:610-624.

162. Ziegler A, Walz B (1989) Analysis of extracellular calcium and volume changes in the compound eye of the honeybee drone, *Apis mellifera*. J Comp Physiol A 165:697-709.

163. Zinkler D, Bentrop J, Paulsen R (1985) Phospholipids of fly photoreceptor membranes: fatty acid and phosphoinositide metabolism. Verh Dtsch Zool Ges 78:303.

List of publications

1. Oberwinkler J, Stavenga DG (1998) Light dependence of calcium and membrane potential measured in blowfly photoreceptors in vivo. J Gen Physiol 112:113-124.

2. Oberwinkler J, Stavenga DG (1998) Is the pupil mechanism of fly photoreceptors a useful calcium probe? In: From structure to information in sensory systems (Taddei-Ferretti C, Musio C, eds), pp 504-508. Singapore: World Scientific.

3. Postma M, Oberwinkler J, Stavenga DG (1999) Does Ca^{2+} reach millimolar concentrations after single photon absorption in *Drosophila* photoreceptor microvilli? Biophys J 77:1811-1823.

4. Marshall NJ, Oberwinkler J (1999) The colourful world of the mantis shrimp. Nature 401:873-874.

5. Oberwinkler J, Stavenga DG (2000) Calcium transients in the rhabdomeres of dark- and light-adapted fly photoreceptor cells. J Neurosci 20:1701-1709.

Summary

What are calcium signals?

Changes in the intracellular calcium concentration are called calcium signals. Calcium signals are crucial for the physiology of most biological cells and therefore for the functioning of whole organisms. Well-established examples of processes that depend on calcium signals are: the synaptic transmission of information between two nerve cells, the contraction of muscles and the storage of information in memory. Often, a calcium signal is generated by calcium ions flowing from the extracellular space into the cell through small channels in the membrane. The in-flowing calcium ions can increase the intracellular calcium concentration rapidly and by as much as 10, sometimes even 100, times because the intracellular calcium concentration usually is very low. The increase of the calcium concentration can be readily detected by molecules that bind to calcium ions. The calcium-binding molecules subsequently regulate physiological processes of the cell, depending on whether they are bound to calcium.

An important aspect of calcium signaling is that it can be localized, i.e., the calcium concentration can be different in different parts of the cell. Because calcium ions normally can move quite fast and freely inside the cells, which tends to equalize the calcium concentration between the different parts, cells have developed special mechanisms to maintain the localization of calcium signals. One possibility is to place the calcium channels to remote parts of the cell body that are linked to the rest of the cell only via narrow connections (Figure 7.1a). Another possibility is to place molecules that extrude calcium ions from the cell very close to the channels through which calcium ions flow in (Figure 7.1b). Finally, high concentrations of substances binding to the in-flowing calcium ions can constrain the region of increased calcium concentration (Figure 7.1c).

Below, I will show that the light sensitive cells in the eyes of flies, called the photoreceptor cells, use all of these possibilities to produce changes of the

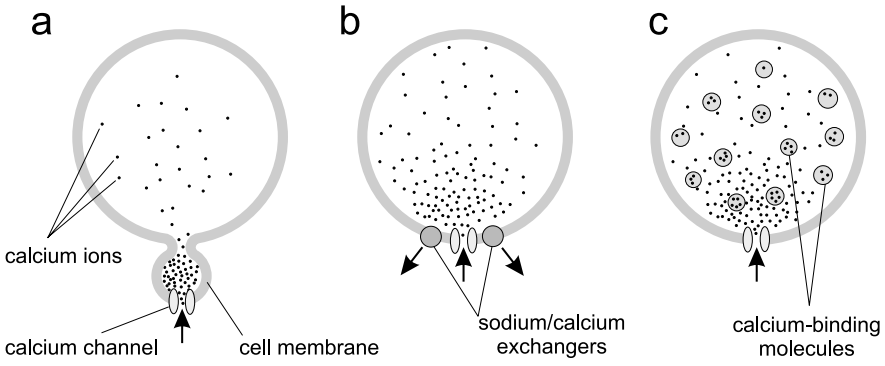

FIGURE 7.1: Three principles allowing to constrain the increase of the intracellular calcium concentration to a part of the cell. a) The calcium channels, through which the calcium enters the cell (upward arrows) are located in a small part of the cell that is linked to the rest of the cell only via a narrow connection. b) Molecules that extrude the in-flowing calcium back to the outside (the sodium/calcium exchangers) are located close to the calcium channels. c) A high concentration of calcium binding molecules is present in the cell.

calcium concentration that are extremely large and highly localized. This makes the photoreceptor cells of flies an attractive object for the study of local calcium signals.

The fly photoreceptor cell, the model system studied in this thesis

Photoreceptor cells respond to light with a change of the electrical potential between the inside and the outside of the cell. A complex biochemical cascade, which is not yet fully understood, underlies the generation of this electrical signal. It starts with the absorption of light by special molecules called rhodopsin. The final result of the chain of biochemical events is that channels in the membrane open (Figure 7.2b), allowing ions, especially calcium ions to enter the cell, thus changing the electrical potential.

The channels that open during light stimulation are not uniformly distributed in the cell membrane, but are concentrated in the rhabdomere (Figure 7.2a, b). The rhabdomere consists of a large number of microvilli, tiny, tube-like protrusions of the cell membrane, that are packed together to form a highly ordered stack. In addition to the channels, most other molecules necessary for generating the electrical signal, including the rhodopsin molecules, are located in the microvilli (Figure 7.2b). The microvilli are all connected

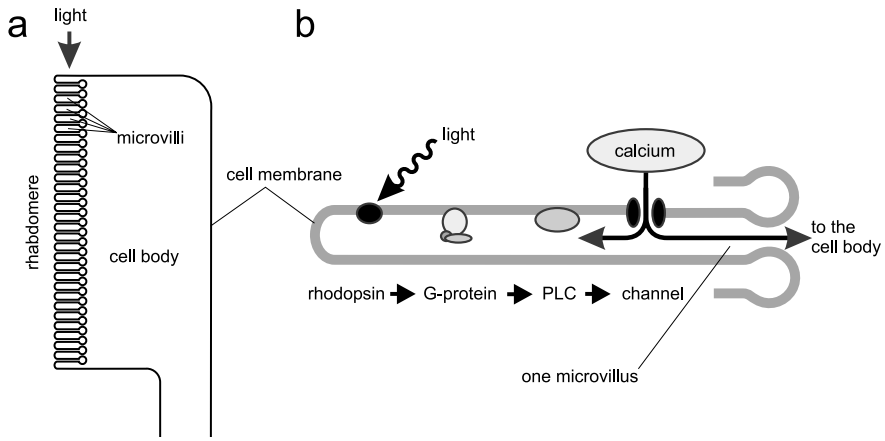

FIGURE 7.2: a) Schematic drawing of a fly photoreceptor cell. It consists of a cell body and a rhabdomere that is made of a large number of microvilli. b) Each microvillus contains rhodopsin molecules that absorb light and thereby are activated. The activation of the rhodopsin molecule is signaled to the calcium channels via a G-protein and a phospholipase C (PLC). The molecules that transport the signal between the PLC and the channels are not yet identified. The final result of the signaling cascade is that the channels open and thereby allows calcium to flow into the microvilli. Therefore the calcium concentration increases in the microvilli and calcium diffuses from the microvilli into the cell body.

to the cell body via a small neck that reduces the speed of diffusion of calcium ions from the microvilli in the large cell body (as shown in Figure 7.1a). Therefore, and because the microvilli are so small, calcium ions flowing into the microvilli rapidly and strongly increase the calcium concentration there. However, there remains a significant calcium flux due to diffusion from the microvilli into the cell body that causes the calcium concentration to rise there as well.

Measuring the calcium concentration in photoreceptor cells in the intact eye of flies

A very popular method to measure the calcium concentration inside cells is to introduce substances, so-called calcium indicator dyes, into the cell that change their optical properties when they bind to calcium. For example, the calcium indicator dyes I used in this thesis emit green fluorescence light when they are illuminated with blue light. Because the intensity of the emitted

green light is stronger when the calcium indicator dyes bind to calcium, one can infer the concentration of calcium by measuring the intensity of the emitted green light. This optical method allows measuring the calcium concentration with a temporal resolution of about a millisecond. I could show that the calcium concentration, especially in the rhabdomere, can rise very quickly. Thus, the high temporal resolution of the optical measuring technique turned out to be indeed necessary

I introduced the calcium indicator dyes into the cell by dissolving them in water and transferring this solution into a tiny pipette made of glass. To approach the photoreceptor cells with the pipette, it is sufficient to cut a small hole in one part of the cornea of the fly's eye. The other parts of the eye are not damaged by this operation. The very tip of this pipette is less than a micrometer wide, and it is possible to push with this small tip through the membrane of a photoreceptor cell without seriously damaging the cell. When the tip of the electrode is inside the photoreceptor cell, the calcium indicator dye can diffuse into the cell. In addition, it is thus possible to measure the electrical potential between the inside and the outside of the cell by connecting the pipette to an electrical amplifier. This technique, however, only works well when the cells that are impaled with the pipette are not too small. I therefore used the relatively large blowflies (*Calliphora vicina*) for this work.

The main results of my thesis

CHAPTER 2: Measuring the calcium concentration in cells remaining in the intact organ can be difficult. Accordingly, the calcium concentration inside fly photoreceptor cells was previously only measured after the photoreceptor cells had been isolated from each other. However, cells in the intact eye are much healthier, and are not vulnerable to damage by the high light intensities necessary for the measurement of the calcium concentration. Isolated photoreceptor cells, however, can not withstand these light intensities. Using photoreceptor cells in the (almost) intact eye, I could quantitatively measure how the calcium concentration, averaged throughout the whole cell, depends on the intensity of the stimulating light. Surprisingly, stimulating the photoreceptor cells with bright light intensities induces the calcium concentration to reach values, that are about 10 times higher than those normally found in other cell types. Calcium indicators can only measure the calcium concentration in a certain range. Because of the large changes of the calcium concentration in the fly photoreceptor cells, I had to use several

types of indicator dyes. However, this also has an advantage. Comparing the measurements obtained with the different calcium indicator dyes, I could determine the calcium concentration in the photoreceptor cells much more accurately than it would have been possible with only one calcium indicator dye.

CHAPTER 3: Because of the special geometry of the fly photoreceptor cells, I expected that the calcium concentration in different parts of the cell is not always the same. It seemed especially interesting to know the calcium concentration in the rhabdomere, as the calcium influx takes place only there. It turned out that working on photoreceptor cells in the intact eyes has an additional advantage. I could show that the natural optics of the fly's eye are perfectly suited to measure the calcium concentration in the rhabdomere. My results clearly demonstrate that the calcium concentration in the rhabdomere can indeed be very different from the average calcium concentration in the cell. Turning on the stimulating light causes the calcium concentration in the rhabdomere to rise extremely fast and to reach extraordinarily high values being more than 10 times higher than the already high average calcium concentrations. These high calcium concentrations exist only for a short time in the rhabdomere, because the calcium concentration decays rather rapidly after having reached its maximum. This form of a calcium signal is often called a calcium transient. Calcium transients are thought to be very important, e.g., for the proper functioning of synapses. Quite likely, the calcium transients in the rhabdomere are also very important for the functioning of the photoreceptor cells. However, previously calcium transients in the rhabdomere had only been postulated on theoretical grounds, while here I could demonstrate their existence and quantitatively measure their time course.

CHAPTER 4: All cells that allow calcium to enter also need to extrude it. This is also true for the photoreceptor cells of flies. This process, the calcium extrusion, is only poorly understood in fly photoreceptor cells, and many other systems too. Here I show that calcium is extruded from fly photoreceptor there, where it flows in, i.e. from the rhabdomere. I arrived at this conclusion by theoretically analyzing the diffusion of calcium ions in the photoreceptor cells. When the calcium extrusion takes place in the rhabdomere, I calculated that the calcium concentration should have the same value everywhere throughout the photoreceptor cell, after the decay

of the calcium transients. If the calcium extrusion takes place elsewhere, the calcium concentrations in the rhabdomere and in the other parts of the cell should be considerably different. To test these predictions, I measured the distribution of the calcium concentration in a single cell with a so-called confocal microscope. I could show that the calcium concentration throughout the cell is indeed constant, after the initial calcium transient has decayed. Therefore, the molecules that remove calcium ions from the cell (so-called sodium/calcium exchangers) are located in or close to the rhabdomere. This shows that the design principle illustrated in Figure 7.1b is realized in fly photoreceptor cells. As a consequence of this design, one should expect that calcium is removed faster from the rhabdomere than from other parts of the cell, when the stimulating light is turned off. Again, experimental testing showed this hypothesis to be correct. Because the calcium concentration in the rhabdomere determines the sensitivity of the photoreceptor cell, quickly removing calcium from the rhabdomere improves the speed with which the sensitivity recovers. This should be a clear functional advantage for the flies. In an increasing number of other cell types both calcium influx channels and calcium extruding are found in the membrane of small, separate parts of the cell. This is probably caused by functional advantages, similar to those that I have demonstrated here, of this design principle.

CHAPTER 5: In fly photoreceptor cells two different types of sodium/calcium exchangers are believed to be present. The two types have different properties, since one of them needs potassium ions to function, but not the other. Until now, it was unknown which type of sodium/calcium exchanger is located in the rhabdomere of fly photoreceptor cells. To investigate this question, I isolated photoreceptor cells of the fruitfly (*Drosophila melanogaster*) and studied them with the so-called patch-clamp technique. This technique has the advantage that it is possible to precisely control the concentration of ions inside and outside of the cell. When I removed potassium completely from the inside and the outside of the cell, the sodium/calcium exchanger molecules still worked. This is a strong indication that sodium/calcium exchanger molecules are present in the rhabdomere that do not depend on potassium ions.

CHAPTER 6: Describing the processes that take place inside a cell mathematically allows evaluating critically the understanding of the whole system. By comparing predicted and measured results, a mathematical model addi-

tionally provides the means to constrain values that have not yet been measured. In order to test the information I gathered in the previous Chapters, I developed a mathematical model that describes the relevant processes in the photoreceptor cells. It describes the influx of calcium ions, their diffusion in the various regions of the cell and their extrusion from the rhabdomere. It furthermore takes into account all other known processes in the cell that influence the electrical potential between the cell's inside and outside. Using the measured calcium concentration in the rhabdomere as starting point, I used the model to predict the change of the electrical potential and compared them with my measurements. It turned out that the predictions of the model match with the measured traces rather well, provided the parameters the values of which have not yet been determined are chosen reasonably. The calculations also confirm that there is a considerable amount of calcium-binding molecules inside the rhabdomere (as indicated in Figure 7.1c). A further advantage is that the model cab be used to quantitatively predict how other ion concentrations, that have not yet been measured, change during light stimulation. For example, the model predicts that the calcium concentration between the microvilli of the rhabdomere, i.e. in the extracellular space of the rhabdomere, decreases quickly and considerably, due to the strong calcium influx at the beginning of the light stimulation. I was able to confirm this, using again optical measuring techniques. The model developed here therefore seems to reasonably describe the movement of calcium ions in the different parts of the photoreceptor cell.

This model thus nicely rounds off the four years of research I have been conducting on the influx, the diffusion and the extrusion of calcium ions in the fly photoreceptor cells, because it integrates the results described in the previous Chapters with the already available knowledge.

Outlook

It has long been recognized that calcium signals in fly photoreceptor play a very important role for the functioning of these cells. An increase of the calcium concentration, caused by light stimulation, is necessary for the desensitization of the photoreceptor cells. Changing the sensitivity is crucial for photoreceptor cells that need to operate equally well under very different illumination conditions, e.g. on a cloudy dawn and on a bright, sunny day. Light adaptation is a very complex phenomenon, which influences many biochemical processes in the photoreceptor cells. Having described how the calcium concentration changes in different parts of the photoreceptor cell, it

is now possible to ask how precisely the local calcium concentrations regulate the physiology of these cells. In order to answer this question, it will be necessary to identify the molecules that interact with calcium ions, and what the effect of this interaction on their physiological function is. These data then can be combined in order to improve our understanding of the complex phenomenon light adaptation. The findings of this thesis may help to achieve this goal. I expect that the insight obtained from working on photoreceptor cells will contribute to similar research in other cell types and to our general understanding of calcium signals.

Samenvatting

Wat zijn calciumsignalen?

Veranderingen van de intracellulaire calciumconcentratie worden calciumsignalen genoemd. Calciumsignalen zijn erg belangrijk voor de fysiologie van de meeste biologische cellen en daarom ook voor het functioneren van hele organismen. Goed uitgewerkte voorbeelden van belangrijke calciumsignalen zijn: de overdracht van informatie van de ene zenuwcel naar de andere via synapsen, de contractie van spieren, en het opslaan van informatie in het geheugen. Vaak worden calciumsignalen opgewekt doordat calciumionen uit de extracellulaire ruimte de cellen binnenstromen. De binnenkomende calciumionen kunnen vrij snel de intracellulaire calciumconcentratie met een factor 10 en soms ook met een factor 100 verhogen, omdat normaal de intracellulaire calciumconcentratie erg laag is. De verhoging van de calciumconcentratie kan worden gedetecteerd door moleculen waaraan het calcium zich kan binden. Sommige calciumbindende moleculen kunnen dan, als zij aan calcium zijn gebonden, de fysiologische processen in de cel beïnvloeden.

Een belangrijk aspect van calciumsignalen is dat ze gelokaliseerd kunnen optreden. Dat wil zeggen dat op verschillende plaatsen in de cel de calciumconcentratie niet dezelfde hoeft te zijn. Omdat calciumionen normaalgesproken zich in de cellen redelijk snel kunnen verplaatsen, hetgeen de calciumconcentraties overal gelijk zou maken, hebben veel cellen speciale mechanismen ontwikkeld om de calciumsignalen te beperken tot een klein gebied. Een mogelijkheid om dat te bereiken is door de calciumkanalen op plaatsen neer te zetten die alleen via nauwe verbindingen met de rest van de cel verbonden zijn (figuur 8.1a). Een ander optie is om moleculen die het calcium weer uit de cel kunnen transporteren dicht bij de kanalen waardoor het calcium binnenstroomt te plaatsen (figuur 8.1b). Ook het aanwezig zijn van een hoge concentratie van calciumbindende moleculen kan helpen het gebied van verhoogde calciumconcentratie te beperken (figuur 8.1c).

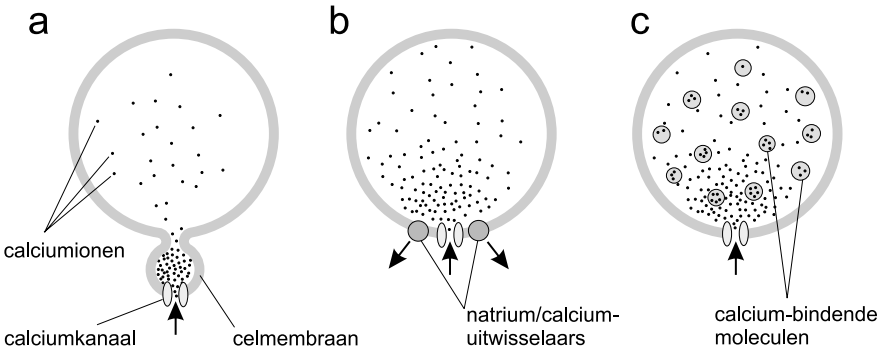

FIGUUR 8.1: Drie principes om de verhoging van de intracellulaire calciumconcentratie tot een deel van de cel te beperken. a) De calciumkanalen, waardoor het calcium binnenstroomt (naar boven gerichte peilen), bevinden zich in een klein gebied van de cel, dat alleen via een nauwe verbinding aan de rest van de cel is gekoppeld. b) Moleculen die het binnengestroomde calcium weer naar buiten kunnen transporteren (de natrium/calcium-uitwisselaars) worden dichtbij de calciumkanalen geplaatst. c) Een hoge concentratie calciumbindende moleculen is in de cel aanwezig.

Ik zal hieronder laten zien dat de lichtgevoelige cellen in het oog van vliegen, die ook fotoreceptorcellen worden genoemd, van al deze mogelijkheden gebruik maken om erg gelokaliseerde, ongekend hoge en snelle veranderingen van de calciumconcentratie te produceren. De lichtgevoelige cellen in het vliegenoog zijn daarom zeer attractief om lokale calciumsignalen te bestuderen.

De fotoreceptorcellen van vliegen, het model systeem dat ik heb bestudeerd

Fotoreceptorcellen van vliegen reageren op licht met een verandering van de elektrische spanning tussen het binnen- en buitenmilieu van de cel. Dit elektrische signaal wordt gegenereerd door een complexe biochemische reactieketen die nog niet helemaal wordt begrepen. De eerste stap is dat speciale moleculen, rhodopsine genoemd, het licht absorberen. Het uiteindelijke resultaat van de reactieketen is dat kanalen in het membraan worden opengezet (figuur 8.2b). Door deze kanalen kunnen ionen, vooral calciumionen, de cel binnenstromen, waardoor de elektrische spanning verandert.

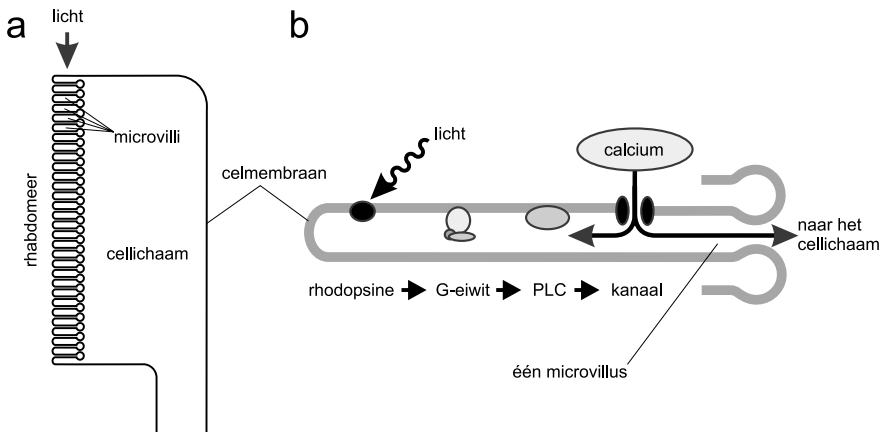

FIGUUR 8.2: a) Schets van een fotoreceptorcel van een vlieg. Zo'n cel bestaat uit het cellichaam en het rhabdomeer, dat uit zeer vele microvilli is opgebouwd. b) In elke microvillus zitten rhodopsinemoleculen die het licht absorberen en daardoor worden geactiveerd. De activatie van het rhodopsinemolecuul wordt dan via een G-eiwit en een phospholipase C (PLC) molecuul aan de calciumkanalen doorgegeven. De moleculen die het signaal tussen de PLC en de kanalen transporteren, zijn nog niet goed bekend, maar uiteindelijk gaan de kanalen open waardoor calcium de microvilli kan binnenstromen. Het calcium hoopt zich in eerste instantie op in de microvilli, maar diffundeert vervolgens naar het cellichaam.

De kanalen, die tijdens de stimulatie met licht opengaan, zijn niet overal in het celmembraan te vinden, maar alleen in het rhabdomeer (figuur 8.2a, b). Het rhabdomeer bestaat uit een zeer groot aantal microvilli, erg kleine uitstulpingen van het celmembraan, die in een zeer regelmatig opgebouwde stapeling naast elkaar liggen. Behalve de kanalen zijn de meeste andere moleculen, die een rol spelen bij het genereren van het elektrische signaal, ook in de microvilli gelokaliseerd (figuur 8.2b). Dat geldt speciaal voor de rhodopsinemoleculen. De microvilli zijn via een nauwe verbinding, de nek, met het cellichaam verbonden. De diffusie van calciumionen vanuit de microvilli naar het cellichaam zal daardoor enigszins worden vertraagd (zoals in figuur 8.1a is aangeduid). Daarom, en ook omdat de microvilli zo klein zijn, kan de calciumconcentratie in de microvilli snel en sterk verhoogd worden. Maar ook in het cellichaam verhoogt de calciumconcentratie tijdens stimulatie met licht aanzienlijk door de diffusie van calciumionen vanuit het rhabdomeer.

Hoe ik de calciumconcentratie in de fotoreceptorcellen in het intacte vliegenoog heb gemeten

Een vaak toegepaste methode om de calciumconcentratie binnen de cellen te meten is speciale kleurstoffen (zogenoemde indicatorkleurstoffen) in de cellen te brengen, waarvan de optische eigenschappen veranderen wanneer zij aan calcium binden. De door mij gebruikte indicatorkleurstoffen fluoresceren in het groen als zij met blauw licht worden bestraald. De intensiteit van de fluorescentie wordt sterker als de indicatorkleurstoffen aan het calcium kunnen binden. Door de intensiteit van de fluorescentie, het uitgezonden groene licht, te meten kan men dus de calciumconcentratie bepalen. Deze methode maakt het mogelijk om de veranderingen van de calciumconcentratie met een hoge temporele oplossing (in de praktijk ongeveer 1 milliseconde) te meten. Ik heb kunnen aantonen dat de calciumconcentratie, vooral in het rhabdomeer, erg snel kan toenemen. Zo'n hoge temporele resolutie is dus ook echt nodig.

Ik heb de indicatorkleurstoffen in de fotoreceptorcellen kunnen brengen door de kleurstof in water op te lossen en de zo verkregen oplossing in een kleine glaspipet te doen. Om met die glaspipet bij de fotoreceptorcellen te komen is het alleen nodig om een kleine opening in een deel van de cornea van het oog te snijden, waardoor de pipet in het oog kan worden gebracht. De rest van het oog wordt door deze operatie niet verstoord. De doorsnede van het uiterste puntje van de gebruikte glaspipetten is minder dan een micrometer, waardoor het mogelijk is om met die punt het celmembraan te penetreren zonder de cel merkbaar te beschadigen. Als de punt van het glaspipet binnen de cel is, kan de indicatorkleurstof vanuit het pipet in de cel diffunderen. Op die manier is het daarbij nog mogelijk de elektrische spanning tussen binnen- en buitenkant van de cel te meten. Daarvoor moet alleen het glaspipet met een elektrische versterker worden verbonden. Deze methode kan alleen worden toegepast wanneer de cellen, waarin de glaspipet wordt gestoken, niet te klein zijn. Ik heb daarom voor deze experimenten de relatief grote bromvliegen (*Calliphora vicina*) gebruikt.

De hoofdresultaten van mijn onderzoek

HOOFDSTUK 2: Het kan behoorlijk lastig zijn om de calciumconcentratie in cellen te meten, die nog in het intacte orgaan zitten. Voordat ik met het werk voor mijn promotie begon was misschien daarom de calciumconcentratie in fotoreceptorcellen van vliegen alleen maar gemeten in cellen die van elkaar geïsoleerd waren. Maar fotoreceptorcellen die nog in het oog zitten zijn veel

gezonder en kunnen heel goed tegen het enorm felle licht dat nodig is voor de metingen van de calciumconcentratie. Geïsoleerde fotoreceptorcellen kunnen daar niet tegen. Doordat ik dus fotoreceptorcellen gebruikte die in het nog (bijna) intacte oog zaten kon ik bepalen hoe de calciumconcentratie, gemiddeld over de hele cel, afhangt van de intensiteit van het stimulerende licht. Toen ik met hoge lichtintensiteiten stimuleerde zag ik tot mijn verbazing dat de calciumconcentratie in de fotoreceptorcellen maar liefst 10 keer hoger kon worden dan wat normaalgesproken in andere celtypes wordt gemeten. De indicatorkleurstofjes hebben een ernstige beperking, want ze kunnen alleen in een bepaald concentratiebereik goed op veranderingen van de calciumconcentratie reageren. Omdat de calciumconcentratie in de fotoreceptorcellen zo sterk kan veranderen, moest ik dus meerdere soorten indicatorkleurstoffen gebruiken. Dit leverde extra werk op, maar had ook weer een bijzonder voordeel. Door de signalen van de verschillende kleurstoffen met elkaar te vergelijken, kon ik de calciumconcentratie veel nauwkeuriger bepalen dan het mogelijk zou zijn geweest met alleen één indicatorkleurstof.

HOOFDSTUK 3: Omdat de fotoreceptorcellen van de vlieg zo'n unieke geometrie hebben, had ik het vermoeden, dat de verandering van de calciumconcentratie in verschillende delen van de cel niet altijd gelijk zou kunnen zijn. Het leek vooral interessant de calciumconcentratie in het rhabdomeer te weten te komen, omdat de calciuminstroom alleen daar plaatsvindt. Het bleek dat het werken met fotoreceptorcellen in het intacte oog extra voordelen had. Ik kon aantonen, dat de natuurlijke optica van het vliegenoog bij uitstek geschikt is om naar de calciumconcentratie in het rhabdomeer te kijken. Mijn resultaten tonen heel duidelijk aan, dat de calciumconcentratie in het rhabdomeer inderdaad zeer sterk kan afwijken van de gemiddelde calciumconcentratie in de cel. Als het stimulerende licht wordt aangezet, gaat de calciumconcentratie in het rhabdomeer veel sneller omhoog dan in de rest van de cel, en wel naar waarden die nog eens meer dan tien keer hoger zijn dan de, sowieso al hoge, gemiddelde calciumconcentratie in de cel. Maar deze extreem hoge calciumconcentraties bestaan maar voor een korte tijd, want de calciumconcentratie in het rhabdomeer neemt na zijn maximum ook weer snel af. Zoiets wordt wel een calciumtransiënt genoemd. Calciumtransiënten zijn erg belangrijk, bijvoorbeeld voor het doorgeven van elektrische signalen bij synapsen. Het is waarschijnlijk dat de calciumtransiënten in het rhabdomeer ook belangrijk zijn voor de werking van de fotoreceptorcellen. Er is daarom al eerder verondersteld dat calciumtransiënten in het rhabdomeer

optreden, maar ik kon hier voor het eerst hun bestaan aantonen en kwantitatief bepalen hoe de calciumconcentratie tijdens zo'n transiënt verandert.

HOOFDSTUK 4: Alle cellen die een calciuminstroom toestaan moeten op een gegeven moment dat calcium ook weer naar buiten zien te krijgen. Dat geldt ook voor de fotoreceptorcellen van vliegen. Over dit proces, de calciumextrusie, is, ook in vele andere systemen, betrekkelijk weinig bekend. Ik laat in dit hoofdstuk zien dat het calcium naar buiten wordt gepompt op vrijwel dezelfde plaats waar het ook binnenkomt, het rhabdomeer. Tot deze conclusie ben ik gekomen door de diffusie van calcium theoretisch te analyseren. Ik kon uitrekenen dat de calciumconcentratie overal in de cel dezelfde moet zijn, uiteraard nadat de calciumtransiënten zijn afgelopen, mits de calciumextrusie ook in het rhabdomeer plaats vindt. Als de calciumextrusie elders was gelokaliseerd zouden de calciumconcentraties in het rhabdomeer en andere delen van de cel nooit dezelfde waarden kunnen hebben. Om deze voorspellingen te testen, heb ik met behulp van een zogenoemde confocale microscoop de verdeling van de calciumconcentratie in de fotoreceptorcellen bepaald. Daarmee kon ik aantonen, dat, na afloop van de calciumtransiënten, de calciumconcentratie inderdaad overal dezelfde waarde heeft. De moleculen die het calcium naar buiten transporteren (de natrium/calcium-uitwisselaars) moeten daarom in of dichtbij het rhabdomeer zitten. In de fotoreceptorcellen van de vliegen is dus het in figuur 8.1b geschetste principe gerealiseerd. Een consequentie van dit principe zou moeten zijn dat, wanneer het stimulerende licht wordt uitgezet, het calcium sneller uit het rhabdomeer wordt verwijderd dan uit de anderen delen van de cel. De experimenten waarmee ik deze vraagstelling heb onderzocht laten duidelijk zien dat deze hypothese juist is. Omdat de calciumconcentratie in het rhabdomeer de gevoeligheid van de fotoreceptorcellen bepaalt, verhoogt het snel verwijderen van calcium uit het rhabdomeer de snelheid waarmee de gevoeligheid van de cellen herstelt. Voor het zien van de vliegen is dit waarschijnlijk van groot belang. Er worden trouwens steeds meer systemen bekend waar én de calciumkanalen én de moleculen die het calcium weer naar buiten werken in het membraan van kleine, afzonderlijke delen van de cel zitten. De functionele voordelen van dit ontwerpprincipe, overeenkomstig aan die ik hier heb laten zien, zijn daar waarschijnlijk verantwoordelijk voor.

HOOFDSTUK 5: Er wordt verondersteld dat in de fotoreceptorcellen van vliegen twee verschillende types natrium/calcium-uitwisselaars aanwezig zijn.

Die twee types hebben verschillende eigenschappen, want de ene kan niet zonder kaliumionen werken, maar de andere wel. Tot dusver was nog niet bekend, welk type in het rhabdomeer van de fotoreceptorcellen voorkomt. In een speciaal onderzoek daarnaar heb ik fotoreceptorcellen van het fruitvliegje (*Drosophila melanogaster*) geïsoleerd en met de patch-clamp-techniek bestudeerd. Deze techniek heeft het voordeel dat de ionenconcentraties binnen en buiten de cellen nauwkeurig kunnen worden gecontroleerd. Toen ik de kaliumionen binnen en buiten de cel volledig verwijderde, werkten de natrium/calcium-uitwisselaars nog steeds. Dit is een sterke aanwijzing, dat natrium/calcium-uitwisselaars in het rhabdomeer zitten, die geen kalium voor hun functioneren nodig hebben.

HOOFDSTUK 6: Door de processen die in een cel gebeuren op een wiskundige manier te beschrijven, kan kritisch worden getoetst hoe goed het hele systeem wordt begrepen. Het is met een wiskundig model soms ook mogelijk de waarden van parameters die nog niet bekend zijn te berekenen. Daarvoor is het meestal nodig voorspellingen van het model met resultaten die wel zijn gemeten te vergelijken. Om de resultaten uit de voorafgaande hoofdstukken te toetsen heb ik een wiskundig model van de relevante processen in de fotoreceptorcel ontwikkeld. Dit model beschrijft de instroom van calciumionen, hun diffusie in de verschillende delen van de fotoreceptorcel en de calciumextrusie vanuit het rhabdomeer. Verder worden in het model alle anderen bekende processen beschreven die de elektrische spanning tussen de binnen- en buitenkant van de cel beïnvloeden. Uitgaand van de gemeten calciumconcentratie in het rhabdomeer heb ik met het model berekend hoe de elektrische spanning zou moeten veranderen. Deze voorspelling heb ik dan met mijn metingen vergeleken. Het bleek dat de voorspellingen van het model best goed met de gemeten resultaten overeenkwamen, wanneer de waarden voor de nog niet goed bekende parameters verstandig werden gekozen. Deze berekeningen bevestigden ook dat er een redelijk grote hoeveelheid van calciumbindende moleculen in het rhabdomeer zitten (zoals in figuur 8.1c is geschetst). Een bijzonder voordeel van het model is dat het gebruikt kan worden om kwantitatief te voorspellen hoe de concentraties van ionen veranderen die nog niet zijn gemeten. Bijvoorbeeld zou, volgens de modelberekeningen, de calciumconcentratie tussen de microvilli, dus in de extracellulaire ruimte, aan het begin van een lichtstimulatie snel en behoorlijk sterk moeten afnemen, vanwege de sterke instroom van calcium in de microvilli. Met behulp van optische meettechnieken kon ik laten zien dat

ook deze voorspelling klopt. Het door mij ontwikkelde model kan kennelijk de calciumstromen tussen de verschillende delen van de cel op een redelijke manier beschrijven.

Dit model is dus een mooie afronding van mijn vier jaren onderzoek aan de instroom, diffusie en extrusie van calciumionen in de fotoreceptorcellen van vliegen, want het voegt de kennis die ik in de eerdere hoofdstukken heb opgedaan samen met de inzichten die al langer bekend waren tot één geheel.

Hoe zou dit onderzoek verder kunnen gaan?

Het is al lang bekend dat de calciumsignalen in de fotoreceptorcellen van vliegen een belangrijke rol spelen voor het functioneren van deze cellen. Een toename van de calciumconcentratie, geïnduceerd door stimulatie met licht, is nodig voor het afnemen van de gevoeligheid van de fotoreceptorcellen. Het aanpassen van de gevoeligheid, ook lichtadaptatie genoemd, is van cruciaal belang voor fotoreceptorcellen die goed moeten kunnen werken onder sterk wisselende lichtcondities, bijvoorbeeld tijdens een donkere, bewolkte ochtend en tijdens een heldere, zonnige middag. Lichtadaptatie is een zeer complex fenomeen, waarbij een heleboel biochemische processen in de fotoreceptorcel worden beïnvloed. Omdat ik heb gemeten hoe de calciumconcentratie verandert in de verschillende delen van de fotoreceptorcel zou het nu mogelijk moeten zijn om te onderzoeken hoe de lokale calciumconcentraties de fysiologie van deze cellen precies reguleert. Om deze vraag te beantwoorden is het nodig om te bepalen welke moleculen met het calcium interactie hebben en wat de effecten van deze interactie op de fysiologische functie van deze moleculen zijn. Deze gegevens kunnen dan worden geïntegreerd in een algemeen model om zo het ingewikkelde fenomeen lichtadaptatie beter te kunnen begrijpen. De resultaten van dit boekje zouden daarbij kunnen helpen. Uiteraard heb ik de verwachting dat de zo aan fotoreceptoren verworven inzichten een bijdrage zullen leveren aan vergelijkbaar onderzoek naar calciumsignalen in andere celtypes.

Acknowledgments

The last four years have been a fantastic and most rewarding time for me. I have had the great opportunity to work on a subject that fascinated me from the very beginning and continues to do so up to now. I owe this opportunity to my promotor, Doekele Stavenga, and I want to thank him for making it possible for me to do my PhD in Groningen. I furthermore want to thank him for the direct and supportive way he supervised me during the four years. His ideas, insight, keen interest and enthusiasm as well as his criticism were indispensable for the work described in this thesis.

I also want to thank Hein Leertouwer and Jannes Land who helped me a lot with the technical aspects of the work. Without their knowledge and dedication, it would have been impossible to perform most of the experiments described in this thesis. Ben Pijpker helped me sorting out problems with computers and the people from the electronics workshop often enough had to repair some part of my equipment. I could always count on Jan Tinbergen to help me out with almost any problem, notably with breeding the flies; I also enjoyed having his opinion and suggestions regarding my work.

I have been very lucky to be able to spend three months in the lab of Roger Hardie, where I learned how to patch-clamp *Drosophila* photoreceptors; the work described in Chapter 5 was done during this stay. I also had the occasion to visit the lab of Matti Weckström in Oulu. The discussions with Roger and Matti have been most interesting and helpful and I am very glad that both have accepted to participate in the committee for my promotion.

In the second half of my time as PhD student, Marten Postma joined the group and started to work on modeling the ion fluxes in the photoreceptor cells. I have learned a lot from this collaboration, and I hope very much that this will continue. The theoretical work in Chapters 4 and 6 profited tremendously from Marten's expertise on numerical calculations.

When I arrived four years ago in the Netherlands, the other PhD students at that time, Esther Wiersinga-Post, Arjen van der Schaaf, Marten Jansen, Kees Schilstra and Lieke Poot, made me feel at home quickly. They, together

with the other members of the Biophysics group created an atmosphere in which it was a pleasure to work. I would like to thank them all.

I am most grateful for the constant support and encouragement that I have received from my parents, not only during the last four years. Finally, I want to thank Sandrine. Without her understanding support, encouragement and tolerance, this thesis would not have been possible in its present form.